Title
Two Degree of Freedom Optimal Control for Nonlinear Systems with Parameter Uncertainty

Author
Shaffer, Richard

Publication Date
2019

Peer reviewed|Thesis/dissertation

UNIVERSITY OF CALIFORNIA
SANTA CRUZ

TWO DEGREE OF FREEDOM OPTIMAL CONTROL FOR NONLINEAR SYSTEMS WITH PARAMETER UNCERTAINTY

A dissertation submitted in partial satisfaction of the
requirements for the degree of

DOCTOR OF PHILOSOPHY

in

APPLIED MATHEMATICS AND STATISTICS

by

Richard Shaffer

March 2019

The Dissertation of Richard Shaffer
is approved:

Professor Qi Gong, Chair

Professor Mark Karpenko

Professor Hongyun Wang

Professor Abhishek Halder

Lori Kletzer
Vice Provost and Dean of Graduate Studies

Table of Contents

List of Figures

List of Tables

Abstract

Two Degree of Freedom Optimal Control for Nonlinear Systems with Parameter Uncertainty

by

Richard Shaffer

This dissertation explores some of the ways that optimal control can be used to mitigate the effects of parametric uncertainty on the control's ability to achieve a desired endpoint condition on the state variables. Standard optimal control solutions rely on precise knowledge of parameter values which are difficult to measure in many practical applications. The result is that, when implementing the designed controls, there is likely to be some error between the desired state trajectories and the actual system outputs. Usually these errors are managed using feedback control using sensor measurements to correct the state deviations on the fly. However, recently there has been promising work done for generating controls which operate in the open-loop for generating state trajectories which are inherently robust to uncertainty in the parameters.

One avenue of applying optimal control for managing parameter uncertainty is unscented optimal control which borrows the low sample discretization of the Unscented Transform for approximating a Riemann-Stieltjes integral of an objective function. This method has proven effective for generating open-loop controls. In this dissertation we explore a family of sensitivity function based optimal control problems, which utilizes an approximation of the response to parameter deviations through a Taylor series, which can be used to likewise generate open-loop controls. We then use these sensitivity based problems as a lens for exploring the unscented control problem. Furthermore, we identify conditions for equivalence

between the two optimal control problems. These inherently robust open-loop trajectories represent a single degree of freedom control.

In addition to generating the open-loop controls for a more robust state trajectory, this dissertation provides a problem formulation for generating a set of time-varying feedback gains. These gains use sensor measurement for both the sensitivity function based problem as well as the unscented problem frameworks. The unscented problem avoids linearizing the error dynamics which is shown to be advantageous for designing the feedback gains. The use of feedback gains represents a second degree of freedom when combined with a more robust open-loop control significantly improving the performance.

These concepts are demonstrated on a simulated nonlinear double gimbal mechanism with flexible effects where the unscented feedback control gives a nearly 100% decrease in variance of the error of the trajectory endpoints and 82% in the case of the purely open-loop. The mathematical model of the double gimbal as a second order set of differential equations represents a prevalent mechanical system in engineering. The controls generated by the neighboring unscented problem demonstrate a significant improvement in the robustness to the parameter uncertainty over the standard controls. The utility of these concepts is further illustrated experimentally using a nonlinear two link robotic arm with flexible joints.

For my family who supported me.

Acknowledgments

I would like to first acknowledge the efforts of my advisors Qi Gong and Mark Karpenko. You both have my gratitude for your guidance over the years.

Additionally, thank you to my AMS support group for the unforgettable friendships and Harleigh Marsh for his help and his willingness to be an enthusiastic sounding board.

Finally, I want to acknowledge and thank my family. I would like to thank my parents for setting an example to strive for, my siblings for pushing me to want to do better, and my best friend for taking the journey with me and giving me motivation.

Chapter 1

Introduction

This dissertation focuses on optimal control of nonlinear systems with uncertainty. In this chapter we will review fundamental theory of optimal control and existing computational methods for mitigating the effects of parametric uncertainty in optimal control framework.

1.1 Optimal Control Problem Formulation and Pontryagin's Principle

In this section optimal control is outlined from problem formulation through an application of Pontryagin's Minimization Principle. The necessary conditions for optimality are generated and form a boundary value problem for the optimal control candidate.

Consider a system with state variables $x(t) \in \mathbb{R}^{n_x}$ with control inputs $u(t) \in \mathbb{R}^{n_u}$ subject to dynamics

$$\dot{x}(t) = f(x, u, t), \tag{1.1}$$

the goal is to design the control inputs to minimize the Bolza cost functional

$$J = E(x_f, t_f) + \int_{t_0}^{t_f} F(x(t), u(t))dt, \tag{1.2}$$

which includes a measure on the final state of the system and a running measure involving the state and control. In addition to the dynamic constraints, the problem formulation includes boundary conditions on the states and time

$$\psi(x(t_f), t_f) = 0, \quad x(t_0) = x_0. \tag{1.3}$$

From the states, controls and endpoint constraints in Eqs. (1.1)-(1.3) the optimal control problem can be formulated using the problem statement

$$x(t) \in \mathbb{R}^{n_x}, \quad u(t) \in \mathbb{R}^{n_u}$$

$$(OP) \begin{cases} \text{Min} & J = E(x_f, t_f) + \int_{t_0}^{t_f} F(x(t), u(t))dt \\ \text{S.t.} & \dot{x}(t) = f(x(t), u(t)) \\ & x(t_0) = x_0 \\ & \psi(x(t_f), t_f) = 0. \end{cases}$$

Applying Pontryagin's Maximization Principle to problem (OP) generates the necessary conditions for a candidate optimal control. The scalar valued Hamiltonian is defined as

$$H(\lambda(t), x(t), u(t)) = F(x(t), u(t)) + \lambda^T[f(x(t), u(t))], \tag{1.4}$$

and the Endpoint Lagrangian

$$\overline{E}(\nu, x_f, t_f) = E(x_f, t_f) + \nu^T \psi(x_f, t_f),$$

where $\lambda(t)$ are the adjoint states and ν are the constant Lagrange multipliers associated with the constraint $\psi(x(t_f), t_f) = 0$. The adjoint states satisfy the dynamics

$$\dot{\lambda} = -\frac{\partial H}{\partial x},$$

with terminal Transversality Condition

$$\lambda(t_f) = \left.\frac{\partial \overline{E}}{\partial x}\right|_{t=t_f}.$$

The Hamiltonian Minimization Condition gives

$$\left.\frac{\partial H}{\partial u}\right|_{x=x^*(t), u=u^*(t)} = 0, \ \forall t \in [t_0, t_f].$$

This set of necessary conditions forms a boundary value problem, which can be solved numerically resulting in so-called indirect methods. Alternatively, the optimal control problem (OP) can be discretized (in time domain) into a finite dimensional optimization problem; then solved by nonlinear programming solvers. Such methods are called direct methods. In such direct methods, necessary conditions from minimum principle can be used for verification and validation of numerical optimal solutions [3].

1.2 Effects of Parameter Uncertainty

In practice, implementing the controls designed from the optimal control problem in the previous section will not precisely produce the outputs expected. This can have different causes including the fact that in many applications the parameters used to define a mathematical model are frequently difficult or expensive to

measure precisely. Uncertainty in the model parameters as a result of measurement difficulty can have undesirable effects on the ability to design maneuvers and requires that special attention be paid to the existence of this uncertainty. This can be conceptualized by, instead of considering a state trajectory for a set of nominally assumed parameters, a set of trajectories each of which is a trajectory associated to a different value of the parameter in the distribution of the uncertainty.

A demonstration of the effects of model parameter uncertainty using a nonlinear fixed wing unmanned areal vehicle (UAV) is provided in the following section.

1.2.1 Nonlinear UAV Example

In this section, a three degree of freedom (3DOF) model of a fixed-wing UAV is used to develop optimal maneuvers between waypoints and to demonstrate the effects of parameter uncertainty. The dynamics use (x, y, z) as the position states in a flat-Earth NED reference frame and velocity, v, along with a generalization of Euler angles for orientation [4]. This model includes control over the rate of change of the bank angle, μ, which co-ordinates yaw and roll, and angle of attack, α. The thrust, T, is assumed (initially) to be constant. The states (γ, σ) are the flight path elevation angle and the heading angle of the craft and the parameters (m, g) are the mass of the vehicle and gravity. The variables (u_α, u_μ) are the

designed signals used to control the UAV.

$$(3DOF)\begin{cases} \dot{x} = v\cos(\gamma)\cos(\sigma) \\ \dot{y} = v\cos(\gamma)\sin(\sigma) \\ \dot{z} = v\sin(\gamma) \\ \dot{v} = \frac{1}{m}(-D + T\cos\alpha) - g\sin\gamma \\ \dot{\gamma} = \frac{1}{mv}(L\cos\mu + T\cos\mu\sin\alpha) - \frac{g}{v}\cos\gamma \\ \dot{\sigma} = \frac{1}{mv\cos\gamma}(L\sin\mu + T\sin\mu\sin\alpha) \\ \dot{\alpha} = u_\alpha \\ \dot{\mu} = u_\mu. \end{cases}$$

In this model, L and D are the lift and drag obtained using the standard equations:

$$\begin{aligned} L &= \tfrac{1}{2}\rho v^2 S C_L \\ D &= \tfrac{1}{2}\rho v^2 S C_D, \end{aligned} \tag{1.5}$$

where S is the reference wing area, ρ is the air density, and (C_L, C_D) are the lift and drag coefficients given by

$$C_L = (C_{x0} + C_{xa}\alpha)\sin\alpha - (C_{z0} + C_{za}\alpha)\cos\alpha, \tag{1.6}$$

$$C_D = -(C_{x0} + C_{xa})\cos\alpha - (C_{z0} + C_{za}\alpha)\sin\alpha. \tag{1.7}$$

Referring to (1.6)–(1.7), the lift and drag coefficients are computed from four parameters $(C_{x0}, C_{xa}, C_{z0}, C_{za})$. The exact values of these coefficients are unknown and have to be estimated experimentally. Thus, they are considered as uncertain parameters, but with a known probability distribution function.

Using the 3DOF model it is possible to formulate the problem of navigating

between two waypoints as an optimal control problem. To this end, denote the dynamics of the UAV model as

$$\dot{x} = f(x(t), u(t), p)$$

where p is a vector of parameters and the state and control vectors are given by

$$\begin{aligned} x &:= (x, y, z, v, \gamma, \sigma, \alpha, \mu) \in \mathbb{R}^8 \\ u &:= (u_\alpha, u_\mu) \in \mathbb{R}^2. \end{aligned}$$

The minimum time trajectory between two waypoints can be obtained by solving the following standard optimal control problem

$$(SOP) \begin{cases} \text{Minimize} & J[x(\cdot), u(\cdot), t_f] := t_f \\ \text{Subject to} & \dot{x} = f(x(t), u(t), p) \\ & (x(t_0), t_0) = (x_0, t_0) \\ & e(x(t_f, p), t_f; p) = x_f, \\ & u_\alpha \in [-0.05, 0.05] \\ & u_\mu \in [-0.05, 0.05] \end{cases}$$

where x_0 is the initial condition of the UAV, x_f is the desired endpoint condition for the waypoint. In all simulations presented in this chapter, the initial condition $(x_0, y_0, z_0) = (0, 0, 600)$, and final condition $(x_f, y_f, z_f) = (1000, 1000, 600)$ are used. These boundary conditions represent a simple canonical turn maneuver that requires the UAV begin and end at a specific location and altitude.

Assuming exact values of the uncertain parameters, $(C_{x0}, C_{xa}, C_{z0}, C_{za})$, are known, the optimal control problem can be solved using, for example, psuedospectral optimal control theory [5, 6, 7, 8]. Shown in Figure 1.1 is a minimum time

trajectory obtained by the software DIDO [3] with the nominal parameter values

$$(C_{x0}, C_{xa}, C_{z0}, C_{za}) = (-0.0355, 0.003, -0.055, -5.6).$$

The UAV is driven precisely to the desired waypoint, as seen in Figure 1.1.

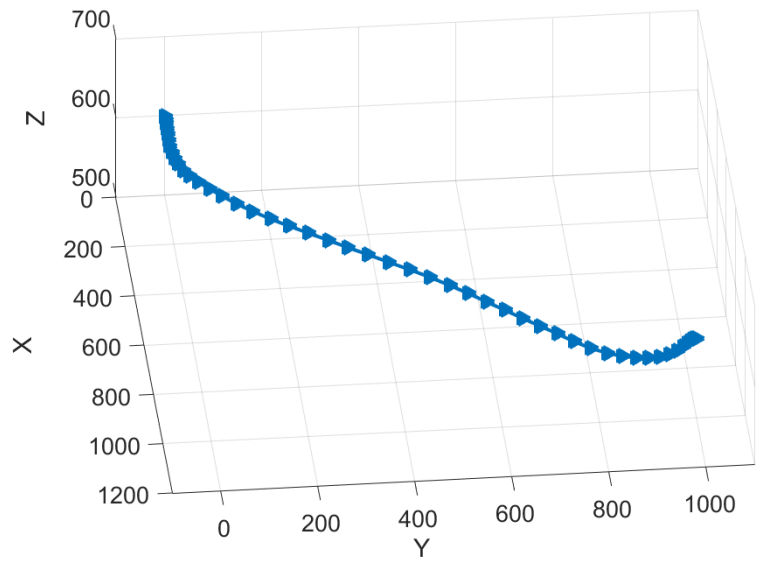

Figure 1.1: Minimum time turn trajectory for standard optimal control problem with nominal model.

However, a problem arises if any uncertainty is introduced into the model, for example the parameters used in (1.6)–(1.7). The issue is easily seen in Figure 1.2 where trajectories are plotted by propagating the computed controls for various values of the uncertain parameter C_{x0}. Variation in C_{x0} was determined, for this maneuver, to have a large effect on the dynamics. A normal distribution centered at the nominal value $C_{x0} = -0.03554$ with a deviation of 20% was assumed. Figure 1.2 demonstrates that propagating the open-loop optimal control generate trajectories that may significantly deviate from the desired waypoint. The mean error and the Euclidean miss distance from the waypoint are given in Table 1.1 for a Monte Carlo simulation comprising 1000 runs. As shown in Table 1.1, there

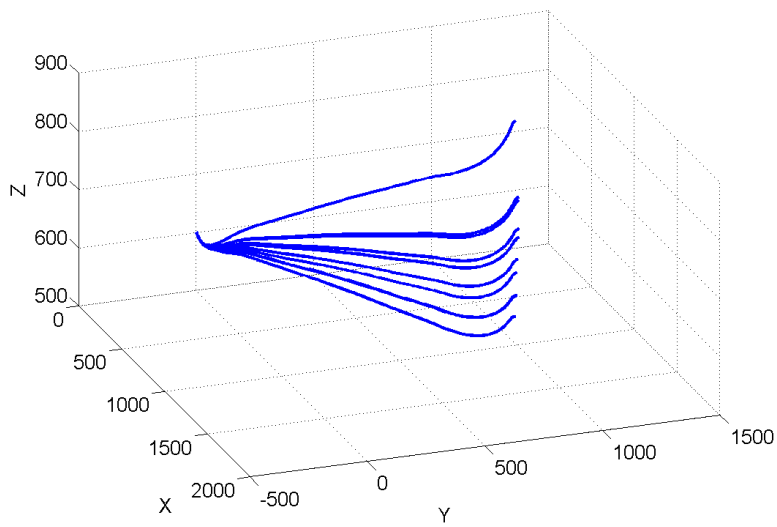

Figure 1.2: Monte Carlo trajectory tube for the standard nominal-only optimal control under parameter uncertainty.

Target Parameter	Error Mean	Standard Deviation (m)
x	0.7%	10.9
y	1.2%	10.4
z	17.5%	80.7
Miss Distance	106 (m)	83.2

Table 1.1: Component-wise relative errors for the Euclidean miss distance from the desired endpoint using standard optimal control.

is an average error of over 100 meters from the intended waypoint with a standard deviation of 83 meters. Clearly, without an explicit consideration of uncertainty in the design of optimal control, it is virtually impossible to precisely target the waypoint under uncertainty.

1.3 Riemann-Stieltjes Optimal Control

Methods for mitigating the effects of uncertainty are important in the field of optimal control. Frequently, it is assumed that feedback type control, which

relies on accurate state sensors, are used, however, recently open-loop control has been demonstrated for designing state trajectories and controls which are consider directly the potential for uncertainty. In this section, an optimal control problem formulation for minimizing a cost functional which is given as a Riemann-Stieltjes integral is reviewed [9, 10, 11, 12, 13]. For the system with dynamics

$$\dot{x} = f(x, u; p), \quad x(0) = x_0, \tag{1.8}$$

and states $x(t) \in \mathbb{R}^{n_x}$ and model parameters $p \in \mathbb{R}^{n_p}$ can be modified to

$$\begin{aligned} \dot{x} &= f(x, u; p), \\ \dot{p} &= 0, \end{aligned}$$

which shifts the parameter uncertainty in the system to uncertainty purely in the initial conditions. For a fixed value of the initial conditions, a standard deterministic cost functional for optimal control is given as

$$J[x(t), u(t)], \tag{1.9}$$

which can be adjusted to include the uncertainty in the initial conditions

$$J_u[x(t, x_0), u(t); x_0].$$

For any given value of the initial condition x_0, a real-valued J_u is generated, however, the uncertainty in the initial condition, which are not decision variables in this case, requires a modification to the cost functional.

A Riemann-Stieltjes integral, an integral of a real function with respect to a

real measure,

$$\int f(x)dg(x), \tag{1.10}$$

in context of the initial condition uncertainty

$$\int_{\Omega} \cdots d\alpha(x_0), \tag{1.11}$$

where Ω is the support of the uncertainty PDF in the initial conditions and $\alpha(x_0)$ is a given joint cumulative distribution function (CDF) of the uncertainty [11, 1]. Combining the Riemann-Stieltjes integral with the uncertain cost functional J_u

$$\int_{\Omega} J_u[x(t, x_0), u(t); x_0]d\alpha(x_0), \tag{1.12}$$

is a functional of a functional [11]. The Riemann-Stieltjes integral of Eq. (1.12) the uncertain cost functional provides the avenue for formulating an optimal control problem to generate the state control pair $(x(t), u(t))$ which minimizes the uncertain cost functional J_u over the full support of the uncertainty in the initial conditions x_0

$$J_{RS}[x(t, x_0), u(t); x_0] = \int_{\Omega} J_u[x(t, x_0), u(t); x_0]d\alpha(x_0). \tag{1.13}$$

Given the uncertain cost functional generated by a standard cost functional,

$$J_u = E(x_0, x_f) + \int_{t_0}^{t_f} F(x(t, x_0), u(t); x_0)dt,$$

the Riemann-Stieltjes cost functional is defined as

$$\begin{aligned} J_{RS} &= \int_{\Omega} E(x_0, x_f) d\alpha(x_0) \\ &+ \int_{\Omega} \left[\int_{t_0}^{t_f} F(x(t, x_0), u(t); x_0) dt \right] d\alpha(x_0) \\ &= \int_{\Omega} \tilde{E}(x_0, x_f) d\alpha(x_0) \end{aligned}$$

Using this cost functional an optimal control problem can be formulated as [11]

$$x(t) \in \mathbb{R}^{n_x}, \quad u(t) \in \mathbb{R}^{n_u}, \quad x_0 \in \Omega$$

$$\begin{cases} \text{Min} & J_{RS}[x(t, x_0), u(t); x_0] = \int_{\Omega} \tilde{E}(x_0, x_f) d\alpha(x_0) \\ \text{S.t.} & \dot{x}(t) = f(x(t, x_0), u(t); x_0) \\ & \int_{\Omega} \psi(x_0, x(t_f)) d\alpha(x_0) \leq 0, \end{cases}$$

where $\psi()$ is a vector function which constrains the state trajectory inputs. The costates $\lambda(t, x_0)$ of this problem formulation are given by

$$-\dot{\lambda} = \partial_x H(\lambda(t, x_0), x(t, x_0), u(t)), \tag{1.14}$$

where the Pontryagin Hamiltonian is given as

$$H(\lambda, x, u) = \lambda^T f(x(t, x_0), u(t); x_0). \tag{1.15}$$

Similarly, the constant endpoint multiplier ν is used in defining the endpoint Lagrangian as

$$\bar{E}(\nu, x_0, x_f) := \tilde{E}(x_0, x_f) + \nu^T \psi(x_0, x_f).$$

To derive the necessary conditions for the Riemann-Stieltjes optimal control

problem it is useful to introduce a semidiscretization approximation of the cost functional J_{RS} and take the limit.

Using the derivative of a CDF is the random variables PDF, the integral of the Riemann-Stieltjes problem can be written as

$$J_{RS}[x(t,x_0),u(t);x_0] = \int_\Omega J_u[x(t,x_0),u(t);x_0]g(x_0)dx_0 \tag{1.16}$$

where $g(x_0)$ is the PDF associated with the initial condition uncertainty. This integral can be approximated by discretizing over the support of the uncertainty

$$J_{RS} = \lim_{n\to\infty}\sum_{i=1}^{n} J_u[x^i(t,x_0^i),u(t);x_0^i]g(x_0^i)\Delta x_0 \tag{1.17}$$

where the notation x_0^i refers to a discrete sample of x_0 in its support and the Δx_0 are generated as a set of non overlapping intervals over Ω

$$\bigcup_{i=1}^{n}\Delta x_0^i = \Omega.$$

In the same fashion, the integral of the endpoint constraint can be discretized

$$\int_\Omega \psi(x_0,x_f)g(x_0)dx_0 = \lim_{n\to\infty}\sum_{i=1}^{n}\psi(x_0^i,x_f)g(x_0^i)\Delta x_0. \tag{1.18}$$

Combining the discretizations of the endpoint cost functional and the endpoint constraint function the endpoint Lagrangian is defined as

$$\int_\Omega \bar{E}(\nu,x_0,x_f,)g(x_0)dx_0 = \lim_{n\to\infty}\sum_{i=1}^{n}\bar{E}(\nu,x_0^i,x_f)g(x_0^i)\Delta x_0. \tag{1.19}$$

These discretizations motivate a analogous discretization of the state dynamics

$$\dot{x} = f(x(t, x_0), u(t)) \tag{1.20}$$

as

$$\begin{aligned} \dot{x}^1 &= f(x^1, u), \\ \dot{x}^2 &= f(x^2, u), \\ &\vdots \qquad (1.21) \\ \dot{x}^n &= f(x^n, u), \qquad (1.22) \end{aligned}$$

where the shorthand notation x^i refers to the state associated with a given sample of the uncertain initial condition $x^i = x(t, x_0^i)$. Additionally, the costates in Eq. (1.14) follow the same discretization over the uncertainty

$$\begin{aligned} -\dot{\lambda}^1 &= \partial_{x_1} H(\lambda^1, x^1, u), \\ -\dot{\lambda}^2 &= \partial_{x_2} H(\lambda^2, x^2, u), \\ &\vdots \qquad (1.23) \\ -\dot{\lambda}^n &= \partial_{x_n} H(\lambda^n, x^n, u), \end{aligned}$$

Following the discretization of the state and costate systems leads to the construction of the integral of the Riemann-Stieltjes Hamiltonian

$$H_{RS} = \sum_{i=1}^{n} (\lambda^i)^T f(x^i, u) g(x_0^i) \Delta x_0 = \int_\Omega \lambda^T f(x(t, x_0), u; x_0) g(x_0) dx_0. \tag{1.24}$$

Combining the discretizations of the Riemann-Stieltjes problem and truncating the sums to a finite value of n, a standard deterministic optimal control problem

can be formulated as [11, 14]

$$x^i \in \mathbb{R}^{n_x}, \quad u(t) \in \mathbb{R}^{n_u}, i = 1, 2, ..., n$$

$$\begin{cases} \text{Min} & J_{RS}[x(t, x_0), u(t); x_0] = \sum_{i=1}^{n} J_u[x^i(t, x_0^i), u(t); x_0^i] g(x_0^i) \Delta x_0 \\ \text{S.t.} & \dot{x}^1 = f(x^1, u), \\ & \dot{x}^2 = f(x^2, u), \\ & \vdots \\ & \dot{x}^n = f(x^n, u), \\ & \sum_{i=1}^{n} \psi(x_0^i, x_f) g(x_0^i) \Delta x_0 \leq 0, \end{cases}$$

which, in the limit of as n increases towards infinity, optimal control $u^*(t)$ generated satisfies the Hamiltonian Minimization Condition

$$\begin{aligned} u^*(t) &= \arg\min_{u(t)} \sum_{i=1}^{n} (\lambda^i)^T f(x^i, u) g(x_0^i) \Delta x_0 \\ &= \arg\min_{u(t)} \int_{\Omega} \lambda^T f(x(t, x_0), u; x_0) g(x_0) dx_0. \end{aligned}$$

Thus, the Riemann-Stieltjes optimal control problem formulation as a discretized standard deterministic optimal control problem generates the Pontryagin necessary conditions required for an optimal control candidate in the limit as the number of samples goes to infinity [11]. The difficulty in generating the solution to this optimal control problem lies in the dimensionality, even in the finite sample version the dimension of the states quickly increases with the number of samples. One avenue of mitigating the curse of dimensionality is to choose a discretization which doesn't require a large number of samples to converge [11, 15, 1, 14] . Along this line is a recently defined unscented optimal control problem formulation.

1.3.1 Unscented Optimal Control

The difficulty of the discretized Riemann-Stieltjes optimal control problem from the previous section derives from the large dimensionality of the state space resulting from the requirement of large numbers of samples to converge to the desired integral values. This curse of dimensionality calls for special attention to be paid when choosing the sampling method as to keep the dimensionality as low as possible. To this end, unscented optimal control [15, 14] is one possible method.

Currently, no assumptions on the form of the cost functional have been made, however, in practice it is likely that the cost function will specifically target the effects of the parameter uncertainty. A useful measure of the effect of the uncertainty on the trajectory endpoints of the system can be formed as a norm squared error [1]

$$J_u[x(t_f, p); p] = \|x(t_f, p) - x_f\|^2$$

where x_f is the target endpoint value. The dynamics of the state variables are given by

$$\dot{x} = f(x(t, p), u(t); p),$$

where $p \in \mathbb{R}^{N_p}$ is a vector of constant parameters with unknown values. Furthermore, the assumption that the unknown parameters p are subject to a given probability density function of $g(p)$ is required. If one takes the nominal value (mean) of the parameter and designs an open loop control $u(t)$ with respect to this particular value of p, there is no guarantee that the trajectory will reach the desired final state. In general, when p is unknown, it may not be possible to

find an open-loop control to steer the system exactly to the final point. The cost functional of the Riemann-Stieltjes problem then becomes

$$J_{RS} = \int_{\Omega} \|x(t_f, p) - x_f\|^2 g(p) dp$$

which describes the distance of the trajectory endpoints for all values of the uncertain parameter to the desired final condition. In general a change of coordinates can be used to ensure that the desired endpoint is the origin which allows us to construct the cost functional as

$$J_{RS} = \int_{\Omega} \|x(t_f, p)\|^2 g(p) dp,$$

without loss of generality. Conceptually, this cost functional motivates the following optimal control formulation:

$$x \in \mathbb{R}^{N_x}, \quad u \in \mathbb{R}^{N_u}, \quad p \in \Omega := supp(p)$$

$$(RS^{\infty}) \begin{cases} \text{Minimize} & J_{RS} = \int_{\Omega} \|x(t_f, u, p)\|^2 g(p) dp. \\ \text{Subject to} & \dot{x}(t, p) = f(x(t, p), u(t), t; p) \\ & (x(t_0, p), t_0) = (x^0, t^0) \end{cases}$$

Problem (RS$^{\infty}$) belongs to a special case of Riemann Stieltjes (RS) optimal control introduced and studied in Ref. [15, 14, 16]. Such optimal control formulations well capture the effect of unknown parameters on the control objective (in our case, regulating the state to the origin). However, solving such Riemann Stieltjes (RS) optimal control problems with nonlinear dynamics and control constraints is nontrivial. Several approaches have been proposed in the literature [11, 9, 10]. Among them, the unscented optimal control method attracts a large

amount of attention [17, 18]. In the following, we briefly review the unscented optimal control as a method for solving Problem (RS$^\infty$). Unscented optimal control combines the unscented transform of Julier et al [19, 20] and standard optimal control theory to formulate a problem that accounts for, and manages, parametric uncertainty by approximating problem (RS^∞) [15, 14, 11]. The controls developed from the unscented problem can improve the robustness of a system under uncertainty using open-loop controls by approximating the effects of the uncertainty using sampled points. This problem formulation leads to a deterministic optimal control problem that can utilize existing computational methods to solve, such as psuedospectral methods [3, 7].

In unscented control, the uncertain parameters p is discretized over the parameter space

$$supp(p) \subset R^{N_p}$$

into a finite number of nodes

$$p_i, \qquad i = 1, 2, ..., n.$$

The choice of the nodes, p_i, depends on the PDF of the parameter, p. Then the integral in the cost functional is approximated as a weighted finite sum as

$$\int_\Omega \|x(t_f, u, p)\|^2 g(p) dp \quad \approx \quad \sum_{i=1}^{n} w_i \|x(t_f, u, p_i)\|^2,$$

where w_i, $i = 1, 2, \ldots, n$, are weights associated with the nodes p_i. The semi-discretization, i.e., discretization in parameter space while keeping time domain continuous, results in the following high-dimensional deterministic optimal control problem

$$x^i \in \mathbb{R}^{N_x}, \quad u \in \mathbb{R}^{N_u}, \quad i = 1, 2, ..., n$$

$$(US^n) \begin{cases} \text{Minimize} & J_{US} = \sum_{i=1}^{n} w_i \|x(t_f, u, p_i)\|^2 \\ \text{Subject to} & \dot{x}^1 = f(x^1, u; p_1) \\ & \vdots \\ & \dot{x}^n = f(x^n, u; p_n) \\ & (x^i(t_0, p_i), t_0) = (x_0, t_0) \\ & u_{lower} \leq u \leq u_{upper} \\ & p_i \in supp(p), \ \forall \ i = 1, 2..., n, \end{cases}$$

where x^i is a shorthand notation for $x(t; p_i)$, the state trajectory driven by the control $u(t)$ with the parameter p fixed at the value p_i. It is obvious that the semi discretized problem, (US^n), is an approximation of the original optimal control Problem (RS$^\infty$). A number of theoretical results have been published to establish the consistent and convergent approximation of the problem (RS^∞) under mild technical assumptions [10, 9, 21].

As the number of uncertain parameters grows, the number of sampling points, p_i, required to adequately characterize the uncertainty can increase quickly. This leads to a large increase in dimensionality of the optimal control problem (US^n) which can become computationally intensive to solve. Thus, it is important to choose an efficient discretization of the parameter space, i.e., p_i, $i = 1, 2, ..., n$. For this purpose, sigma points based on the unscented transformation can be used [11, 15]. Such discretization points are based on the PDF of the parameter, and can achieve high accuracy with a relatively low number of discrete parameter samples. For example, for a single uncertain parameter with Gaussian PDF, only two sigma points are needed, which results in a semi-discretized optimization

problem with only two copies of the dynamics. As the dimension of the parameter, p, or the complexity of the PDF, $g(p)$ increases, the number of sigma points also increase, but typically at a rate much slower than other sampling techniques. Unscented optimal control methods have been successfully applied to solve a variety of optimal control problems with uncertainty. For example, waypoint navigation of a fixed-wing UAV and control of a satellite [17]

1.3.2 Unscented UAV Waypoint Navigation

In order to manage the uncertainty in the parameters of the UAV, an application of unscented optimal control is used. In this section, this method is outlined. More details can be found in [15, 14, 22, 17].

We apply unscented optimal control to UAV waypoint navigation. To illustrate the idea, we consider only one uncertain parameter, C_{x0}, which is known to have a large effect on the turn maneuver of interest.

Aiming to minimize the mean error of the UAV terminal position, we design the following cost functional:

$$J[x(\cdot,\cdot), u(\cdot), t_f] := \int_{-\infty}^{\infty} (\Delta x_f^2 + \Delta y_f^2 + \Delta z_f^2) d\Phi(p),$$

where

$$\begin{aligned} \Delta x_f &= x(t_f; p) - x_f \\ \Delta y_f &= y(t_f; p) - y_f \\ \Delta z_f &= z(t_f; p) - z_f \end{aligned}$$

and (x_f, y_f, z_f) is the designated endpoint. $\Phi(p)$ is the CDF of uncertain parameter $p = C_{x0}$.

Assuming that uncertainty in C_{x0} has a Gaussian distribution $\mathcal{N}(-0.03554, 0.0012^2)$, the corresponding sigma points are given by the shifted Hermite-Gauss quadrature points, $p_1 = -0.0343,\ p_2 = -0.0367$. Thus, the cost functional can be discretized as

$$\begin{aligned} J &= \frac{1}{\sqrt{2\pi\sigma_p^2}} \int_{-\infty}^{\infty} (\Delta x_f^2 + \Delta y_f^2 + \Delta z_f^2) e^{\left(-\frac{(p-\mu_p)^2}{2\sigma_p^2}\right)} dp \\ &\approx \sum_{i=1}^{2} w_i [(x^i(t_f, p_i) - x_f)^2 + (y^i(t_f, p_i) - y_f)^2 \\ &\qquad + (z^i(t_f, p_i) - z_f)^2], \end{aligned}$$

where the mean $\mu_p = -0.03554$ and standard deviation $\sigma_p = 0.0012$. The cost functional only contains terms involving the terminal state. It is also possible to include path constraints in the problem formulation in order to control the dispersion over time [16].

The resulting unscented optimal control problem is summarized in the follow-

ing for the dynamics of the UAV ($3DOF$)

$$x^i := (x^i, y^i, z^i, v^i, \gamma^i, \sigma^i, \alpha^i, \mu^i) \in \mathbb{R}^8, \ i = 1, 2$$

$$u := (u_\alpha, u_\mu) \in \mathbb{R}^2$$

$$p := C_{x0} \sim \mathcal{N}(-0.03554, 0.0012^2)$$

$$(UAV^1) \begin{cases} \text{Minimize} & J[x^1(\cdot), x^2(\cdot), u(\cdot), t_f] \\ \text{Subject to} & \dot{x}^1 = f(x^1, u, p_1) \\ & \dot{x}^2 = f(x^2, u, p_2) \\ & (x^1(t_0, p_1), t_0) = (x_0^1, t^0) \\ & (x^2(t_0, p_2), t_0) = (x_0^2, t^0) \\ & u_\alpha \in [-0.05, 0.05] \\ & u_\mu \in [-0.05, 0.05]. \end{cases}$$

The new discretized problem has the form of a standard deterministic optimal control problem, which can be solved using standard tools. For the simulations presented in this paper we used the MATLAB® toolkit DIDO© [1] which implements the spectral method [23, 24] for solving optimal control problems.

Figure 1.3 shows the angle of attack and the bank angle for both the unscented problem, UAV^1, and standard optimal control problem, SOP. There is a clear difference in the angle of attack and bank angle for the unscented problem. This variation allows the endpoint error to be significantly reduced over the standard solution with only a small increase in flight time. The Monte Carlo trajectory tube, obtained by propagating the unscented control for various values of the uncertain parameters, is plotted in Figure 1.4.

Comparing Figure 1.4 to Figure 1.2 there are clear differences in the shapes of

[1] http://www.mathworks.com/products/connections/product_detail/prod- uct_61633.html and http://www.ElissarGlobal.com

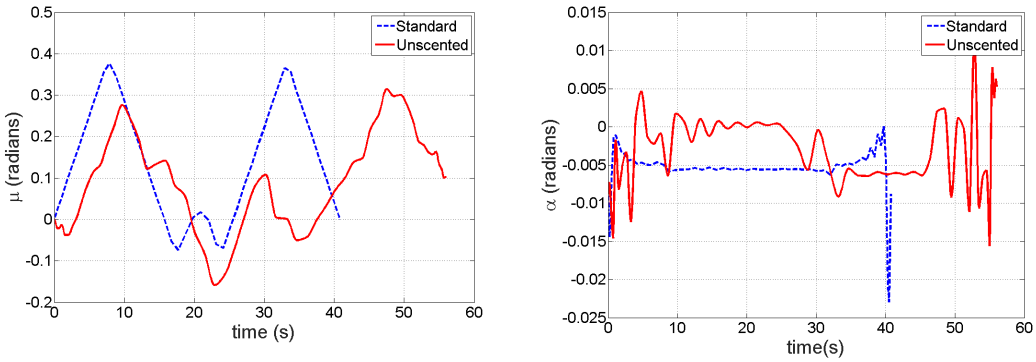

Figure 1.3: Bank angle and angle of attack for the standard and unscented control solutions.

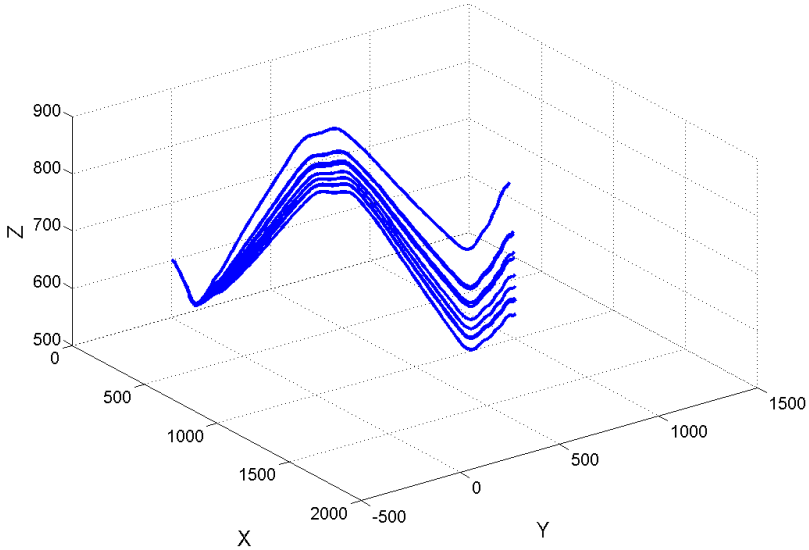

Figure 1.4: Monte Carlo trajectory tube for the unscented optimal control.

trajectories for the span of the uncertain parameters. The unscented controls are observed to induce altitude changes in an effort to minimize the terminal error.

Table 1.2 shows the data for the unscented problem, which can be compared to the data from Table 1.1. The error and standard deviation in the x state has increased slightly in the unscented problem as a trade-off for a significant decrease in the error and standard deviation of the other two position states. This is

desirable because the end result is that the mean miss distance for the unscented

Target Parameter	Error Mean	Standard Deviation (m)
x	1.3%	11.4
y	.52%	5.0
z	12.5%	55.3
Miss Distance	76.1 m	54.2

Table 1.2: Component-wise relative errors for the euclidean miss distance from the desired endpoint for the unscented optimal control with constant thrust

problem is much smaller (76.1 m), which is nearly a 30% improvement over the original problem (see Table 1.1). A 35% decrease in the standard deviation of the terminal errors is also obtained. Thus, unscented control can be applied in order to increase the accuracy of open-loop waypoint navigation. Moreover, this result is achieved using only two copies of the dynamics associated with the two sigma points used to describe the parameter uncertainty in C_{x0}.

Figure 1.5 shows, graphically, the effectiveness of the new unscented problem formulation. Using the Monte Carlo simulations done for Tables 1.1 and 1.2 we plot the mean and covariance for both the unscented and the standard optimal control problem for each combination of the position error states. The covariance ellipses for the unscented problem show an obvious reduction in the dispersion of the terminal errors.

1.4 Dissertation Outline and Contributions

In this dissertation optimal control of nonlinear systems with parameter uncertainty is the main focus. These problems are prolific in the field of engineering and many examples, such as the fixed wing UAV, can be found across many areas of engineering.

In the second chapter a problem for minimizing the effects of parameter un-

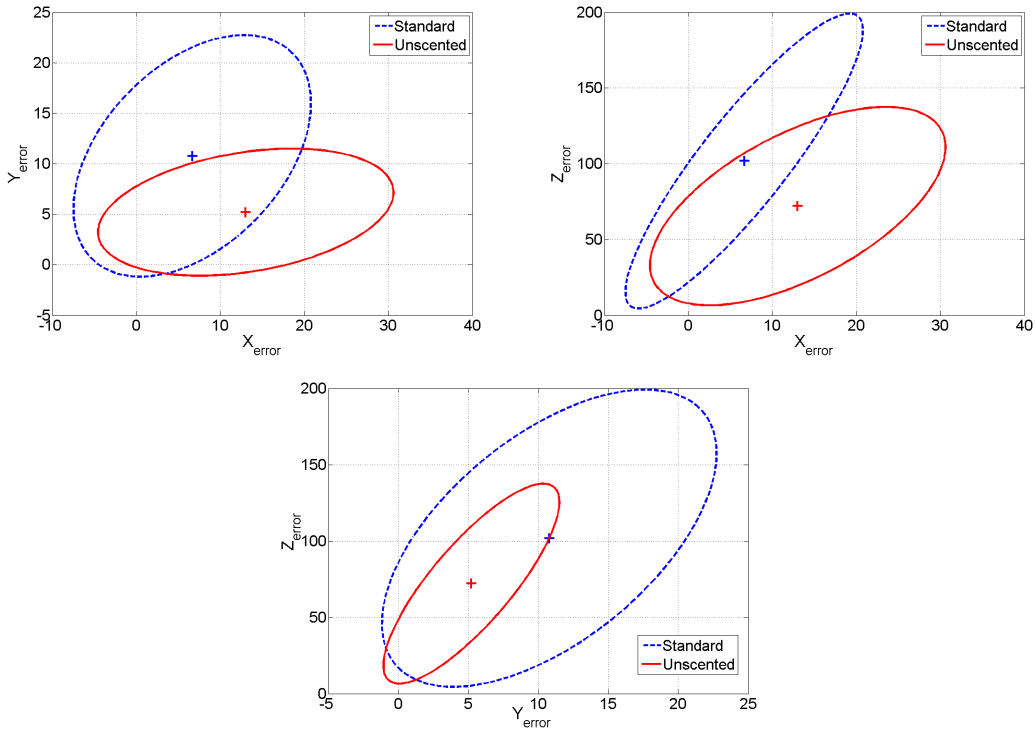

Figure 1.5: Comparison of covariance for each position state combination from Monte Carlo simulations of unscented and standard control

certainty which are approximated by terms derived from a Taylor expansion of deviations from a nominal parameter value is outlined. This method is related to the more classical approach of using a linearization provided by the Taylor series of any potential uncertainty given as the sensitivity functions, but is extended to show that considering higher order Taylor series can be important. An example Zermelo type problem is then used to motivate the connection between this approximation of the uncertainty with the unscented and Riemann-Steiltjes control covered in this introduction. These methods can be viewed as having the same goals and are fundamentally connected. This connection provides a new lens with which to view the unscented optimal control. A simple spring mass system, which is linear in its dynamics, is used to illustrate that purely considering the first order sensitivity functions given by a linear approximation of parameter uncertainty is

potentially insufficient and it is advantageous to include the higher order terms of the expansion into the control problem. Alternatively, the unscented optimal control problem can be used which does not require the perturbation dynamics to be derived yet still manages high order effects of the uncertainty.

In the third chapter a two degree of freedom type optimal control is considered which includes an open-loop control for designing a nominally optimal control while a time-varying set of feedback gains are used to manage the effects of the parameter uncertainty. A problem using the linearization of the uncertainty is defined for generating the feedback gains which is connected to neighboring optimal control. Along the same lines of avoiding linearization through sampling, a new type of optimal control problem formulation is outlined for the full nonlinear error states that is discretized according to unscented optimal control. The advantage of avoiding the linearization is again demonstrated using the simple linear spring-mass system.

In the fourth chapter an application of the methods from the previous chapters is used on a nonlinear double gimbal model. These mechanical systems are pervasive in many engineering fields and specifically a motivation involving repositionable antenna on board satellites is presented. The various methods for generating controls for the model parameter uncertainty is showcased and provides clear advantages in controlling the gimbal when the stiffness parameter is uncertain.

In the fifth chapter a multi link robotic arm with flexible effects which is a physical example of the type of system explored in the previous chapter is investigated. This system includes twenty model parameters, some of which are likely to be subject to measurement uncertainty.

Ultimately, this dissertation explores the unscented optimal control problem for managing parameter uncertainty in the open-loop by considering its connection

to an optimal control problem which is formulated by using a Taylor expansion of the nonlinear dynamics about an assumed nominal parameter values. The unscented problem can be effective at controlling high order effects of the parameter uncertainty without the need to derive the Taylor expansions. Furthermore, a new framework for generating feedback controls for achieving a pre-designed maneuver based on the unscented optimal control problem is outlined. The open-loop and feedback unscented controls are demonstrated effective for managing the effects of parameter uncertainty on achieving desired endpoint conditions for mechanical systems given by a flexible double gimbal used for repositionable antennas and for multi link robotic arms.

Chapter 2

Relationship Between Sensitivity Function Based and Unscented Optimal Control

The Riemann-Stieltjes optimal control problem and its unscented approximation are relatively new methods for mitigating parameter uncertainty for nonlinear systems. The advantage of sampling the distribution of the uncertain parameters instead of a more classical linearization of the dynamics around a nominal value makes the unscented optimal control a powerful tool. In contrast, linearizing the effects of deviations in the parameter value can be advantageous in cases where the linear neighborhood captures the majority of the effects of uncertainty. This leads to an optimal control problem that uses the sensitivity functions for general nonlinear dynamical systems. A comparison of the two types of optimal control of the uncertain systems on a nonlinear control problem motivates the connection between the optimal control problem formulations. In this chapter, we review an optimal control problem formulation based on the concept of sensitiv-

ity function. The method produces state trajectories which are less sensitive to parameter deviations. This sensitivity based problem is then used to investigate the Riemann-Stieltjes optimal control problem described in the Introduction.

2.1 Sensitivity Function-Based Optimal Control

When considering a nonlinear model with uncertain parameters $p \in \mathbb{R}^{N_p}$ with state trajectories $x(t, u; p) \in \mathbb{R}^{N_x}$, a first order Taylor Expansion around the trajectory given for a nominal value p_0 [25] is:

$$x(t, u; p_0 + \Delta p) = x(t, u; p_0) + \left.\frac{\partial x(t, u; p)}{\partial p}\right|_{x^{\text{Nom}}, u^{\text{Nom}}, p_0} (\Delta p) + \mathcal{O}(||\Delta p||^2), \quad (2.1)$$

where p_0 is a vector of nominal parameter values and Δp is a small perturbation from the nominal value. Conventionally the first order partial derivatives are defined as the sensitivity functions $s(t) \in \mathbb{R}^{N_x \times N_p}$ and are given by [25]

$$s(t) = \left.\frac{\partial x(t)}{\partial p}\right|_{x^{\text{Nom}}, u^{\text{Nom}}, p_0} = \begin{bmatrix} \frac{\partial x_1}{\partial p_1} & \dots & \frac{\partial x_1}{\partial p_n} \\ \frac{\partial x_2}{\partial p_1} & \dots & \frac{\partial x_2}{\partial p_n} \\ \vdots & \vdots & \vdots \\ \frac{\partial x_n}{\partial p_1} & \dots & \frac{\partial x_n}{\partial p_n} \end{bmatrix}.$$

Truncating Eq. (2.1) to first order leaves

$$x(t, u; p_0 + \Delta p) \approx x(t, u; p_0) + s(t)(\Delta p). \quad (2.2)$$

The partial derivative of the state trajectory with respect to the model parameters gives a local measure of the effect of small variations to the parameter values.

For a general nonlinear dynamical system

$$\dot{x}(t, u; p) = f(x, t, u; p), \qquad x(0) = x_0, \tag{2.3}$$

the dynamics for the trajectories given by the approximation in Eq. (2.2) becomes

$$\dot{x}(t, u; p_0 + \Delta p) \approx f(x, t, u; p_0) + \dot{s}(t)(\Delta p), \tag{2.4}$$

which provides a set of differential equations for the sensitivity function dynamics $\dot{s}(t)$ with initial conditions $s(0) = 0$.

The dynamics of sensitivity functions is given in [25]

$$\dot{s}(t) = A(t, p_0)s(t) + B(t, p_0), \qquad s(t_0) = 0, \tag{2.5}$$

where

$$A(t, p_0) = \left.\frac{\partial f}{\partial x}\right|_{x^{\text{Nom}}, u^{\text{Nom}}, p_0} \quad \text{and} \quad B(t, p_0) = \left.\frac{\partial f}{\partial p}\right|_{x^{\text{Nom}}, u^{\text{Nom}}, p_0},$$

$A(t, p_0)$ is the Jacobian of the state dynamics evaluated along the nominal trajectory $x(t, p_0)$ at the nominal parameter value p_0 and $B(t, p_0)$ is a matrix of the partial derivatives of the explicit dependence of the dynamics on the model parameters.

The sensitivity functions can be managed using feedback control, for example a linear time-varying feedback control of the form

$$u(t, x) = K(t)x + g(t),$$

as will shown in a following section. In many real world applications, it can become important to consider the case when states cannot be accurately measured in

real time which is required for feedback control. Recently there has been interest in methods for generating open loop controls which, without the use of feedback, can successfully operate when the model parameters are uncertain. To this end the information provided by the sensitivity functions can be applied in an optimal control setting for open loop control. This type of sensitivity based optimal control problem has been used to develop open loop controls that manage parametric uncertainty in path planning problems [26, 27] and endpoint sensitivity optimization [28].

For a generic nonlinear plant of the form given by Eq. (2.3) the associated sensitivity functions can be appended to the state dynamics of an optimal control problem. This allows for explicit consideration of the sensitivity trajectories in the cost functional and/or endpoint constraints generating an optimal control problem formulation for open loop control which produces insensitive trajectories and which can be solved using existing computational optimal control methods.

In practice, the choice of cost functional can take many forms involving the endpoints of the sensitivity functions in addition to the full sensitivity state trajectories as

$$J[x(\cdot), s(\cdot), u(\cdot), t_f] = E(s(t_f), s(t_0), x(t_f), x(t_0)) + \int_{t_0}^{t_f} F(s(t), x(t), u(t))dt.$$

In many applications involving regulating a system to a desired final target the goal of the design can be to reduce the uncertain parameter's effect on the endpoint of the system states. This translates to minimizing the sensitivity function values at the final time, or written as a cost functional

$$J[x(\cdot), s(\cdot)] = \|s(t_f)\|^2$$

involving a suitable norm, such as the Frobenius norm, of the sensitivity function matrix, $s(t)$, at the final time. This measure provides a convenient and smooth measure of the local disturbance to the endpoints caused by deviations in the parameter from the assumed nominal.

This endpoint sensitivity measure can be used to formulate and optimal control problem for driving the nominal system trajectory to a desired endpoint, for example

$$(SENS)\begin{cases} \text{Minimize} & J[x(\cdot), s(\cdot), u(\cdot)] = ||s(t_f)||^2 \\ \text{Subject to} & \dot{x} = f(x, u; p_0) \\ & \dot{s} = A(t, p_0)\Big|_{x^{\text{Nom}}, u^{\text{Nom}}, p_0} s(t) + B(t, p_0)\Big|_{x^{\text{Nom}}, u^{\text{Nom}}, p_0} \\ & (x(t_0, u; p_0), t_0) = (x_0, t_0) \\ & (s(t_0), t_0) = (0, t_0) \\ & x(t_f, u; p_0) = x_f \\ & u_{lower} \leq u \leq u_{upper}, \end{cases}$$

where the sensitivity functions have been appended to the dynamic states and a final condition $x(t_f, p_0)$ has been imposed on the nominal state trajectory. By straightforward modification, this optimal control problem can also include constraints on the sensitivity and state trajectories through the addition of path constraints. In addition, the cost functional can be changed to include penalties for states and control effort with no modification to the dynamic constraints.

Applying Pontryagin's minimization principle to the sensitivity function based problem $(SENS)$ generates the necessary conditions for optimality. The Hamiltonian is given by

$$H(\lambda_x, \lambda_s, x, s, u) = \lambda_x^T \dot{x} + \lambda_s^T [\dot{s}]$$

where $[\dot{s}]$ is a vector created by stacking the column vectors of $s(t)$. The costates are subject to dynamics

$$\begin{aligned} -\dot{\lambda}_x &= \partial_x H(\lambda_x, \lambda_s, x, s, u) \\ -\dot{\lambda}_s &= \partial_s H(\lambda_x, \lambda_s, x, s, u). \end{aligned} \tag{2.6}$$

The Hamiltonian Minimization Condition can then be constructed as

$$u^*(t) \quad = \quad \arg\min_{u(t)} \left[\lambda_x^T \dot{x} + \lambda_s^T [\dot{s}] \right].$$

There is no inherent restriction to the first order sensitivity measure, in fact, extending the expansion in Eq. (2.1) to include an arbitrary number of higher order terms allows for a larger neighborhood of the uncertainty to be considered. The cost functional involving the norm of the sensitivity endpoints can likewise be expanded conceptually as

$$J[x(\cdot), s_1(\cdot), s_2(\cdot), ..., s_n(\cdot)] = \|s_1(t_f)\|^2 + \|s_2(t_f)\|^2 + \cdots + \|s_n(t_f)\|^2$$

where $s_i(t_f)$ refers to the i-th order sensitivity function. The dynamics of the higher order terms can be derived by continuing to evaluate the higher-order derivatives with respect to the parameter values, for example

$$s_2(t) = \left.\frac{\partial^2 x}{\partial p^2}\right|_{x^{\text{Nom}}, u^{\text{Nom}}, p_0}, \qquad \dot{s}_2(t) = \frac{\partial^2 \dot{x}}{\partial p^2}.$$

Furthermore, it is possible to incorporate the higher order sensitivity terms into the optimal control problem $(SENS)$ by adjusting the cost functional as

above and appending the sensitivity dynamics $\dot{s}_i(t)$ for $i = 1, 2, ..., n$ as

$$
(SENS^n) \begin{cases}
\text{Min} & J[x(\cdot), s_1(\cdot), s_2(\cdot), ..., s_n(\cdot)] = \sum_{k=1}^{n} \|s_k(t_f)\|^2 \\
\text{S.t.} & \dot{x}_0 = f(x_0, u; p_0) \\
& \dot{s_1}(t) = \phi_1(x_0, s_1, u, t) \\
& \dot{s_2}(t) = \phi_2(x_0, s_1, s_2, u, t) \\
& \vdots \\
& \dot{s_n}(t) = \phi_n(x_0, s_1, ..., s_n, u, t) \\
& (x(t_0, u; p_0), t_0) = (x_0, t_0) \\
& (s_i(t_0), t_0) = (0, t_0), \ i = 1, 2, ..., n \\
& x(t_f, u; p_0) = x_f \\
& u_{lower} \leq u \leq u_{upper}.
\end{cases}
$$

In the limit as the number of sensitivity orders increases $n \to \infty$, the Taylor expansion of the parameter sensitivity function converges to the global effect parameter deviations under suitable assumptions on the dynamics. This sensitivity function based problem formulation is useful, however, it is limited by the requirement that each sensitivity function must be derived prior to constructing the optimal control problem. This limitation usually results in only the first order sensitivity functions being implemented.

In the next section, we will demonstrate the effectiveness of the sensitivity function based optimal control for an example nonlinear system. This motivates the comparison between senstivity based optimal control and unscented optimal control.

2.2 Motivating Example: The Zermelo Problem

Zermelo type problems with uncertainty have been used to conceptualize some space operations and have recently been the subject of unscented optimal control application[1]. These types of problems characterize a steering problem of a ship in uncertain wind conditions where the wind strength is an uncertain parameter. Dynamics of an example Zermelo problem with position states (x, y) and controls $(u_1(t), u_2(t))$ could be given by [1, 14]

$$\dot{x}(t) = py^3 + u_1(t)$$
$$\dot{y}(t) = u_2(t),$$

where the parameter p has a nominal value, $p_0 = 10$, and the uncertainty is assumed to be Gaussian centered around the nominal value with standard deviation $\sigma = 2$. The control objective is to steer the ship from an initial condition $(x_0, y_0) = (2.25, 1)$ to the final target at the origin. The controls are bound by the relation $u_1^2 + u_2^2 = 1$ and there exist no other path constraints on the dynamic states.

To apply the unscented optimal control approach for the Zermelo problem, a cost functional of the form of Eq. (2.11) for two weighted sample points is used,

which results in the following discretized problem with the form of US^n:

$$x^i \in \mathbb{R}^2, \quad u \in \mathbb{R}^2, \quad i = 1, 2$$

$$(Z^n) \begin{cases} \text{Minimize} & J = \sum_{i=1}^{2} w_i (x_i^2(t_f) + y_i^2(t_f)) \\ \text{Subject to} & \dot{x}_1 = p_1 y_1^3 + u_1(t) \\ & \dot{y}_1 = u_2(t) \\ & \dot{x}_2 = p_2 y_2^3 + u_1(t) \\ & \dot{y}_2 = u_2(t) \\ & (x_1(t_0), y_1(t_0)) = (2.25, 1) \\ & (x_2(t_0), y_2(t_0)) = (2.25, 1) \\ & t_f = 3.41 \\ & u_1^2(t) + u_2^2(t) = 1, \end{cases}$$

with sample points $(p_1, p_2) = (8, 12)$ and weights $w_{1,2} = .5$. The sample points and weights are chosen according to the Unscented Transform's sigma points. This two sample approximation of the Riemann-Stieltjes optimal control problem is a low dimension optimal control problem for minimization of the second moment of the endpoints of the sigma point states.

The sensitivity-based optimal control problem, involves minimizing the norm of the sensitivity functions at the final time and enforces zero endpoint error for the trajectory. This problem formulation is given by

$$x \in \mathbb{R}^2, \quad s \in \mathbb{R}^2, \quad u \in \mathbb{R}^2$$

$$(ZS) \begin{cases} \text{Minimize} & J = s_1^2(t_f) + s_2^2(t_f) \\ \text{Subject to} & \dot{x} = p_0 y^3 + u_1(t) \\ & \dot{y} = u_2(t) \\ & \dot{s}_1 = y^3 \\ & \dot{s_2} = 0 \\ & (x(t_0), y(t_0), s_1(t_0), s_2(t_0)) = (2.25, 1, 0, 0) \\ & (x(t_f), y(t_f)) = (0, 0) \\ & t_f = 3.41 \\ & u_1^2(t) + u_2^2(t) = 1. \end{cases}$$

The first order sensitivity dynamics indicated that the y state are insensitive to the parameter.

Problem (Z^n) and (ZS) can be solved using standard computational optimal control techniques, in this case psuedospectral optimal control, to generate control signals that minimize their respective cost functionals and, in effect, minimize the variance of the endpoint trajectories for parameter values $p \in supp(p)$.

Figure 2.1 shows controls signals for the two optimal control problems. These control profiles seem to be nearly identical, indicating that the two different methods aim to achieve the same goal. Propagating the control signals through the dynamics of the Zermelo problem generates state trajectories for specific sampled values of the uncertain parameter p. By propagating the controls for many values of the parameter using a Monte Carlo simulation, the effectiveness of the control signals becomes clear. Figure 2.2 shows these Monte Carlo simulations for Gaussian and uniform distributions of the parameter p.

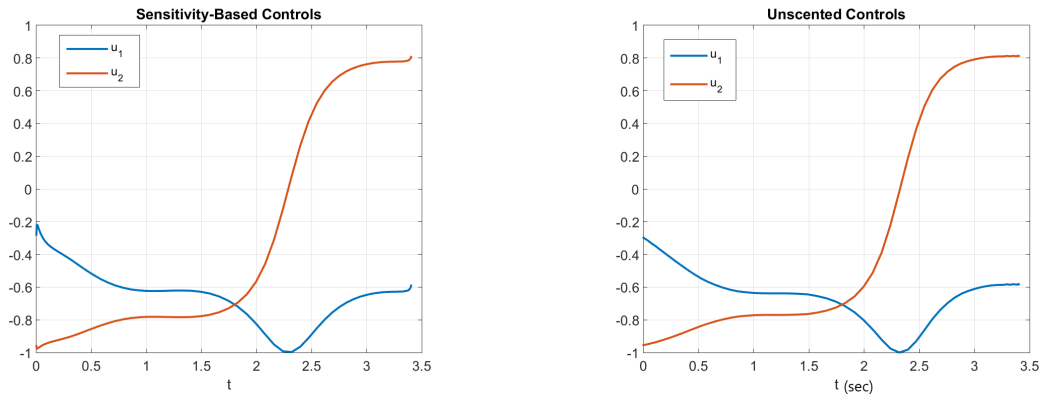

Figure 2.1: Control profiles for the sensitivity based and unscented optimal control problems after [1].

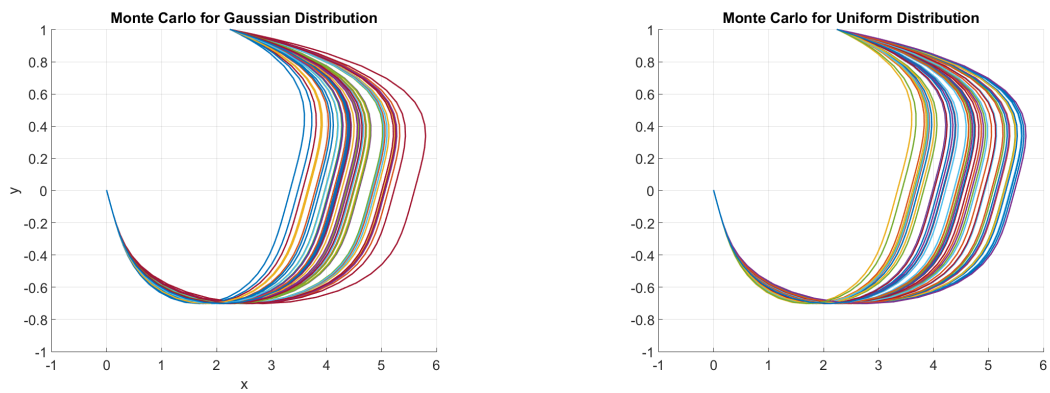

Figure 2.2: Propagated state trajectories using the unscented controls for sampled values of the uncertain parameter for the Gaussian and uniform distributions after [1].

When choosing the sigma points and weights according to some mild conditions developed below for the unscented discretization, the specific distribution of the uncertain parameter is considered. Interestingly, it is clear from Figure 2.2 that, for this problem, the distribution seems not to impact the effectiveness of the controls. Figure 2.2 demonstrates that, independent of the two distributions sampled for the Monte Carlo simulation, the variance of the endpoints is nearly zero for all sampled parameter values.

The mean endpoint errors of the states for the two optimal control problems

Error	Unscented	Sens($s(t_f)$)
x (m)	0.0005	0.0001
y (m)	0.0007	0.0005

Table 2.1: Mean endpoint error of each state for the optimal control formulations.

are given in Table 2.1 for a Monte Carlo simulation comprising 1000 sampled parameter values. It is clear from the Table and Figure 2.2 that the endpoint error from the origin for both sets of control signals is small and that there is little variance of the endpoints. In fact, the controls nearly eliminate all variance in the endpoints. This property indicates a complete insensitivity to the parameter at the trajectory endpoints which can be seen by plotting the sensitivity functions of the x state for both optimal control problems in Figure 2.3.

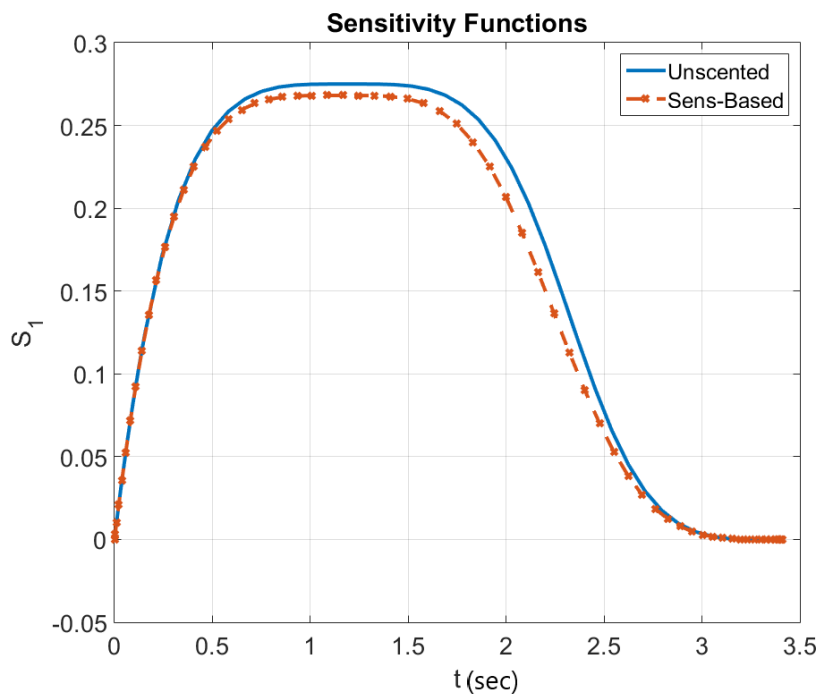

Figure 2.3: Senstivity functions of position state x for both the unscented and sensitivity based trajectories.

The sensitivity function for both the propagated unscented and senstivity optimal controls decrease to zero at the final time. In the case of the Zermelo problem,

the second and higher order sensitivity functions are zero so controlling the first order endpoint sensitivity to zero is sufficient for reducing higher orders to zero.

Conceptually, the open loop problem for sensitivity reduction and the unscented optimal control both aim to reduce the effects of parameter uncertainty on a desired endpoint by designing open-loop trajectories that are more robust. The sensitivity based problem uses a linearization around the nominal trajectory while the unscented control uses information about the distribution of the uncertainty, which can theoretically provide a more global approximation. The sensitivity functions can be used to help understand the machinations of the unscented optimal control and in this case of the Zermelo problem can help identify how connected the nearly identical controls are.

The approximation

$$x(t, u; p) \approx x(t, u; p_0) + s(t)(p - p_0) \tag{2.7}$$

can be explored to establish a connection between the uncertain optimal control problem (RS^∞) and the semi-discretized optimal control problem (US^n). Based on the Riemann-Stieltjes cost functional

$$J_{RS} = \int_\Omega \|x(t_f, u; p)\|^2 g(p) dp,$$

the cost function of the problem (RS^∞) can be approximated as

$$J_{RS} \approx \int_\Omega \|x(t_f, u; p_0) + s(t_f)(p - p_0)\|^2 g(p) dp. \tag{2.8}$$

Expanding the norm in the integral gives

$$\begin{aligned} J_{RS} \approx & \int_{\Omega} \|x(t_f, u; p_0)\|^2 g(p)dp + \int_{\Omega} \|s(t_f)(p - p_0)\|^2 g(p)dp \\ & +2 \int_{\Omega} x^T(t_f, u; p_0) s(t_f)(p - p_0) g(p)dp. \end{aligned}$$

Choosing the nominal parameter values to be the expectation of the associated distribution

$$p_0 = \int_{\Omega} pg(p)dp$$

allows the cost function to be simplified to

$$J_{RS} \approx \|x(t_f, u; p_0)\|^2 + \int_{\Omega} \|s(t_f)(p - p_0)\|^2 g(p)dp. \tag{2.9}$$

Denoting the column vectors of $s(t)$ as

$$[s^1(t), s^2(t), \cdots, s^{N_p}(t)]$$

and the vector

$$p = [p^1, p^2, \cdots, p^{N_p}]^T,$$

along with the assumption that all parameters are independently distributed, the second term in Eq. (2.9) can be written as the sum

$$\sum_{i=1}^{N_p} \|s^i(t_f)\|^2 \int_{\Omega} (p^i - p_0^i)^2 g_i(p^i)dp^i = \sum_{i=1}^{N_p} \|s^i(t_f)\|^2 (\sigma^i)^2,$$

where $(\sigma^i)^2$ is the variance of the $i-th$ parameter p^i. Thus

$$J_{RS} \approx \|x(t_f, u; p_0)\|^2 + \sum_{i=1}^{N_p} ||s^i(t_f)||^2 (\sigma^i)^2. \tag{2.10}$$

The cost functional approximation of J_{RS} is comprised of the sum of the norm of the endpoints of the nominal trajectory and the norm of the first order endpoint sensitivities scaled by the parameter variances.

Now consider the cost function in the unscented optimal control problem (US^n) with only two sample points, (p_1, p_2) and weights, (w_1, w_2)

$$J_{US} = w_1(\|x(t_f, u; p_1)\|^2) + w_2(\|x(t_f, u; p_2)\|^2). \tag{2.11}$$

Using the approximation from Eq. (2.7) the unscented cost function can be expanded to

$$\begin{aligned} J_{US} \approx (w_1 + w_2)\|x(t_f, u; p_0)\|^2 \\ + \left[w_1\|s(t_f)(p_1 - p_0)\|^2 + w_2\|s(t_f)(p_2 - p_0)\|^2\right] \\ +2x^T(t_f, u; p_0)s(t_f)\left[w_1(p_1 - p_0) + w_2(p_2 - p_0)\right]. \end{aligned} \tag{2.12}$$

The approximation provides a basis for choosing the weights (w_1, w_2) and the sample points (p_1, p_2), which is explained in the following.

Consider a particular choice of weights $w_1 = w_2 = \frac{1}{2}$, and sampling points

$$\begin{aligned} p_1 &= p_0 + \sigma \\ p_2 &= p_0 - \sigma, \end{aligned}$$

where $\sigma \in R^{N_p}$ is the standard deviation of the uncertain parameter p. These

represent the sigma points of the unscented transform. Eq. (2.12) is simplified to

$$J_{US} \approx ||x(t_f, u; p_0)||^2 + \sum_{i=1}^{N_p} \|s^i(t_f)\|^2 (\sigma^i)^2. \tag{2.13}$$

Now by comparing Eq.(2.10) with Eq.(2.13), it can be seen that the cost functionals in problem (RS^∞) and problem (US^n) can both be approximated by the addition of the final variance with nominal parameter value p_0 and the variance of the parameters scaled by the sensitivity function. Therefore, when the higher order effect $\mathcal{O}\left(\|p - p_0\|^2\right)$ on the state trajectory $x(t, u, p)$ can be neglected, unscented optimal control can serve as a good approximation of the uncertain optimal control problem (RS^∞) even with just two samples, for the case of a single uncertain parameter.

From above derivations, it is clear that in the case where the approximation given by Eq. (2.7) is exact,

$$x(t, u; p) = x(t, u; p_0) + s(t)(p - p_0),$$

the unscented cost functional in (US^n) is exactly equivalent to the one in (RS^∞). In other words, the discretization in the parameter space introduces no approximation errors,

$$\int_\Omega \|x(t_f, u; p)\|^2 g(p) dp \quad = \quad \sum_{i=1}^{2} w_i \|x(t_f, u; p_i)\|^2.$$

For this case, optimal solution to problem (RS^∞) can be obtained by solving the unscented optimal control problem with the cost function in Eq. (2.11) with two weighted samples, for any number of uncertain parameters (as long as they are independently distributed) and no information about their distributions other

than the mean and variance.

When the higher order sensitivity functions are neglected the unscented problem can be reduced to a first order sensitivity based optimal control problem. However, these higher order effects can still influence the robustness of the trajectories. Unscented optimal control provides a formulation which does not depend on the derivation of higher order sensitivity functions yet can still be effective for managing the higher order effects.

Additionally, the equivalency between the cost functionals of the two optimal control problems can be further explored to account for higher order sensitivity functions.

2.3 Riemann-Stieltjes and Sensitivity Functions

The Zermelo problem example demonstrated that there is a fundamental connection between the unscented approximation of the Riemann-Stieltjes cost functional and the cost functional used in minimizing the sensitivity function approximation of deviations in parameter values. This concept can be expanded to include dynamics which have higher order sensitivity effects according to

$$x(t, p_0 + \Delta p) = x(t, p_0) + \left.\frac{\partial x(t,p)}{\partial p}\right|_{x^{\mathrm{Nom}}, u^{\mathrm{Nom}}, p_0} (\Delta p) + \mathcal{O}(\Delta p^2), \tag{2.14}$$

for a single uncertain parameter. Including a larger number of uncertain parameters preserves the following results, assuming the uncertainty distributions of the parameters are independently distributed, and can be done using the Taylor series in its multi-index notation form.

Assuming that the nominal parameter value p_0 is the mean of the parameters PDF, the uncertainty in the model parameter has now been shifted to the origin,

denoting this shifted uncertain parameter Δp with support $\Delta\Omega$.

A Riemann-Stieltjes cost functional for minimizing the spread of the trajectory endpoints around the nominal endpoint can be formulated as

$$J_{RS} = \int_{\Delta\Omega} \|x(t_f, u; p_0 + \Delta p)\|^2 g(\Delta p) d\Delta p.$$

The norm squared of the error term can be expanded as a sum over the squared endpoint errors as

$$\|x(t_f, u; p_0 + \Delta p)\|^2 = \sum_{j=1}^{n_x} \left[x^j(t_f, u; p_0 + \Delta p)\right]^2,$$

where $x^j()$ is shorthand for the $j-th$ element of the state vector.

Along the lines of the sensitivity expansion, for a single uncertain parameter, the perturbed state can be expanded

$$x^j(t_f, u; p) \approx x^j(t_f, u; p_0) + \sum_{m=1}^{n_s} \left(\frac{s_m^j(t_f)}{m!} (\Delta p)^m \right),$$

where $s_m^j(t_f)$ is shorthand for the $m-th$ derivative of the $j-th$ state

$$s_m^j(t_f) = \frac{\partial^m x^j(t_f, u; p)}{\partial p^m}, \text{ and } x_0(t_f, u; p_0) \text{ for } m = 0$$

evaluated at the nominal parameter value and $x(t_f, u; p_0)$. In the limit as the number of sensitivity functions, n_s, goes to infinity the expansion becomes exact in the case when the Taylor expansion converges. Combining the expansions with the original integral, the Riemann-Stieltjes integral takes the form

$$J_{RS} \approx \sum_{j=1}^{n_x} \left[\int_{\Delta\Omega} \left(\sum_{m=0}^{n_s} \left(\frac{s_m^j(t_f)}{m!} (\Delta p)^m \right) \right)^2 g(\Delta p) d\Delta p \right],$$

where the order of the norm and integral have been interchanged. The sum of the squared terms can be expanded according to

$$\left(\sum_{j=1}^{N} y_j\right)^2 = \sum_{j=1}^{N} y_j^2 + \sum_{j=1}^{N} \sum_{\substack{k=1 \\ k\neq j}}^{N} y_j y_k.$$

Using this expansion the sum of the squared sensitivity functions becomes

$$\begin{aligned} J_{RS} \approx & \sum_{j=1}^{n_x} \left[\int_{\Delta\Omega} \sum_{m=0}^{n_s} \left(\frac{s_m^j}{m!}\right)^2 (\Delta p)^{2m} g(\Delta p) d\Delta p\right] \\ + & \sum_{j=1}^{n_x} \left[\int_{\Delta\Omega} \left(\sum_{m=0}^{n_s} \sum_{\substack{k=0 \\ k\neq m}}^{n_s} \left(\frac{s_m^j s_k^j}{m!k!} (\Delta p)^{m+k}\right)\right) g(\Delta p) d\Delta p\right], \end{aligned}$$

where the (t_f) has been dropped. The integral can be brought into the sums over the sensitivity functions because the sensitivity functions themselves have no dependence on the parameter. These integrals will then represent the associated central moment of the distribution of the parameter uncertainty now given by Δp. The central moment of the shifted parameter

$$\mathbb{E}[\Delta p^m] = \int_{\Delta\Omega} \Delta p^m g(\Delta p) d\Delta p, \tag{2.15}$$

is known for a given distribution $g(\Delta p)$. Substituting the associated moments for the integral notation in the expansion of J_{RS}

$$J_{RS} \approx \sum_{m=0}^{n_s} \left[\frac{\|s_m\|^2}{(m!)^2} \mathbb{E}[\Delta p^{2m}]\right] + \sum_{m=0}^{n_s} \sum_{\substack{k=0 \\ k\neq m}}^{n_s} \left[\sum_{j=1}^{n_x} \left(s_m^j s_k^j\right) \frac{\mathbb{E}[\Delta p^{m+k}]}{m!k!}\right],$$

or, using inner product notation,

$$J_{RS} \approx \sum_{m=0}^{n_s} \left[\frac{\|s_m\|^2}{(m!)^2} \mathbb{E}[\Delta p^{2m}]\right] + \sum_{m=0}^{n_s} \sum_{\substack{k=0 \\ k\neq m}}^{n_s} \left[\langle s_m, s_k\rangle \frac{\mathbb{E}[\Delta p^{m+k}]}{m!k!}\right], \tag{2.16}$$

where $\langle s_m, s_k \rangle = s_m^T s_k$ is the inner product between the $m-th$ and $k-th$ order sensitivity function vectors. This formula gives the Riemann-Stieltjes integral as a function of the sensitivity functions where the integrals can be simplified to moments of the distribution of uncertainty. In the case where the higher order sensitivity functions $m \geq 2$ vanish, the expansion collapses

$$\int_{\Delta\Omega} \|x(t_f, u; p_0 + \Delta p)\|^2 g(\Delta p) d\Delta p, = \|x_0(tf, u; p_0)\|^2 + \|s_1(t_f)\|^2 \mathbb{E}[\Delta p^2],$$

as was determined in the context of the Zermelo problem. This sensitivity function-based cost functional can be used to compare with the unscented discretization of the same integral.

The objective of unscented optimal control is to approximate the Riemann-Stieltjes cost functional using the least number of samples, therefore, there is expected to be some error associated to the number of samples used. By comparing the sensitivity function expansion with the unscented approximation, an insight into the source of potential approximation errors can be developed.

In unscented optimal control the cost function

$$J_{RS} = \int \|x(t_f, u; p_0 + \Delta p)\|^2 g(\Delta p) d\Delta p$$

is approximated by a finite set of weighted samples

$$J_{RS} \approx J_{US} = \sum_{i=1}^{N} w_i \|x(t_f, u; p_0 + \Delta p_i)\|^2,$$

where w_i is the weight associated with the sampled parameter deviation Δp_i and N is the number of samples. The sampled states can be expanded in terms of the

nominal states and the sensitivity functions

$$J_{US} \approx \sum_{i=1}^{N} w_i \left[\sum_{j=1}^{n_x} \left(\sum_{m=0}^{n_s} \frac{s_m^j(t_f)}{m!} (\Delta p_i)^m \right)^2 \right] = \sum_{j=1}^{n_x} \left[\sum_{i=1}^{N} w_i \left(\sum_{m=0}^{n_s} \frac{s_m^j(t_f)}{m!} (\Delta p_i)^m \right)^2 \right],$$

which is exact when n_s goes to infinity. Modifying the unscented sum using the inner product and expanding the sum squared term gives

$$J_{US} \approx \sum_{m=0}^{n_s} \left[\frac{\|s_m\|^2}{(m!)^2} \left(\sum_{i=1}^{N} w_i \Delta p_i^{2m} \right) \right] + \sum_{m=0}^{n_s} \sum_{\substack{k=0 \\ k \neq m}}^{n_s} \left[\frac{\langle s_m, s_k \rangle}{m!k!} \left(\sum_{i=1}^{N} w_i \Delta p_i^{m+k} \right) \right], \quad (2.17)$$

where the inner sums

$$\sum_{i=1}^{N} w_i \Delta p_i^{2m}$$

are approximations of the $2m$-th moment of the uncertain parameter. Comparing this approximation with the sensitivity function expansion

$$\begin{aligned} J_{RS} \approx \quad & \sum_{m=0}^{n_s} \left[\tfrac{\|s_m\|^2}{(m!)^2} \int \Delta p^{2m} g(\Delta p) d\Delta p \right] \\ & + \sum_{m=0}^{n_s} \sum_{\substack{k=0 \\ k \neq m}}^{n_s} \left[\tfrac{\langle s_m, s_k \rangle}{m!k!} \int \Delta p^{m+k} g(\Delta p) d\Delta p \right], \end{aligned} \quad (2.18)$$

it is clear that if Eq (2.17) = Eq (2.18) then the cost functional of scaled sensitivity functions and the sampled sum cost functional are equivalent and both capture the Riemann-Stieltjes integral. This is true when the integrals over the parameter, which multiply the sensitivity states, are achieved with the choice of discretization nodes and weights $(w_i, \Delta p_i)$

$$\begin{aligned} \int \Delta p^{2m} g(\Delta p) d\Delta p &\approx \sum_{i=1}^{N} w_i \Delta p_i^{2m} \\ \int \Delta p^{m+k} g(\Delta p) d\Delta p &\approx \sum_{i=1}^{N} w_i \Delta p_i^{m+k}. \end{aligned}$$

Specifically, the weights and sums need to be chosen to capture the moments of the initial assumed uncertainty distribution. For example, when the distribution is Gaussian, the best choice of weights and nodes are optimally given by a Gauss Hermite quadrature rule.

In the case of a Gaussian, the choice of the number of samples is determined by the degree of sensitivity function which contributes to the expansion in Eq. (2.18), i.e. if one wishes to be accurate up to the mth degree sensitivity, one must capture up to the $2m^{th}$ moment of Δp. According to Gauss Hermite Quadrature, in order to approximate the integral

$$\int \Delta p^{2m} g(\Delta p) d\Delta p \;\; \approx \;\; \sum_{i=1}^{N} w_i \Delta p_i^{2m}$$

a choice of

$$N = m + 1$$

minimum, introduces no error to the integral approximation. The error in the unscented discretization of the cost functional then is pushed to the $m+1$ term of the expansion. Ideally the sensitivity expansion converges quickly, otherwise, one can choose enough samples so that the error is pushed into high enough orders to be small, if possible. This indicates that using information about the sensitivity functions, a general rule, for Gaussian distributed parameter uncertainty, is that one should choose the number of sample points to be the order of sensitivity function of interest plus one.

Motivated by the connection between the sensitivity function and unscented approximations of the Riemann-Stieltjes cost functional seen in the Zermelo problem, the equivalence for general sensitivity function expansions holds given the convergence of the expansion. By computing the expansions, a guideline for choos-

ing the number of samples to include in the unscented expansion can be determined given information about the sensitivity functions of the system. Previously, choosing the number of samples is generally done in context of the uncertainty's distribution, which is included in the approximations of the central moments, however, the relationship between samples and sensitivity functions can be used to determine more precisely how many discrete samples a priori.

2.4 Illustrative Example: The Mass Spring

The relationships outlined in the previous section can be observed numerically similar to observing the connections in the Zermelo problem. To this end, a simple mass spring system is used for illustration. The effects of uncertainty in the spring properties can be quantified, which can then be compared with the solutions of an unscented optimal control, a first order sensitivity control, and second order sensitivity control. It will be shown that, even for the relatively simple linear system, controlling the first order sensitivity functions leaves a lot of improvement on the table compared with the unscented and second order sensitivity controls. By including the second order sensitivity terms, the unscented and second order sensitivity controls match very closely in value and performance.

A state space model of the mass spring system with position x and velocity v is given by:

$$\begin{aligned} \dot{x}(t) &= v \\ \dot{v}(t) &= -\frac{1}{m}(kx + cv - u(t)), \end{aligned}$$

where k is the spring constant, m is the mass and c is the linear damping coefficient. In many systems the damping is small and can be neglected, ($c = 0$). For

the nominal model with $(k, m) = (1, 1)$, an optimal control formulation focusing on minimum effort when controlling the system from an initial state $(x, v) = (1, 0)$ to a final state at the origin can be formulated as:

$$x \in \mathbb{R}^2, \quad u \in \mathbb{R}^1$$

$$(S) \begin{cases} \text{Minimize} & J = \int_{t_0}^{t_f} u^2(t)dt \\ \text{Subject to} & \dot{x} = v \\ & \dot{v} = -\frac{1}{m}(kx - u(t)) \\ & (x(t_0), v(t_0)) = (1, 0) \\ & (x(t_f), v(t_f)) = (0, 0) \\ & t_f = 10. \end{cases}$$

This problem does not consider uncertainty and can therefore be solved for the control signal which drives the system to the origin. Figure 2.4 shows the control signal solution to problem (S) and the state trajectories associated with the control.

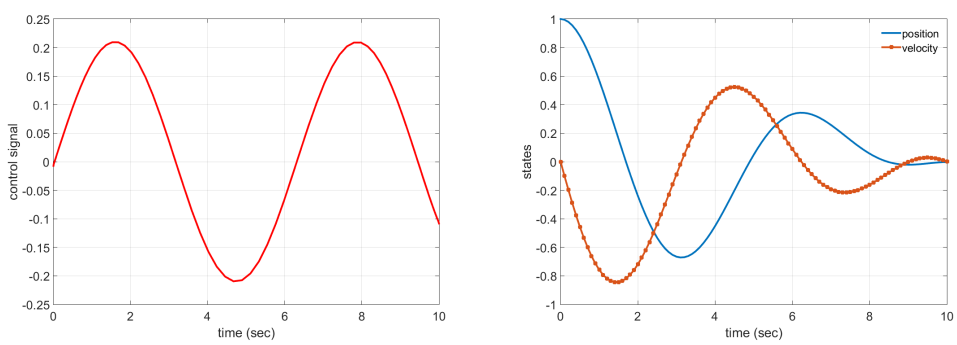

Figure 2.4: Control profile and propagated state trajectories for the nominal control problem.

Considering uncertainty lies in the spring constant k, it is possible compute the first and second order sensitivity functions for this nominal case to illustrate that

the nominal control provides trajectories that are highly sensitive to the uncertain k. These sensitivity functions are shown in Figure 2.5 which indicates that first order effects provide an incomplete picture of the uncertainty.

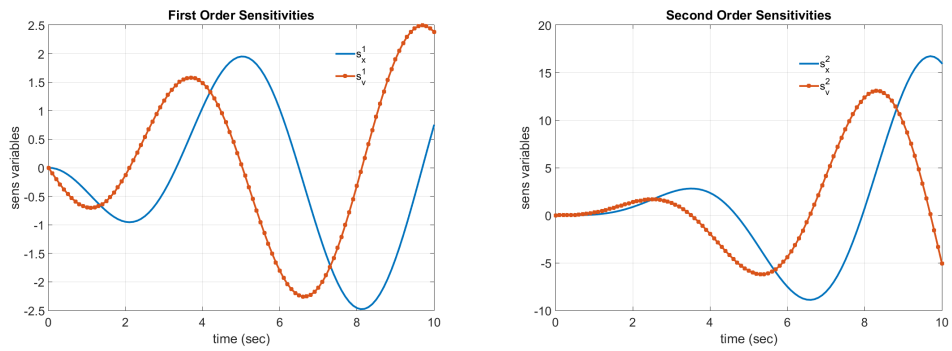

Figure 2.5: First and Second order sensitivity functions for the nominal model.

In order to assess the effects of the parameter sensitivities at the final time, the distance of the endpoint to the origin, a common metric for flexible systems, which gives a measure of residual energy can be defined as:

$$E(t_f) = \sqrt{x(t_f)^2 + v(t_f)^2} \tag{2.19}$$

This metric can be used to determine the effects of the uncertain parameter using a Monte Carlo simulation. Using 1000 samples from $k \in [.8, 1.2]$ for a uniform distribution, the robustness of the nominal controls can be seen in Figure 2.6.

From Figure 2.6 it is clear that the robustness of the designed open loop controls to the uncertain parameter k is poor and that the residual energy increases as the distance from the nominal parameter k_0 increases.

For the mass spring system with no damping, an optimal control problem in the form of problem $(SENS)$ can be formulated to reduce the endpoint sensitivity of the mass' trajectory at the origin while including a penalty on the control effort.

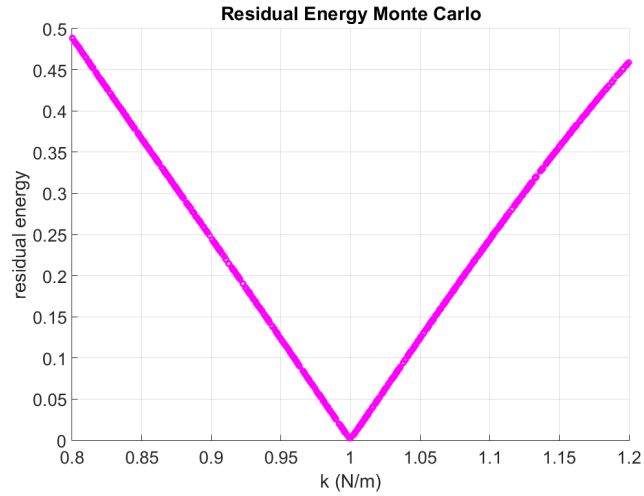

Figure 2.6: Residual energy for random parameter samples in $k \in [.8, 1.2]$.

$$x \in \mathbb{R}^2, \quad s \in \mathbb{R}^2, \quad u \in \mathbb{R}^1$$

$$(SS^1) \begin{cases} \text{Minimize} & J = \int_{t_0}^{t_f} u^2(t)dt + s_x^2(t_f) + s_v^2(t_f) \\ \text{Subject to} & \dot{x} = v \\ & \dot{v} = -\frac{1}{m}(kx - u(t)) \\ & \dot{s}_x = s_v \\ & \dot{s}_v = -\frac{1}{m}(x - ks_x) \\ & (x(t_0), v(t_0), s_x(t_0), s_v(t_0)) = (1, 0, 0, 0) \\ & (x(t_f), v(t_f)) = (0, 0) \\ & t_f = 10, \end{cases}$$

where the first order sensitivity function has been appended to the state dynamics and the cost function now includes the norm of the endpoint sensitives as in problem $(SENS)$. This optimal control problem aims to minimize the first order sensitivity effects on the nominal case and can be solved computationally. The control profile is shown in Figure 2.7.

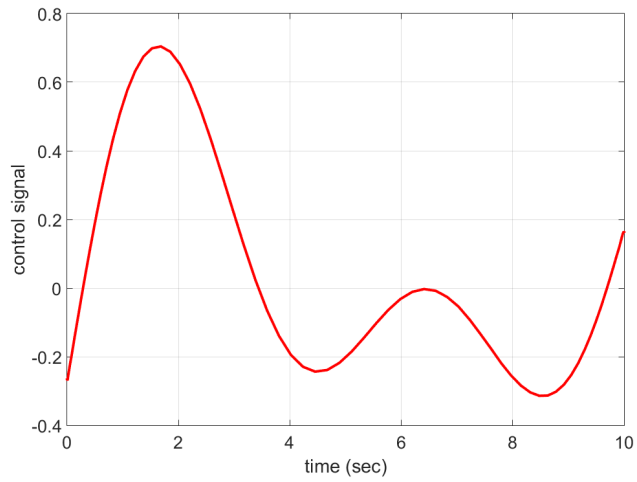

Figure 2.7: Control profile for the first order sensitivity control problem.

By computing the first and second order sensitivity functions, seen in Figure 2.8, it is clear that the optimal control problem (SS^1) is effective at reducing the first order sensitivity at the trajectory endpoint to zero. In addition, by minimizing the first order endpoint sensitivity, the second order endpoint sensitivity also appears to have been reduced.

The improvement to the robustness of the control signal is demonstrated using the same residual energy metric as before in Figure 2.9. By controlling the first order endpoint sensitivity the control signal provides trajectories that are clearly more robust than the nominal control. However, Figure 2.8 shows the second order endpoint sensitivity still has an effect on the robustness of the control.

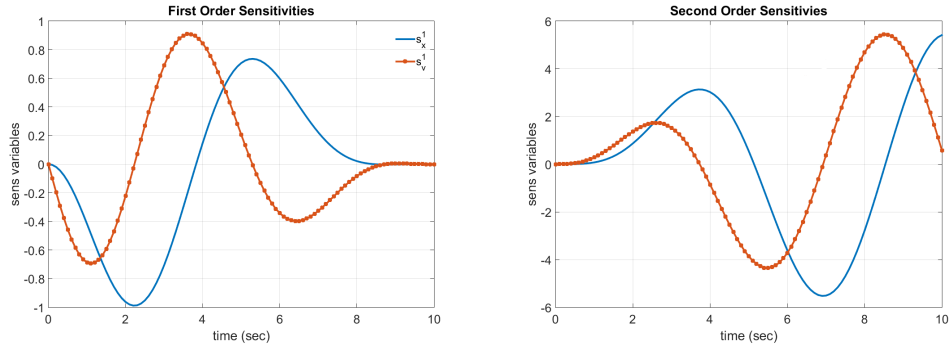

Figure 2.8: First and second order sensitivity functions for the first order sensitivity control problem.

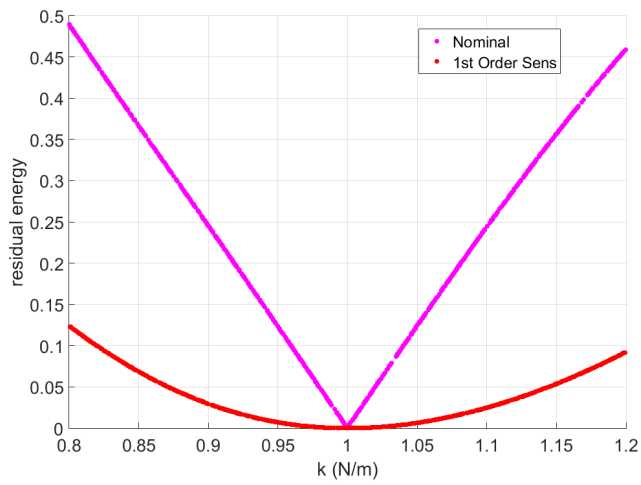

Figure 2.9: Residual energy for the nominal and sensitivity control problems.

In order to compare the effectiveness of the robust controls, an unscented

optimal control problem can be formulated for the linear spring mass example as:

$$x^i \in \mathbb{R}^2, \quad u \in \mathbb{R}^1, \quad i = 1, 2, 3$$

$$(S^n) \begin{cases} \text{Minimize} & J = \int_{t_0}^{t_f} u^2(t)dt + \sum_{i=1}^{3} w_i(x_i^2(t_f) + v_i^2(t_f)) \\ \text{Subject to} & \dot{x}_1 = v_1 \\ & \dot{v}_1 = -\frac{1}{m}(k_1 x_1 + c v_1 - u(t)) \\ & \dot{x}_2 = v_2 \\ & \dot{v}_2 = -\frac{1}{m}(k_2 x_2 + c v_2 - u(t)) \\ & \dot{x}_3 = v_3 \\ & \dot{v}_3 = -\frac{1}{m}(k_3 x_3 + c v_3 - u(t)) \\ & (x_i(t_0), v_i(t_0)) = (0, 0) \\ & t_f = 10. \end{cases}$$

This formulation is an unscented discretization for three sample points using the spherical simplex sigma points [29]

$$w = [0.25, 0.375, 0.375], \qquad k = [1, 0.8845, 1.1155].$$

The sigma points and weights are chosen for a nominal value $k_0 = 1$ and the uniform distribution. Figure 2.10 shows the control profile for the unscented optimal control problem. Computing the sensitivity functions for the trajectories obtained from the unscented control problem shown in Figure 2.11, it is clear that the endpoint sensitivities are no longer zero for the first order, however, the second order endpoint sensitivity has been greatly reduced even compared to the solution of the minimum endpoint sensitivity formulation.

Once again, computing the residual energy for the uniform distribution of k, the robustness of the optimal control problem is shown in Figure 2.12. The un-

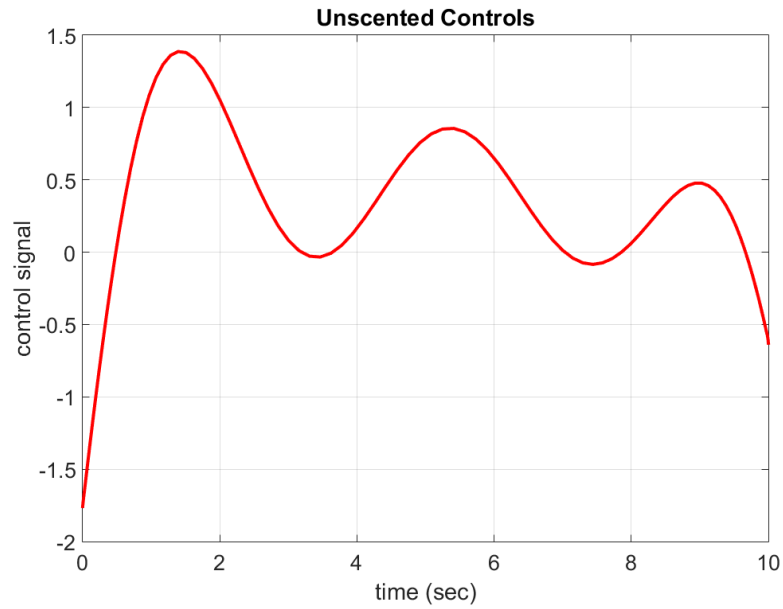

Figure 2.10: Control profile for the unscented control problem.

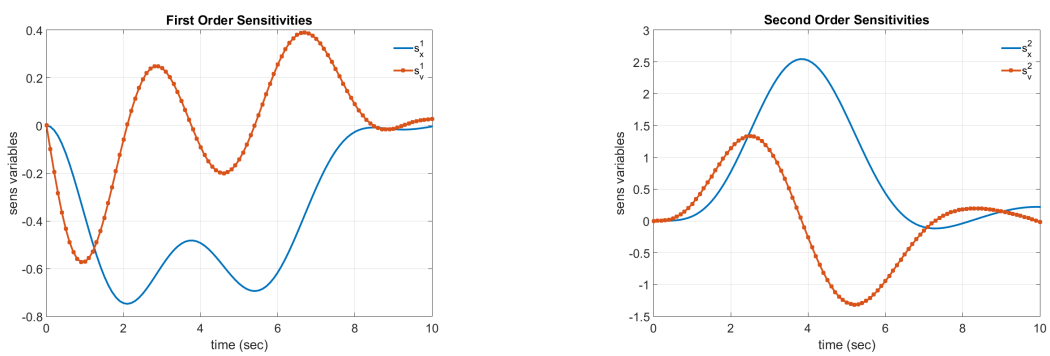

Figure 2.11: Sensitivity functions for the unscented control problem.

scented optimal control problem effectively influences the higher order sensitivities without the need to explicitly include information about the sensitivity functions. In cases where the dynamics are nonlinear and sufficiently complicated, or the parameters appear in the dynamics in a complicated way, the unscented optimal control problem provides a straightforward way to manage the higher order sensitivities.

To demonstrate the effectiveness of unscented optimal control on the higher

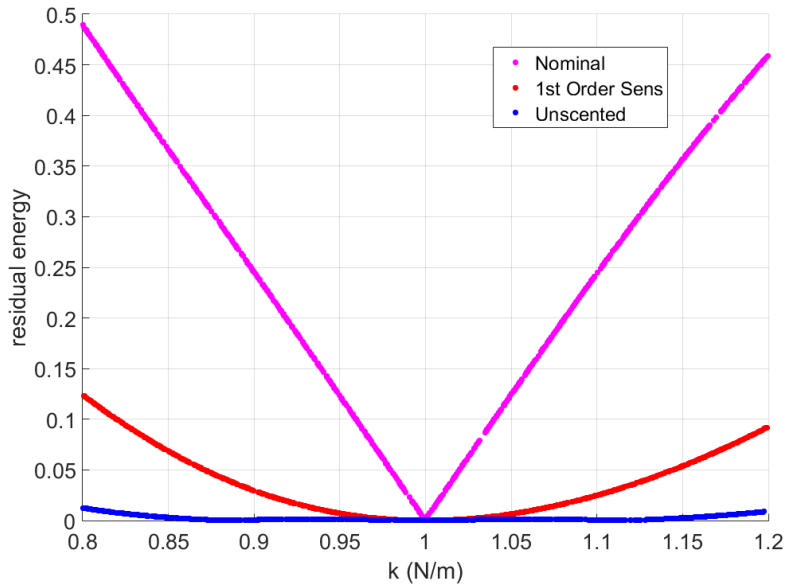

Figure 2.12: Residual energy for the nominal, sensitivity and unscented control problems.

order sensitivity terms an optimal control problem which explicitly includes the first and second order sensitivity functions can be formulated as:

$$x \in \mathbb{R}^2, \quad s \in \mathbb{R}^2, \quad s^2 \in \mathbb{R}^2, \quad u \in \mathbb{R}^1$$

$$(SS^2) \begin{cases} \text{Minimize} & J = \int_{t_0}^{t_f} u^2(t)dt + s_x^2(t_f)^2 + s_v^2(t_f)^2 \\ \text{Subject to} & \dot{x} = v \\ & \dot{v} = -\frac{1}{m}(kx - u(t)) \\ & \dot{s}_x = s_v \\ & \dot{s}_v = -\frac{1}{m}(x - ks_x) \\ & \dot{s^2}_x = s_v^2 \\ & \dot{s^2}_v = -\frac{1}{m}(2s_x - ks_x^2) \\ & (x(t_0), v(t_0), s_x(t_0), s_v(t_0)s_x^2(t_0), s_v^2(t_0)) = (1, 0, 0, 0, 0, 0) \\ & (x(t_f), v(t_f), s_x(t_f), s_v(t_f)) = (0, 0, 0, 0) \\ & t_f = 10, \end{cases}$$

where the first order endpoint sensitivity has been included as an endpoint constraint and the norm of the second order endpoint sensitivities have been included in the cost functional. Solving this problem gives the control profile in Figure 2.13.

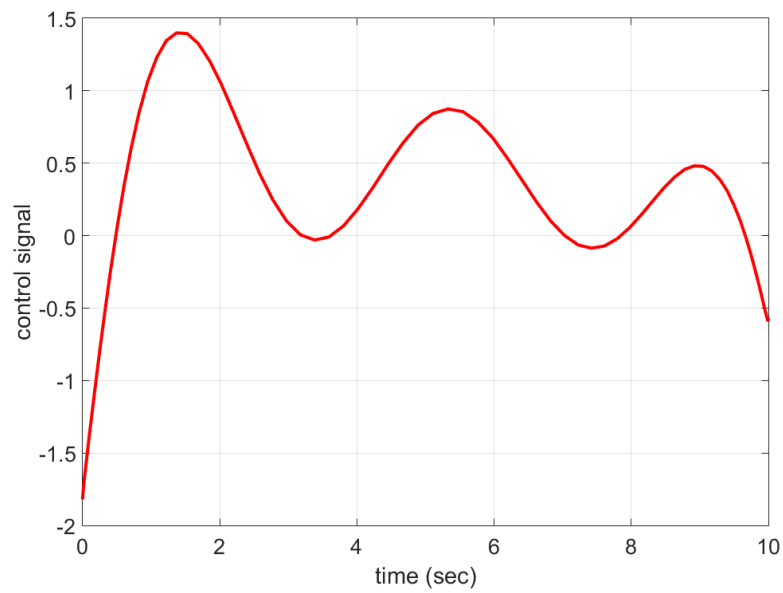

Figure 2.13: Control profile for the second order sensitivity control problem.

Figure 2.14 shows the sensitivity functions for the controls found by solving problem (SS^2). Both the first and second order sensitivity functions have been successfully reduced to zero.

Computing the residual energy for problem (SS^2) shown in Figure 2.15, the robustness is clearly improved when compared to problem (SS^1). However, the unscented control still appears to be marginally more robust. This indicates that controlling the first and second order endpoint sensitivity is not completely sufficient and that the unscented effectively manages even higher order sensitivities.

The relationship between a Riemann-Stieltjes optimal control problem and

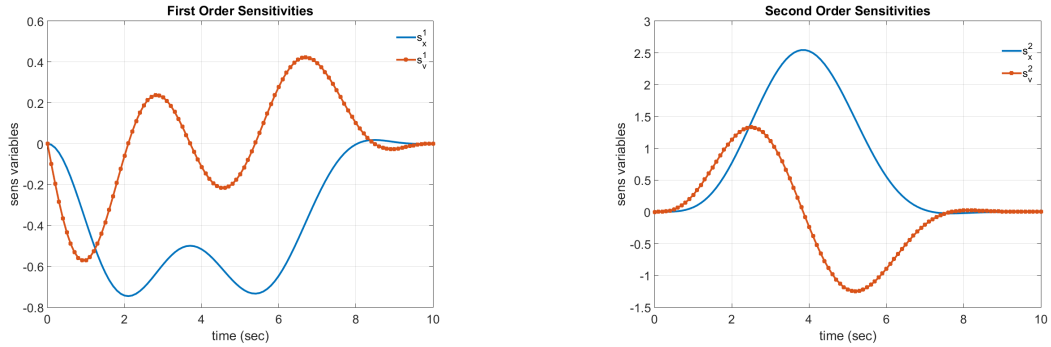

Figure 2.14: Sensitivity functions for the second order sensitivity control problem.

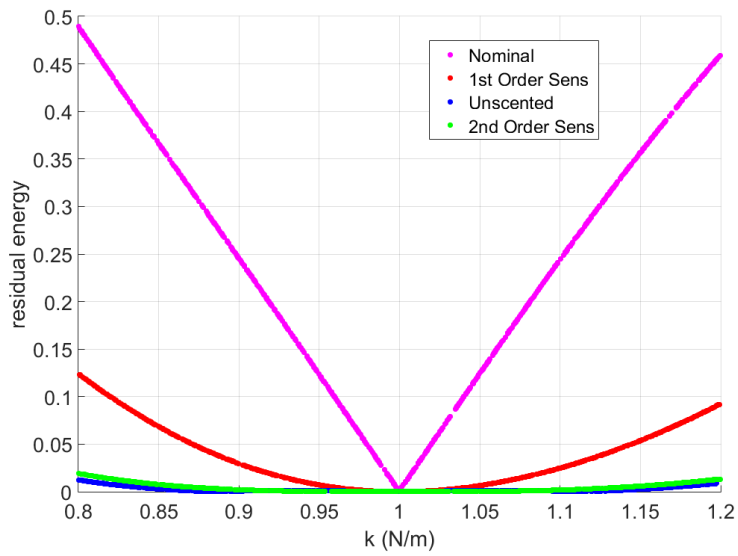

Figure 2.15: Residual energy for nominal, first and second order sensitivity and unscented control problems.

the sensitivity function based optimal control problem is clear in the equivalence of their respective cost functionals. By scaling the sensitivity functions by the moments of the uncertain, a cost functional which matches the integral defining the second moment of the endpoint errors of the Riemann-Stieltjes problem is obtained. Furthermore, the information provided by the sensitivity functions can be used to help determine the sufficient number of sample points required to capture a necessary order of sensitivity. The linear spring mass example demonstrates that

simply considering the first order sensitivity functions can be insufficient for true uncertainty mitigation and that the unscented optimal control problem is able to effect higher order sensitivity functions without the need to derive the sensitivity functions.

While the cost function equivalence between a sensitivity-based, Riemann-Stieltjes, and its unscented approximation, was outlined in the previous section, there is still the question about whether the solution to one is a solution to the other. For this linear spring example it appears that the second order sensitivity problem provides a very similar solution to the three point unscented problem. By observing the Hamiltonian Minimization Condition for both problem formulations the concept of equivalent solutions can be defined.

Given the Riemann-Stieltjes optimal control problem with linear spring mass dynamics for the endpoint error and uncertain stiffness parameter

$$x \in \mathbb{R}^{N_x}, \quad u \in \mathbb{R}^{N_u}, \quad k \in \Omega := supp(k)$$

$$(LSRS) \begin{cases} \text{Minimize} & J_{RS} = \int_\Omega \|x(t_f, u; k)\|^2 g(k) dk. \\ \text{Subject to} & \dot{x}(t, u; k) = A(k)x + Bu \\ & (x(t_0, u; k), t_0) = (x^0, t^0), \end{cases}$$

where the matrices

$$A = \begin{bmatrix} 0 & 1 \\ -\frac{k}{m} & 0 \end{bmatrix}, \qquad B = \begin{bmatrix} 0 \\ -\frac{1}{m} \end{bmatrix}, \tag{2.20}$$

and the solution, according to the Hamiltonian Minimization Condition, can be

stated symbolically as[11]

$$u^*(t) = \arg\min_u \int_\Omega H_{RS}(\lambda(t;p), x(t,u;k), u(t))g(k)dk$$

where, for $\lambda \in \mathbb{R}^{N_x}$,

$$\int_\Omega H_{RS}(\lambda(t;k), x(t,u;k), u(t))g(k)dk = \int_\Omega \lambda^T[A(k)x + Bu]dk.$$

Similar to the expansion used for the cost functionals, the sensitivity functions can be used to expand the integral

$$\int_\Omega \lambda^T[A(k)x + Bu]g(k)dk = \int_\Omega \lambda^T \left(\dot{x}(t,u;k_0) + \sum_{m=1}^{n_s} \left(\frac{\dot{s}_m(t)}{m!}(\Delta k)^m \right) \right) g(k)dk$$

and distributing the PDF functions $g(k)$ followed by splitting the integral over the sensitivity function terms gives

$$\begin{aligned}
&\int_\Omega \lambda^T[A(k)x + Bu]g(k)dk = \\
&\quad \int_\Omega \lambda^T \dot{x}(t,u;k_0)g(p) + \sum_{m=1}^{n_s} \left(\frac{\lambda^T \dot{s}_m(t)}{m!}(\Delta k)^m \right) g(k)dk. \\
&\quad = \left[\int_\Omega \lambda^T g(k)dk \right] \dot{x}(t,u;k_0) + \sum_{m=1}^{n_s} \left(\left[\int_\Omega (\Delta k)^m \lambda^T g(k)dk \right] \frac{\dot{s}_m(t)}{m!} \right).
\end{aligned}$$

The integrated Riemann-Stieltjes Hamiltonian can be viewed as the sensitivity function expansion terms with time-varying multipliers defined by

$$\int_\Omega \frac{(\Delta k)^i}{i!} \lambda^T g(k)dk, \quad i = 1, 2..., n_s \tag{2.21}$$

The optimal control solution of the sensitivity function based problem can be

symbolically written as

$$u^*(t) = \arg\min_u \left[\tilde{\lambda}_0^T \dot{x}(t, u; k_0) + \sum_{m=1}^{n_s} \left(\tilde{\lambda}_m^T \dot{s}_m(t) \right) \right],$$

which has the same structure as the solution of the Riemann-Stieltjes control. In fact, if

$$\tilde{\lambda}_m \approx \int_\Omega \frac{(\Delta k)^m}{m!} \lambda g(k) dk \quad m = 0, 1, 2... \tag{2.22}$$

which describes the costates associated with the $m-th$ order sensitivity function and the integrated and scaled costates of the Riemann-Stieltjes problem, the solution provided by solving the first is equivalent to the second. The unscented approximation to the Riemann-Stieltjes problem discretizes the integrals in Eq. (2.21), which provides an avenue for investigating the costates of a deterministic unscented problem and a sensitivity based problem.

The costates of the unscented problem are derived via the unscented Hamiltonian

$$H_{unsc} = \sum_{i=1}^{N} \lambda_i^T \dot{x}_i(x, t, u; k),$$

which, when combined with Eq. (2.22), gives the relationship between the unscented costates and the sensitivity function based costates

$$\tilde{\lambda}_m \approx \sum_{i=1}^{N} \frac{\Delta k_i^m}{m!} \lambda_i \quad m = 0, 1, 2... \tag{2.23}$$

For the linear spring system, which shows nearly identical solutions for the second order sensitivity and the three point unscented optimal control, the costates of the sensitivity function approximation via Eq. (2.23) can be plotted and com-

pared with the costates of the second order sensitivity problem. Figure 2.16 shows the costates of the two controls.

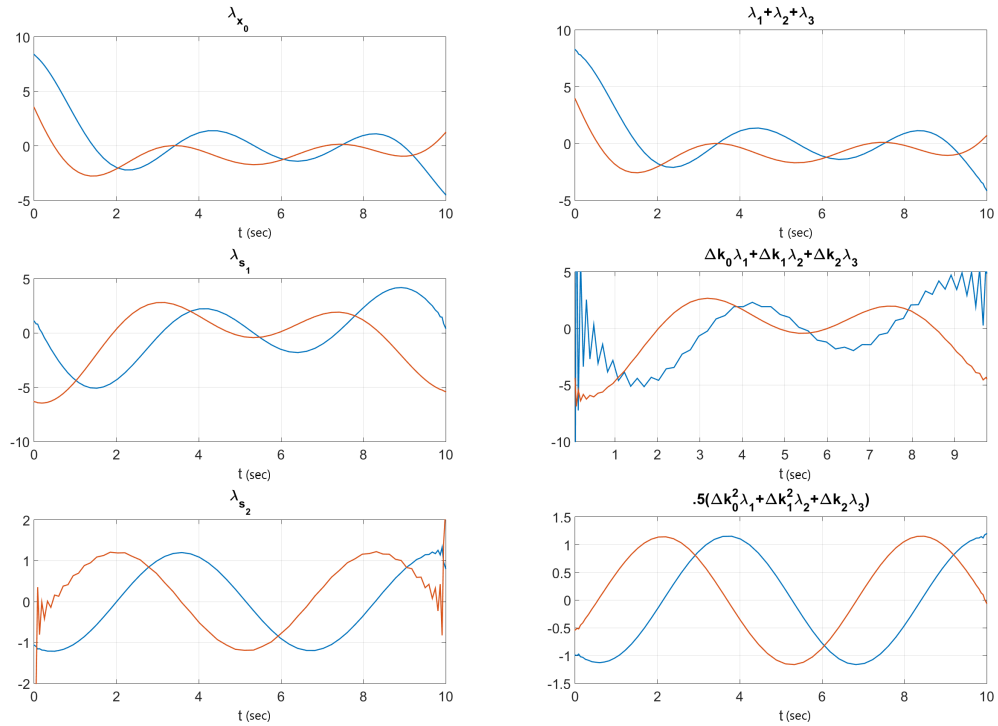

Figure 2.16: Costates of the second order sensitivity problem(left) and the associated function of the unscented costates(right).

Clearly, the relationship defined in Eq. (2.23) for the linear spring mass holds well.

If this relationship between the unscented problem and the sensitivity function-based problem holds then it is clear that the optimal control that solves the argmin condition for one solves both. In order to ensure that this condition is guaranteed for the two control problems the dynamics of the costates must be the same, including the boundary conditions according to the Terminal Transversality Condition

$$\dot{\tilde{\lambda}}_m \approx \sum_{i=1}^{N} \frac{\Delta k_i^m}{m!} \dot{\lambda}_i, \quad \tilde{\lambda}_m(t_f) \approx \sum_{i=1}^{N} \frac{\Delta k_i^m}{m!} \lambda_i(t_f). \tag{2.24}$$

For a general system the terminal condition of the costates can be shown to satisfy this relationship which can be confirmed via comparing the sum of the unscented to the sensitivity costates. The Transversality Condition for the unscented problem is generated by

$$\lambda_i(t_f) = \frac{\partial \bar{J}_{US}}{\partial x(t_f)} = 2w_i x_i(t_f, u; p + \Delta p_i), \tag{2.25}$$

where J_{US} is the the term in the endpoint Lagrangian of the unscented problem containing endpoint states. Passing the $\lambda_i(t_f)$ terms to the infinite sum generates the integral form of the costates

$$\sum_{i=1}^{N} \lambda_i^T(t_f) = \sum_{i=1}^{N} 2w_i x_i(t_f, u; p + \Delta p_i) \approx 2\int_\Omega x(t_f, u; p) g(p) dp \tag{2.26}$$

which can then be expanded

$$\sum_{i=1}^{N} \lambda_i^T(t_f) \;=\; 2\int_\Omega \left(\sum_{m=0}^{n_s} \left(\frac{s_m^j(t_f)}{m!} (\Delta p)^m \right) \right) g(p) dp.$$

According to the relationship in Eq. (2.23), by scaling these costate sums by

$$\frac{\Delta p_i^m}{m!}$$

the terminal value of the sensitivity costates should be recovered. These scaled sums become

$$\begin{aligned} \sum_{i=1}^{N} \frac{\Delta p_i^k}{k!} \lambda_i^T(t_f) &= 2\int_\Omega \left(\sum_{m=0}^{n_s} \left(\frac{\Delta p^k}{k!} \frac{s_m^j(t_f)}{m!} (\Delta p)^m \right) \right) g(p) dp \\ &= 2\sum_{m=0}^{n_s} s_m(t_f) \int_\Omega \frac{\Delta p^{(k+m)}}{k!m!} g(p) dp \\ &= 2\sum_{m=0}^{n_s} s_m(t_f) \frac{\mathbb{E}(\Delta p^{(k+m)})}{k!m!}. \end{aligned} \tag{2.27}$$

The costates of the sensitivity based problem should match given the relationship in Eq. (2.27). To verify this the individual costate terminal conditions, given by

$$\tilde{\lambda}_k(t_f) = \frac{\partial J_{sens}}{\partial s_k} = 2\sum_{m=0}^{n_s} s_m(t_f)\frac{\mathbb{E}(\Delta p^{(k+m)})}{k!m!} \tag{2.28}$$

can be confirmed a match. The costates also need to satisfy the same dynamic constraints. For the linear spring mass example these dynamics are indeed the same which can be confirmed by deriving the costate evolution equations. In fact, for general linear systems, the costate dynamics can be shown to satisfy the same equations.

For linear dynamics

$$\dot{x} = A(p)x + Bu$$

and a single uncertain parameter, the Hamiltonian is

$$H_{sens} = \tilde{\lambda}_{x_0}^T \dot{x}_0 + \tilde{\lambda}_{s_1}^T \dot{s}_1 + \tilde{\lambda}_{s_2}^T \dot{s}_2 + \cdots + \tilde{\lambda}_{s_n}^T \dot{s}_n \tag{2.29}$$

and the dynamics, up to order four, are

$$\begin{aligned}
\dot{x}_0 &= A(p_0)x_0 + Bu \\
\dot{s}_1 &= A(p_0)s_1 + \frac{\partial A(p)}{\partial p}x_0 \\
\dot{s}_2 &= A(p_0)s_2 + 2\frac{\partial A(p)}{\partial p}s_1 + \frac{\partial^2 A(p)}{\partial p^2}x_0 \\
\dot{s}_3 &= A(p_0)s_3 + 3\frac{\partial A(p)}{\partial p}s_2 + 3\frac{\partial^2 A(p)}{\partial p^2}s_1 + \frac{\partial^3 A(p)}{\partial p^3}x_0 \\
\dot{s}_4 &= A(p_0)s_4 + 4\frac{\partial A(p)}{\partial p}s_3 + 6\frac{\partial^2 A(p)}{\partial p^2}s_2 + 4\frac{\partial^3 A(p)}{\partial p^3}s_1 + \frac{\partial^4 A(p)}{\partial p^4}x_0 \\
&\vdots
\end{aligned}$$

where all partial derivatives are evaluated at the nominal parameter value and along the nominal states and can be used to define the dynamics of the costates in Eq. (2.29). The dynamics of the costate associated with the nominal system must satisfy the equation

$$-\dot{\tilde{\lambda}}_{x_0}^T = \frac{\partial H_{sens}}{\partial x_0} = \tilde{\lambda}_{x_0}^T A(p_0) + \tilde{\lambda}_{s_1}^T \frac{\partial A(p)}{\partial p} + \tilde{\lambda}_{s_2}^T \frac{\partial^2 A(p)}{\partial p^2} + \cdots + \tilde{\lambda}_{s_n}^T \frac{\partial^{n_s} A(p)}{\partial p^{n_s}} \quad (2.30)$$

and similarly the costate dynamics for each sensitivity order can be expressed as

$$-\dot{\tilde{\lambda}}_{s_k}^T = \tilde{\lambda}_{s_k}^T A(p_0) + \sum_{i=1}^{n_s-k} \frac{(k+i)!}{i!k!} \tilde{\lambda}_{s_{(k+i)}}^T \frac{\partial^i A(p)}{\partial p^i}. \quad (2.31)$$

The Hamiltonian of the unscented problem

$$H_{unsc} = \sum_{i=1}^{N} \lambda_i^T \dot{x}_i, \qquad \dot{x}_i = A(p_i)x_i + Bu,$$

provide the information necessary to define the unscented costate dynamics with expansion of the Jacobian around the nominal parameter

$$-\dot{\lambda}_i^T = \lambda_i^T \frac{\partial \dot{x}_i}{\partial x_i} = \lambda_i^T A(p_i), \quad A(p_0 + \Delta p) = A(p_0) + \frac{\partial A(p)}{\partial p} + ... + \frac{\Delta p^{n_a}}{n_a!} \frac{\partial^{n_a} A(p)}{\partial p^{n_a}}$$

According to Eq. (2.23) the costate dynamics should be scaled by the appropriate

scaled parameter samples

$$
\begin{aligned}
\sum_{i=1}^{N} -\frac{\Delta p_i^m}{m!}\dot{\lambda}_i^T &= \sum_{i=1}^{N} \frac{\Delta p_i^m}{m!}\lambda_i^T A(p_i) \\
&= \sum_{i=1}^{N} \frac{\Delta p_i^m}{m!}\lambda_i^T \left(A(p_0) + \frac{\partial A(p)}{\partial p} + ... \right) \\
&= \sum_{i=1}^{N} \frac{\Delta p_i^m}{m!}\lambda_i^T A(p_0) + \sum_{j=1}^{n_a}\sum_{i=1}^{N} \frac{\Delta p_i^{m+j}}{j!m!}\lambda_i^T \frac{\partial^j A(p)}{\partial p^j} \\
&= \tilde{\lambda}_{s_m}^T A(p_0) + \sum_{i=1}^{n_s-m} \frac{(m+i)!}{i!m!}\tilde{\lambda}_{s_{(m+i)}}^T \frac{\partial^i A(p)}{\partial p^i} \\
&= -\dot{\tilde{\lambda}}_{s_m}^T .
\end{aligned}
$$

This relationship for linear systems, coupled with the relationship for the Terminal Transversality Conditions, shows that the solution which minimizes the Hamiltonian of the sensitivity based problem also solves the unscented, and therefore the Riemann-Stieltjes, control problems. In general, a similar derivation for nonlinear systems is difficult and can be done on a case by case basis.

2.5 Conclusion

This chapter outlines a problem formulation for systems with parameter uncertainty via the sensitivity functions for both a first and higher order approximation. A motivating example involving a Zermelo type problem was then used to motivate the investigation of the relationship between these sensitivity based control problems and the unscented approximation of a Riemann-Stieltjes optimal control problem reviewed in the introduction. This lead to the conditions for which the cost functionals are equivalent between the problem formulations and also provides a manner of understanding the workings of the relatively new unscented problem using the lens of a more classical approach involving the Taylor expan-

sion of the uncertain parameter, thus bridging a more modern nonlinear control problem with a classical method of linearization. The linear spring example was used to show that, even for a linear system, the linearization of the dynamics around the parameter uncertainty does a poor job of managing the full effects of the uncertainty compared with a higher order approximation and the unscented method for open-loop controls. Extending these ideas to include a method for designing feedback controls, the progression from a linear approximation to a full nonlinear problem will be illustrated in the next chapter.

Chapter 3

Two Degree of Freedom Optimal Control

In the previous chapter we explored the connection between optimal control of the sensitivity functions and unscented optimal control as a means of generating controls which produce trajectories that are robust to deviations in model parameters. Those methods specifically produce open loop controls, which has many useful applications, however, frequently, information about the states can be leveraged to help mitigate unwanted deviations from the designed nominal maneuver. One avenue of including feedback control is through a two degree of freedom structure shown in Figure 3.1. This type of control gives the designer freedom to design a nominal trajectory which satisfies the desired performance criteria while subsequently designing feedback gains which address deviations from the nominal maneuver.

When the objective is to reduce the effects of deviations in the model parameters a sensitivity function approximation of the error from the nominal can be used to design the feedback gains by formulating an appropriate cost functional in a secondary optimal error control problem. The information provided in the

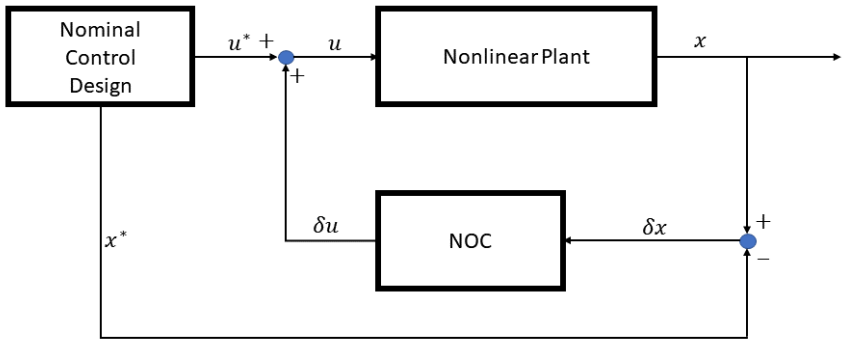

Figure 3.1: Two degree of freedom control for implementing feedforward and feedback controls/neighboring optimal control (NOC).

previous chapter helps construct the cost functional with the objective of minimizing the spread of the endpoints around the nominal endpoint. This method is connected to the well studied neighboring optimal control problem [30, 31].

The connection in the cost functional of a sensitivity optimal control problem and the cost functional of the unscented approximation to the Riemann-Stieltjes optimal control problem motivates a new two degree of freedom problem which utilizes the full nonlinear error state dynamics. In this chapter a new unscented neighboring optimal control problem is generated for general nonlinear systems with uncertainty in initial conditions and model parameters.

3.1 Sensitivity-Based Neighboring Optimal Control

Given a previously designed state and open-loop control pair $(x^{\text{Nom}}, u^{\text{Nom}})$ which is generated for an assumed nominal set of states with model parameter

values and dynamics

$$\dot{x}(t) = f(x, u, t; p_0), \tag{3.1}$$

there is a high likelihood that implementing the control u^{Nom} will not generate exactly the maneuver x^{Nom} in the presence of uncertainty, as previously illustrated. An error state can be defined to describe the difference between the nominally designed trajectory and the actually state produced by implementing the nominal control

$$\delta x(t, u; p) = x(t, u; p) - x^{\text{Nom}} = x(t, u; p) - x(t, u^{\text{Nom}}; p_0), \tag{3.2}$$

where $x(t, u; p)$ is the measured state variable. Using the first order sensitivity function approximation of a small neighborhood around the nominal system to define the error states according to

$$\delta x \approx \left.\frac{\partial x(t, u; p)}{\partial p}\right|_{x^{\text{Nom}}, u^{\text{Nom}}, p_0} = s(t), \tag{3.3}$$

where the sensitivity functions are evaluated along the nominal trajectory, provides a series of error state dynamics via the sensitivity function dynamics

$$\delta \dot{x} \approx \dot{s}(t) = \left.\frac{\partial f(x, u, t; p)}{\partial x}\right|_{x^{\text{Nom}}, u^{\text{Nom}}, p_0} s(t) + \left.\frac{\partial f(x, u, t; p)}{\partial p}\right|_{x^{\text{Nom}}, u^{\text{Nom}}, p_0} \tag{3.4}$$

These dynamics were used in the previous chapter to design the open-loop controls for a more robust maneuver, however, they can similarly be used to generate an optimal feedback rule which leverages the sensitivity function information [18, 32].

In order to define the two degree of freedom control shown in Figure 3.1, the

control is constructed as the sum of a feedforward, $g(t)$, and feedback, $k(x,p)$, control

$$u(t,x) = k(x,p) + g(t),$$

where $k(x,p)$ is a general form which changes depending on the measured state information and $g(t)$ is the feedforward portion which recovers the optimal control along the nominal trajectory. In general, $k(x,p)$ is difficult to design without imposing assumptions on the structure of the feedback. Commonly, a linear type feedback is used due to its convenient structure given by

$$u(t,x) = K(t)x(t,u;p) + g(t), \tag{3.5}$$

where $K(t) \in \mathbb{R}^{n_u \times n_x}$ is a matrix of time-varying feedback gains. The advantage of this feedback structure will become clear. The dynamics given in Eq. (3.4), which use the sensitivity function, approximate the error specifically due to the deviation in the model parameter and are valid in the case of purely open-loop controls, these dynamics must be modified slightly to include the effects of deviation from the nominal control which can be done as

$$\delta\dot{x} \approx \frac{\partial f(x,u,t;p)}{\partial x} s(t) + \frac{\partial f(x,u,t;p)}{\partial p} + \frac{\partial f(x,u,t;p)}{\partial u}\frac{\partial u}{\partial p}.$$

The addition of the

$$\frac{\partial f(x,u,t;p)}{\partial u}\frac{\partial u}{\partial p}$$

term in the error dynamics vanishes for open-loop control, however, control of the

form in Eq. (3.5) becomes

$$\frac{\partial f(x,u,t;p)}{\partial u}K(t)s(t)$$

for

$$\frac{\partial u}{\partial p} = K(t)s(t).$$

The error dynamics then become

$$\delta\dot{x} \approx \left[\frac{\partial f(x,u,t;p)}{\partial x} + \frac{\partial f(x,u,t;p)}{\partial u}K(t)\right]s(t) + \frac{\partial f(x,u,t;p)}{\partial p}. \tag{3.6}$$

The error dynamics given in Eq. (3.6), with initial condition $s(0) = 0$, illustrate the mechanism by which the feedback gains $K(t)$ manage the sensitivity functions. Clearly, the feedback gains aim to stabilize the homogeneous portion of the error approximation provided by the sensitivity functions. Previously, the goal of the sensitivity based optimal control problem was to generate the open-loop control for nominal trajectories such that the Jacobian term in Eq. (3.6) stabilized the sensitivity functions at final time, however, the addition of the second degree of freedom provided by the addition of the feedback contribution gives further direct control of the homogeneous part of the sensitivity functions.

Independent of the method by which the feedback gains $K(t)$ are produced, the feedforward term $g(t)$ can then be defined to ensure that the nominal control is preserved along the nominal trajectory

$$g(t) = K(t)x^{\text{Nom}} - u^{\text{Nom}}. \tag{3.7}$$

With the expanded control and dynamics defined by Eq. (3.6) a measure must be defined to be optimized. For reducing the effects of the uncertainty on the final

endpoint, defining a cost functional, for a single uncertain parameter, according the guidelines defined in the previous chapter for minimizing the second moment of the endpoint spread

$$J_{sens} = \sum_{m=1}^{n_s} \left[\frac{\|s_m\|^2}{(m!)^2} \mathbb{E}[\Delta p^{2m}] \right] + \sum_{m=1}^{n_s} \sum_{\substack{k=1 \\ k \neq m}}^{n_s} \left[\langle s_m, s_k \rangle \frac{\mathbb{E}[\Delta p^{m+k}]}{m!k!} \right],$$

truncated to the first order

$$J_{tdf} = \|s(t_f)\|^2 \mathbb{E}[\Delta p^2], \tag{3.8}$$

provides a candidate objective function for the feedback to optimize. Using this cost functional an optimal control problem can now be defined for designing the feedback gains in the matrix $K(t)$ as

$$s(t) \in \mathbb{R}^{n_x}, \quad K(t) \in \mathbb{R}^{n_u \times n_x}$$

$$\begin{cases} \text{Min} & J_{tdf} = \mathbb{E}[\Delta p^2] ||s(t_f)||^2 \\ \text{S.t.} & \dot{s} = \left[\frac{\partial f}{\partial x} + \frac{\partial f}{\partial u} K(t) \right] s(t) + \frac{\partial f}{\partial p} \\ & s(t_0) = 0. \end{cases}$$

This optimal control problem does not include constraints on the controls in $K(t)$ which presents the problem of allowing any value of feedback effort. Nearly infinite feedback effort would conceptually be able manage any amount of uncertainty, however, this is not realistic. In order to restrict the problem to designing finite feedback gains one option would be to include a constraint on the matrix $K(t)$. A constraint can be constructed as a penalty on the feedback gains by

including a running cost term

$$\int_{t_0}^{t_f} \|K(t)\|^2 dt$$

which can be constructed for any suitable matrix norm. Including this constraint into the optimal control problem

$$s(t) \in \mathbb{R}^{n_x}, \quad K(t) \in \mathbb{R}^{n_u \times n_x}$$

$$\begin{cases} \text{Min} & J_{tdf} = \mathbb{E}[\Delta p^2]||s(t_f)||^2 + \int_{t_0}^{t_f} \|K(t)\|^2 dt \\ \text{S.t.} & \dot{s} = \left[\frac{\partial f}{\partial x} + \frac{\partial f}{\partial u} K(t)\right] s(t) + \frac{\partial f}{\partial p} \\ & s(t_0) = 0. \end{cases}$$

The addition of the constraint aims to avoid the issue of unreasonably large feedback gains. The designer needs to check to ensure that controls generated by this optimal control problem do not cause the implemented control

$$u(t, x) = K(t)x(t, u; p) + g(t)$$

to exceed any control constraints of the original system

$$u^L \leq u(t, x) \leq u^U.$$

Alternatively, a hard constraint can be constructed to aid in avoiding breaching any of the control constraints of the original system. Replacing the control in the control constraint expression

$$u^L \leq K(t)x(t, u; p) + g(t) \leq u^U$$

and replacing the state with

$$x(t, K(t)x + g(t); p + \Delta p) = x^{\text{Nom}} + \delta x$$

gives

$$u^L \leq K(t)[x^{\text{Nom}} + \delta x] + g(t) \leq u^U.$$

From this relationship it is clear that

$$u^L - K(T)x^{\text{Nom}} - g(t) \leq K(t)\delta x \leq u^U - K(t)x^{\text{Nom}} - g(t)$$

thus

$$u^L - u^{\text{Nom}} \leq K(t)\delta x \leq u^U - u^{\text{Nom}}.$$

The δx term is undetermined as it requires the state information provided by measuring the system, however, there is a case to be made for making an assumption on the maximum value of the error δx_{max}. This assumption can be motivated by the sensitivity functions of the nominal system which provide an approximation of the error given the maximum reasonable deviation from the nominal parameter Δp. By considering the worst case scenario a hard constraint can be constructed for the optimal feedback control

$$u^L - u^{\text{Nom}} \leq K(t)\delta x_{max} \leq u^U - u^{\text{Nom}}$$

which provides a reasonable measure of the worst case control effort. This still requires that the control be verified by the designer in implementation. Furthermore, the better the δx_{max} is defined, the better the chance the control will satisfy the original constraint without losing any performance to overconstraint.

The optimal feedback problem then becomes

$$s(t) \in \mathbb{R}^{n_x}, \quad K(t) \in \mathbb{R}^{n_u \times n_x}$$

$$\begin{cases} \text{Min} & J_{tdf} = \mathbb{E}[\Delta p^2]||s(t_f)||^2 + \int_{t_0}^{t_f} \|K(t)\|^2 dt \\ \text{S.t.} & \dot{s} = \left[\frac{\partial f}{\partial x} + \frac{\partial f}{\partial u} K(t)\right] s(t) + \frac{\partial f}{\partial p} \\ & s(t_0) = 0, \\ & u^L - u^{\text{Nom}} \leq K(t)\delta x_{max} \leq u^U - u^{\text{Nom}}. \end{cases}$$

Considering the δx is a function of the sensitivity functions $s(t)$, it makes sense that if the sensitivity functions are small through the maneuver then there is more budget for larger feedback gains in $K(t)$. Along these lines a penalty on the sensitivity states can be included in the running term of the cost functional

$$J_{tdf} = \mathbb{E}[\Delta p^2]||s(t_f)||^2 + \int_{t_0}^{t_f} \|K(t)\|^2 + \|s(t)\|^2 dt$$

which will aim to keep the sensitivity states from growing and allow for larger values of the time-varying feedback gains. For more freedom in the design of the optimal control problem tuning parameters can be included to allow for balancing the endpoint sensitivity and the running sensitivity cost. Combining all these concepts an optimal control for the sensitivity function neighborhood problem is constructed as

$$s(t) \in \mathbb{R}^{n_x}, \quad K(t) \in \mathbb{R}^{n_u \times n_x}$$

$$(SC) \begin{cases} \text{Min} & J_{tdf} = \alpha ||s(t_f)||^2 + \int_{t_0}^{t_f} \|K(t)\|^2 + \beta \|s(t)\|^2 dt \\ \text{S.t.} & \dot{s} = \left[\frac{\partial f}{\partial x} + \frac{\partial f}{\partial u} K(t)\right] s(t) + \frac{\partial f}{\partial p} \\ & s(t_0) = 0, \\ & u^L - u^{\text{Nom}} \leq K(t)\delta x_{max} \leq u^U - u^{\text{Nom}}, \end{cases}$$

where α, β are the tuning parameters. This optimal control problem has similar structure to a Linear Quadratic Regulator (LQR) type problem which is a well studied problem in optimal control. This means that solutions, and the methods of generating solutions, to problem (SC) can be obtained in a number of ways, many of which are computational in nature.

The advantage of the secondary control problem allows the designer to first construct a control according to an assumed nominal system, knowing that deviations occurring in the actual implementation can then be addressed by generating a feedback rule according to problem (SC). The sensitivity neighborhood optimal feedback problem allows for tuning of the balance between a running measure of the sensitivity functions and the sensitivity of the final endpoints in addition to a penalty on the feedback effort. The open-loop term is then designed to guarantee the optimality of the nominal system is preserved in the case that the assumed model parameter was very close to the actual value.

The effectiveness of this two degree of freedom type control can be illustrated using the linear spring mass example considered in the previous chapter. In that section, the uncertainty in the spring parameter was managed using open-loop only control, however, by including feedback it is possible to improve the endpoint error over the range of uncertainty.

Using the feasible trajectory as $(x^{\text{Nom}}, u^{\text{Nom}})$ designed in the previous chapter, the secondary optimal control problem for minimizing the local sensitivity of the linear oscillator system from problem (S) can be formulated in the form of problem (SC) as

$$s \in \mathbb{R}^2, \quad M \in \mathbb{R}^2$$

$$(FC) \begin{cases} \text{Minimize} & J = ||s(t_f)||^2 + \int_{t_0}^{t_f} \left(10||M(t)||^2 + ||s(t)||^2\right) dt \\ \text{Subject to} & \dot{s}(t) = \left[A(k_0) + B(k_0)M(t)\right] s + \left.\frac{\partial A}{\partial k}\right|_{x^{\text{Nom}}, u^{\text{Nom}}, p_0} x^{\text{Nom}} \\ & (s_x(t_0), s_v(t_0)) = (0, 0) \\ & t_f = 10, \end{cases}$$

where $(A(k_0), B(k_0))$ are the coefficient matrices for the mass spring system with the nominal parameter value and a choice of $(\alpha, \beta) = (1, 10)$ has been used. Solving this optimal control problem generates the feedback gains and open loop controls seen in Figure 3.2.

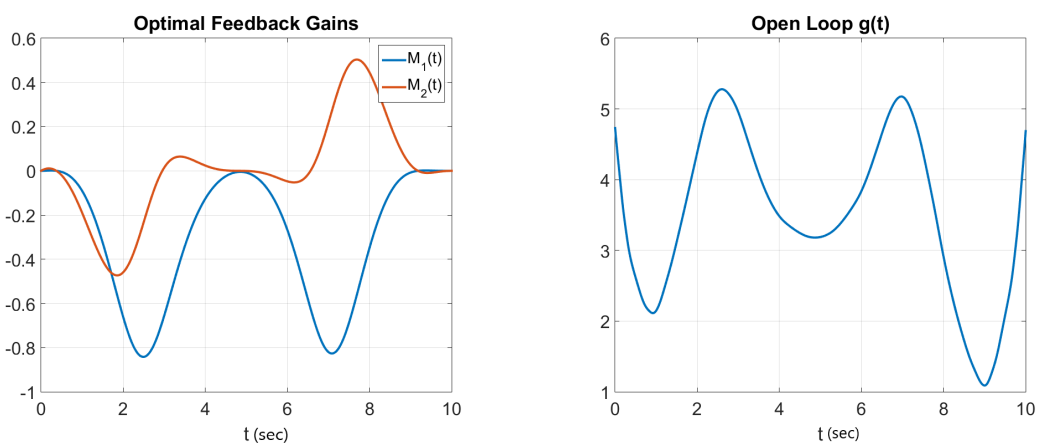

Figure 3.2: Feedback gains for optimal sensitivity reduction (left) and corresponding open loop signal (right).

In order to determine the effectiveness of the optimal gains generated the mean endpoint error for each state and the mean residual energy from the Monte Carlo

simulation described in the previous chapter is shown in Table 3.1.

	Nominal	**Nom TDF**	**Unsc TDF**
x	0.3463	0.0140	0.0141
y	0.2041	0.0089	0.0040
Mean RE	0.4326	0.0176	0.0158
% Change	–	95	97

Table 3.1: Mean endpoint error comparison for a nominal feasible control and the local sensitivity based feedback for the linear spring mass example. Percent change from the nominal performance is also included.

Using the optimal feedback gains obtained from Problem (FC) for a feasible trajectory which does not consider uncertainty, a 95% change in mean residual energy is achieved. This improvement in the robustness of the endpoints is produced as a consequence of the feedback gains which reduce the first order sensitivity functions, however, it was demonstrated that the first order sensitivity functions left a lot of performance on the table compared to the open-loop unscented and second order sensitivity controls. This concept will be used to motivate the unscented feedback control outlined later in this chapter.

As mentioned in the previous section, there are two avenues for managing the sensitivity dynamics which include the feedback, which attempts to stabilize the homogeneous portion of Eq. (3.6), and the Jacobian of the of the system evaluated along the nominally designed control. Therefore, it makes sense that, using a nominal control that is inherently robust to deviations in the parameters, the control effort required by the feedback term can be less than the case of the naively designed nominal control. The feedback gains generated when using the unscented open-loop controls from the previous chapter are shown in Figure 3.3 in comparison to the feedback gains above.

By using the unscented controls propagated at the nominal parameter value as the feasible trajectory, an improvement from the nominal TDF control can

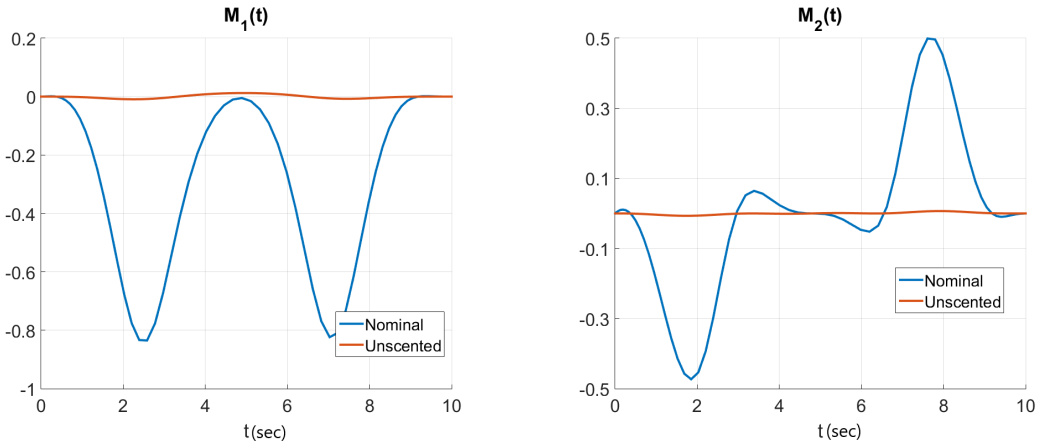

Figure 3.3: Feedback gain comparison between the nominal TDF and unscented TDF problems.

be shown. The TDF control for the unscented open-loop demonstrates a 97% improvement over the nominal and better performance than the nominal TDF case. Figure 3.3 shows that the optimal feedback gains have been greatly reduced in the case of the unscented controls due to its inherently robust nature. This touches upon one of the motivating principles of unscented optimal control which is that, by considering the uncertainty in the model parameters in the design of the open-loop maneuver, it is possible to reduce the dependence on sensor feedback for achieving a desired endpoint condition.

The open-loop control design in the previous chapter demonstrated that the first order sensitivity consideration was not sufficient to account for all the effects of the uncertainty. By using higher order sensitivity functions the performance improvement was greatly increased but requires the designer to derive sensitivity functions for each order. Alternatively, the unscented problem with only three copies of the dynamics for three discrete values of the uncertain parameter value sampled from the assumed distribution effectively managed the higher order effects of the uncertainty. Extending this concept to the case of the two degree of freedom type control for feedback gains motivates a new type of optimal control problem

which uses an unscented control approach to designing the feedback gains outlined for the sensitivity neighborhood. This new optimal control problem, an unscented neighboring control, avoids a linear approximation of the error states and is defined in a following section.

3.1.1 Neighboring Optimal Control

The two degree-of-freedom control for the sensitivity dynamics outlined in the previous section is connected to a type of optimal control which has been studied for reducing plant deviations due to initial condition uncertainty. In optimal control this method is commonly referred to as neighboring optimal control (NOC)[30, 31, 33].

$$\delta x(t) = x(t) - x^{\text{Nom}}(t), \tag{3.9}$$

where x^{Nom} is the desired optimal path and $x(t)$ is the actual path and $\delta x(t)$ are the error states. The objective is to design small deviations from the nominal optimal control

$$\delta u(t) = u(t) - u^{\text{Nom}}(t), \tag{3.10}$$

such that the constraints of the nominal system are satisfied, along with the optimality of the original trajectories, when the initial values of the states differ from the nominal case.

For the case of small deviations from the assumed initial conditions a linear approximation to the nominal state dynamics can be used to model the error

states $\delta x(t)$ with dynamics

$$\delta\dot{x} = \left.\frac{\partial f}{\partial x}\right|_{x^{\text{Nom}},u^{\text{Nom}},p_0} \delta x + \left.\frac{\partial f}{\partial u}\right|_{x^{\text{Nom}},u^{\text{Nom}},p_0} \delta u, \quad \delta x(t_0) = x_0 - x_0^*, \tag{3.11}$$

where the derivative matrices are evaluated along the nominal control and state. The performance index of interest in the neighboring optimal control problem is the second variation of the original cost functional

$$J = E(x_f, t_f) + \int_{t_0}^{t_f} F(x(t), u(t))dt,$$

given by

$$\begin{aligned} \overline{J} &= \frac{1}{2}\delta x^T(t_f)P(t_f)\delta x(t_f) \\ &+ \frac{1}{2}\int_{t_0}^{t_f} [\delta x^T(t)\ \delta u^T(t)] \begin{bmatrix} Q(t) & M(t) \\ M^T(t) & R(t) \end{bmatrix} \begin{bmatrix} \delta x(t) \\ \delta u(t) \end{bmatrix} dt, \end{aligned}$$

and

$$P(t_f) = \left.\frac{\partial^2 E}{\partial x^2}\right|_{t=t_f}, \quad \begin{bmatrix} Q(t) & M(t) \\ M^T(t) & R(t) \end{bmatrix} = \begin{bmatrix} \frac{\partial^2 F}{\partial x^2} & \frac{\partial^2 F}{\partial x \partial u} \\ \frac{\partial^2 F}{\partial u \partial x} & \frac{\partial^2 F}{\partial u^2} \end{bmatrix},$$

for suitable conditions on the cost function matrices. The Hamiltonian for the error system is given by

$$\overline{H} = [\delta x^T(t)\ \delta u^T(t)] \begin{bmatrix} Q(t) & M(t) \\ M^T(t) & R(t) \end{bmatrix} \begin{bmatrix} \delta x(t) \\ \delta u(t) \end{bmatrix} + \overline{\lambda}^T \delta\dot{x}, \tag{3.12}$$

with adjoint dynamics

$$\dot{\overline{\lambda}} = -Q(t)\delta x(t) - M(t)\delta u(t) - \left.\frac{\partial f}{\partial x}^T\right|_{x^{\text{Nom}},u^{\text{Nom}},p_0} \overline{\lambda}, \tag{3.13}$$

and Terminal Transversality Condition

$$\overline{\lambda}(t_f) = P(t_f)\delta x(t_f). \tag{3.14}$$

The minimized Hamiltonian gives the condition

$$M^T(t)\delta x(t) + R(t)\delta u(t) + \left.\frac{\partial f}{\partial u}^T\right|_{x^{\text{Nom}},u^{\text{Nom}},p_0} \overline{\lambda}(t) = 0. \tag{3.15}$$

Eq. (3.15) can be solved for δu,

$$\delta u(t) = -R(t)^{-1}\left[M^T(t)\delta x(t) + \frac{\partial f}{\partial u}^T \overline{\lambda}(t)\right],$$

for non singular $R(t)$. Assuming the relationship in Eq. (3.14) holds for all t, the control deviation can be formulated as a time-varying linear feedback control

$$\delta u(t) = K(t)\delta x(t). \tag{3.16}$$

Plugging Eq. (3.16) into the linear dynamics given by Eq. (3.11) gives the LTV dynamics for the approximated error states

$$\delta \dot{x} = \left[\frac{\partial f}{\partial x} + \frac{\partial f}{\partial u}K(t)\right]\delta x. \tag{3.17}$$

These dynamic constraints, along with the second variation of the cost function $\overline{J}$, generate a Linear Quadratic Regulator optimal control problem which can be solved for the feedback gains in the matrix $K(t)$ via the Riccati equation. The

optimal control deviation δu have the form of a matrix time-varying feedback gains that are scaled linearly by the error states. This property further motivates the form of the control in Eq. (3.5) which share the same structure. These NOC laws have been used for guidance applications and navigation problems for managing small deviations from the designed trajectories [34].

3.2 Unscented Neighboring Optimal Control

In this section we formulate a new type of neighboring optimal control problem which is an extension of unscented optimal control for systems with model parameter uncertainty. The discretization of the parameter space, opposed to the linearization, provides an avenue for using the full nonlinear error dynamics in the design of the optimal control problem.

Deviations to the nominal trajectory due to error in the model parameters

$$\delta x(t;p) = x(t;p) - x^{\text{Nom}}(t), \tag{3.18}$$

where a nominal parameter value $p = p_0$, is used in the design of the nominal optimal trajectories and control $x^{\text{Nom}}, u^{\text{Nom}}$. In the previous section the error state dynamics were approximated using a linearization around the nominally optimal control and state trajectories and resulted in a LQR type optimal control problem, however, it can be advantageous to approximate a PDF via sampling rather than linearize a generic nonlinear function as seen in the case of the linear mass spring example. This allows for the full nonlinear error dynamics for Eq. (3.18)

$$\delta \dot{x} = f(x, u, t; p) - f(x^{\text{Nom}}, u^{\text{Nom}}, t; p_0), \tag{3.19}$$

to be considered in the design of the feedback control law. Solving Eq. (3.18) for the actual state, along with the control deviation δu, and plugging in to the dynamics in Eq. (3.19) gives the nonlinear system for the error dynamics $\delta x(t)$, however, the parameter p has potential deviation $p = p_0 + \Delta p$ which introduces uncertainty into the error dynamics.

Recently, as reviewed earlier, unscented optimal control (UOC) has been shown to provide a promising avenue for discretization of an uncertain optimal control problem when the exact value of the model parameters are unknown or uncertain. In UOC the parameter uncertainty is assumed to be subject to a PDF, with known mean and variance of initial state $x(t_0; p) \equiv p$, which can be used to generate a set of sigma points in context of the unscented transform on the initial state of the system $\chi_1(t_0), \chi_2(t_0), ..., \chi_{n_\sigma}(t_0)$. For each of the sigma point states, the dynamics are given by the dynamics of the original state system with chosen sigma point values of the parameter as the initial condition. Extending this concept to the states in Eq. (3.18), define an error state for each sigma point

$$\delta\chi_i = \chi_i - x^{\text{Nom}} = x(t; p_i) - x(t; p_0),$$

where the uncertain parameter p is discretized over the parameter space $supp(p)$ into a finite number of nodes $p_i, \quad i = 1, 2, ..., n_\sigma$. The choice of the nodes, p_i, depends on the PDF of the parameter, p, for example for the case of a single uncertain parameter with Gaussian distribution the sigma points are simply the nodes of the Gauss Hermite quadrature with associated weights. The advantage of the UOC optimal control problem is the relatively low number of discrete nodes required to capture the effects of the uncertainty in contrast to Monte Carlo based methods.

Dynamics of the individual sigma point systems are given by Eq. (3.19) for

each value of the parameter

$$\delta\dot{\chi}_i = f(\chi_i, u, t, p_i) - f(x^{\text{Nom}}, u^{\text{Nom}}, t, p_0), \tag{3.20}$$

subject to the initial condition $\delta\chi_i(t_0) = \delta x(t_0, p_i)$. Thus, the UOC problem seeks a control signal which drives the system from $\delta\chi_i(t_0),\ i = 1, 2, ..., n_\sigma$ to a desired final state while minimizing a specified cost function.

The choice of cost functional for an UOC problem varies depending on the desired goal, previously, a weighted sum of the sigma point systems at final time, which approximates the second moment of the terminal state, was used. An example of an unscented cost function utilizes the square of the error states at the terminal time as

$$J_{unsc} = \sum_{i=1}^{n_\sigma} w_i \|\delta\chi_i(t_f)\|^2,$$

where the weights w_i are associated to the specific sigma point. The choice of cost functional in the linear sensitivity neighborhood was developed to mirror this approximation.

So far no assumption on the form of the control deviation δu has been made. Defining $\delta u(t)$ as purely open loop generates a fully open loop control $u(t)$ which manages the error states which is related to the unscented problem previously covered. Additionally, along the lines of the NOC problem formulated for the linear approximated error states, a TDF form of the control which includes linear time-varying feedback gains can be defined as

$$u(t) = u^{\text{Nom}}(t) + K(t)\delta x(t, p). \tag{3.21}$$

The UOC problem for the error sigma point system with the unscented cost function can be formulated as

$$\delta\chi_i \in \mathbb{R}^{n_x}, \quad K(t) \in \mathbb{R}^{n_u \times n_x}, \quad i = 1, 2, ..., n_\sigma$$

$$(UNOC) \begin{cases} \text{Min} & J_{unsc} = \sum_{i=1}^{n_\sigma} w_i \|\delta\chi_i(t_f)\|^2 + \int_{t_0}^{t_f} \|K(t)\|^2 dt \\ \text{S.t.} & \delta\dot{\chi}_1 = f(\chi_1, u, t, p_1) - f(x^{\text{Nom}}, u^{\text{Nom}}, t, p_0) \\ & \vdots \\ & \delta\dot{\chi}_{n_\sigma} = f(\chi_{n_\sigma}, u, t, p_{n_\sigma}) - f(x^{\text{Nom}}, u^{\text{Nom}}, t, p_0) \\ & \delta\chi_i(t_0) = \delta x(t_0, p_i) \\ & \delta u_{lower} \leq \delta u \leq \delta u_{upper} \\ & p_i \in supp(p), \ \forall \ i = 1, 2..., n_\sigma, \end{cases}$$

where a penalty on the control effort has been appended to the unscented cost function similar to problem (SC) as a soft constraint to avoid infinite gains when a control constraint is not present. Problem $(UNOC)$ is a deterministic nonlinear optimal control problem in Bolza form which can be solved computationally.

While a single uncertain parameter has been considered, it is straightforward to extend the problem formulation to include any number of uncertain model parameters consequently increasing the number of sigma points required to accurately capture the impact of the uncertainty. In contrast to the sensitivity neighboring problem, this does not require any derivation of the linear and higher order sensitivity functions, yet still includes the information provided by them.

The optimal control problem $(UNOC)$ with feedback gain matrix $K(t)$, for a sufficient number of sigma points are used, begets the Hamiltonian

$$H_{unsc} = \|K(t)\|^2 + \sum_{i=1}^{n_\sigma} \widetilde{\lambda}_i^T \delta\dot{\chi}_i. \tag{3.22}$$

with adjoint state dynamics and Terminal Transversality Condition

$$\dot{\widetilde{\lambda}}_i = \widetilde{\lambda}_i^T \frac{\partial \delta \dot{\chi}_i}{\partial \delta \chi_i}, \quad \widetilde{\lambda}_i(t_f) = 2w_i \delta \chi_i(t_f). \tag{3.23}$$

The minimized Hamiltonian evaluated at the optimal solution must also satisfy the condition

$$\frac{\partial H_{unsc}}{\partial K_{i,j}} = 0, \; i = 1, .., n_x, \; j = 1, .., n_u. \tag{3.24}$$

Eqs. (3.22) - (3.24) provide conditions for which solutions to Problem $(UNOC)$ can be verified and validated. Additionally, a Monte Carlo simulation over the support of the distribution of uncertainty is useful for verifying the efficacy of the feedback gains generated.

In the same way the mechanics of the unscented problem provide an approximation of the Riemann-Stieltjes optimal control problem in the limit of infinite samples of the uncertain parameters, the unscented neighboring optimal control problem can be viewed as an approximation of a Riemann-Stieltjes control

$$x \in \mathbb{R}^{n_x}, \quad K(t) \in \mathbb{R}^{n_u \times n_x}$$

$$(RSNOC) \begin{cases} \text{Min} & J_{RSNOC} = \int_\Omega \|\delta x(t_f, u; p_0 + \Delta p)\|^2 g(\Delta p) d\Delta p + \int_{t_0}^{t_f} \|K(t)\|^2 dt \\ \text{S.t.} & \delta \dot{x} = f(x, u, t; p) - f(x^{\text{Nom}}, u^{\text{Nom}}, t; p_0) \\ & \delta x(t_0) = \delta x_0 \\ & \delta u^L \leq \delta u \leq \delta u^U \\ & \Delta p \in supp(\Delta p). \end{cases}$$

This optimal control aims to minimize all deviations due to parameter variations in the range of the support of the distribution by generating a set of control perturbations.

The versatility of the unscented neighboring optimal control allows for a wide range of possible constraints such as constraints on the allowable range of feedback gain values, path constraints on trajectories associated with the sigma point samples in addition to constraints which approximate the moments of the error states. Furthermore, while linear feedback gains have been considered here, there is no inherent restriction on the form of δu. When designing a purely open-loop control perturbation the full control becomes the unscented controls for minimizing the second moment of the endpoint error around the nominal endpoint

$$\int_{\Omega} \|x(t, u; p + \Delta p_0) - x(t, u; p_0)\|^2 g(\Delta p) d\Delta p.$$

This section outlined a new optimal control problem for designing feedback and open-loop controls for nonlinear systems with model parameter uncertainty according to the full nonlinear error dynamics. This tool can be very useful in cases where linear neighboring optimal control is used to design the feedback gains but where the linear approximation of the error states is insufficient. This result represents a step forward in optimal control of neighboring trajectories which acknowledges the progress in the field of nonlinear optimal control. Anymore, controllers have the computational power to handle many nonlinear problems and are no longer restricted to linearization for the sake of generating solutions.

In the following section the linear mass spring is once again used, this time to showcase the result of solving the unscented neighboring optimal problem. In order to demonstrate the efficacy of the unscented neighboring optimal control problem in the context of the linear spring mass example the unscented neighbor-

ing control problem

$$\delta x_i \in \mathbb{R}^2, \quad M(t) \in \mathbb{R}^2, \quad i = 1, 2, 3$$

$$(UNS) \begin{cases} \text{Min} & J_{unsc} = \sum_{i=1}^{3} w_i \|\delta x_i(t_f)\|^2 + \int_{t_0}^{t_f} \|M(t)\|^2 dt \\ \text{S.t.} & \delta \dot{x}_1 = A(k_1)(x^{\text{Nom}} + \delta x_1) - A(k_0)x^{\text{Nom}} + BM\delta x_1 \\ & \delta \dot{x}_2 = A(k_2)(x^{\text{Nom}} + \delta x_2) - A(k_0)x^{\text{Nom}} + BM\delta x_2 \\ & \delta \dot{x}_3 = A(k_3)(x^{\text{Nom}} + \delta x_3) - A(k_0)x^{\text{Nom}} + BM\delta x_3 \\ & \delta x_i(t_0) = 0 \\ & k_i \in supp(k), \ \forall \ i = 1, 2, 3, \end{cases}$$

can be used to design the feedback gains $M(t) \in \mathbb{R}^2$. Problem (UNS) uses the same sample discretization and nominal maneuver as in the previous chapter.

The gains for the unscented neighboring control are shown in Figure 3.4 and are noticeably different from the gains generated by the sensitivity neighborhood shown in Figure 3.2. To compare the performance of these unscented gains with

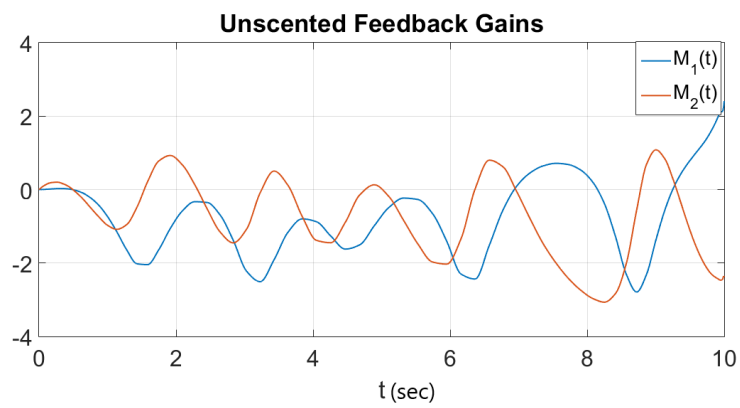

Figure 3.4: Feedback gains generated by problem UNS.

those provided by the sensitivity neighborhood the Monte Carlo simulation for the range of uncertain stiffness parameter is used to compute the mean error of the position and velocity states and the residual energy. This data is shown in

Table 3.2.

	Nominal	**SNOC**	**UNOC**
x	0.3463	0.0140	0.0026
y	0.2041	0.0089	0.0018
Mean RE	0.4326	0.0176	0.0031
% Change	–	95	99.3

Table 3.2: Mean endpoint error comparison for a nominal feasible control and the local sensitivity based and unscented feedback for the linear spring mass example. Percent change from the nominal performance is also included.

There is a marked decrease in both the mean state errors and the residual energy resulting in a 99.3% improvement over the nominal, surpassing that of the sensitivity neighborhood by an order of magnitude. This reiterates the benefit of considering beyond the first order approximation of the error from the nominal, even in the case of a simple linear spring mass system.

3.3 Conclusion

This chapter presents a new way of defining an optimal control problem for the management of deviations from a nominally designed maneuver which are due to parameter uncertainty. The uncertainty is assumed to be subject to a PDF which is then approximated two different ways. One method uses information provided by the first order sensitivity functions, defined via a linearization around the model parameters, while the other methods follows the unscented optimal control framework of discretizing the distribution of the uncertainty which allows for the full nonlinear error dynamics to be used. The advantage of this nonlinear unscented neighboring optimal control is demonstrated in the context of the linear spring example.

In the next chapter, a nonlinear system which has similar structure to the

spring mass investigated so far will be explored to demonstrate the advantage of the controls produced by the methods outlined in this chapter. The advantage of an unscented neighboring control will be clearly illustrated in both the context of feedback and open-loop controls.

Chapter 4

Application to a Non-Linear Double Gimbal Mechanism with Flexibility

As technology advances it has quickly become easier and cheaper to deploy satellites for a range of purposes related to signal relay and communication. These purposes require a high degree of accuracy as small deviations from a desired orientation are amplified by the distance to the target. Figure 4.1 illustrates the potential of undesired wobble when focusing on a target location.

One significant example is NASA's Tracking and Data Relay Satellite (TRDS) program which was established in the early 1970's. The motivation behind this program is to provide near continuous information relay service to missions, for example the Hubble Space Telescope and the International Space Station. This constellation of satellites, which currently consists of nine orbiting satellites, provide a vast improvement over ground station relays as they allow for a consistent relay of signals instead of requiring a waiting period while the satellites orbit into

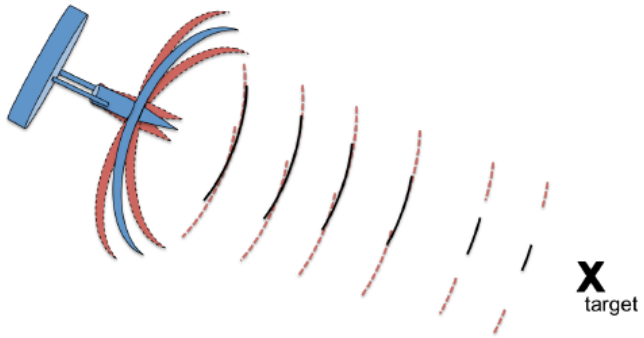

Figure 4.1: Illustration of flexibility effecting ability to target desired objective after [2].

position above the ground stations. Figure 4.2 shows NASA's depiction of the TDRS system.

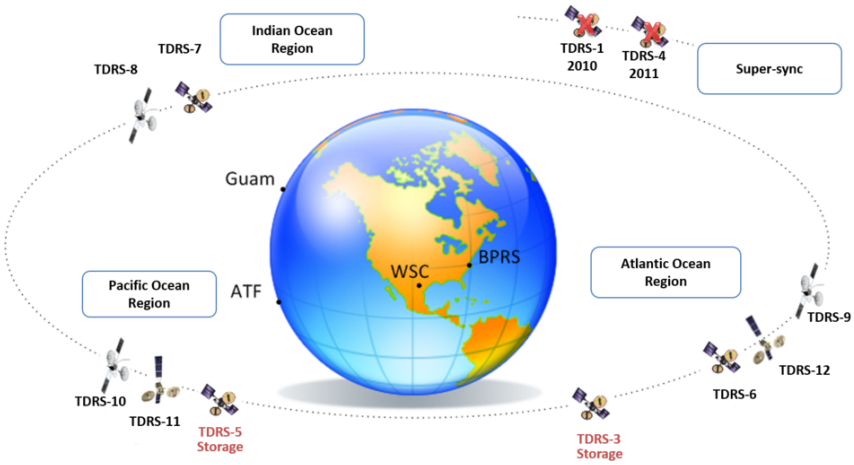

Figure 4.2: NASA's diagram of the TDRS fleet. (`https://www.nasa.gov/directorates/heo/scan/services/networks/tdrs_main`)

Each of these satellites depend on antennas in order to communicate with their partners and the ground stations, for example Figure 4.3 shows a third generation satellite, of which there are currently three with the last having been launched in August 2017. The large array of adjustable antennas must be capable of being directed precisely in order to maintain signal links.

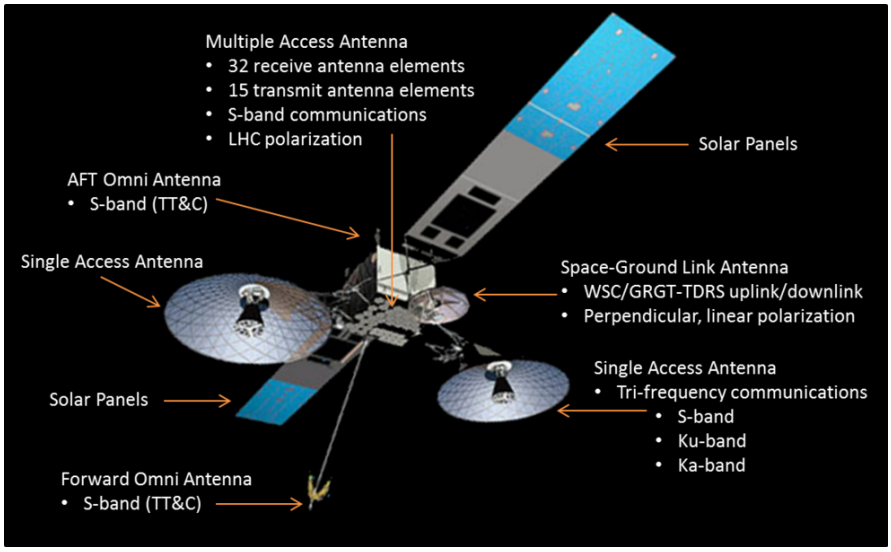

Figure 4.3: Diagram of a third generation satellite member of the TDRS fleet detailing the operable antennas.

Commonly, the models used for antenna systems aboard the crafts are linear and implement feedback control in order to ensure that any reorientation of the antenna avoids inducing unwanted vibrations or drift. However, these linear models require a slow maneuver time in order to avoid the need for modeling the highly nonlinear flexible effects [35].

In contrast to the common practice of feedback control, recently, the need for open loop design of satellite maneuvers has been proposed in order to both combat the costly repairs and maintenance to sensors and to operate when sensor malfunctions occur in addition to implementing optimal time slews [18]. A difficulty with employing open loop controls is that uncertainty in the model has an impact on the designed control's ability to achieve the desired goal and can even effect the feedback mechanism's ability to track. Recently, optimal control theory has been shown to be effective in designing open loop controls which are more robust to uncertainty in model parameters, such as a zero gyro maneuver designed for the Hubble Space Telescope [15]. Furthermore, robust open loop controls can po-

tentially help relieve some of the burden on the feedback tracking mechanism by designing trajectories that explicitly consider potential uncertainty in the model leading to better performance overall.

This chapter presents and compares optimal control problem formulations for generating open loop and feedback controls which specifically aim to manage parameter uncertainty in a nonlinear model of a double gimbaled system with flexible effects via the control frameworks presented in the previous chapter.

4.1 Flexible Gimbal Model

In this chapter a model of a flexible gimbal from [36, 2] is utilized. Figure 4.4 shows a double-gimbal mechanism (DGM) which connects a flexible antenna to the body of the craft and also shows a schematic for a rod with a flexible joint. This flexible rod structure is used to model the flexible connections between the bodies of the gimbal. The spring constant k represents the flexibility of the rod and allows for displacement between the rotor and the rod end and the parameter c represents the torsional damping due to any dissipative mechanism.

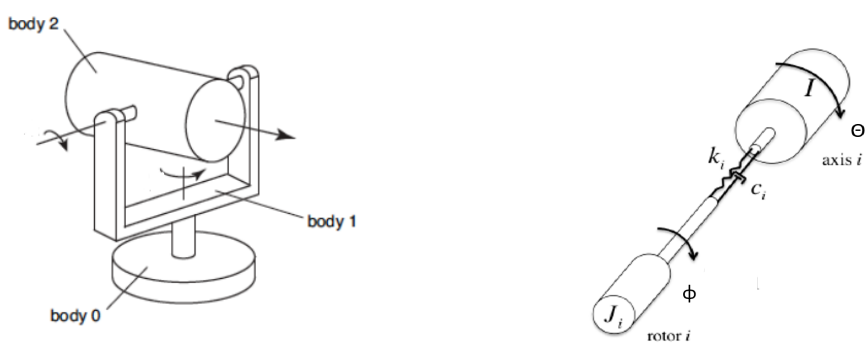

Figure 4.4: Two body gimbal diagram, where body 1 represents azimuth angle and body 2 represents elevation angle, (left) and flexible joint schematic (right), after [2].

The model describing the angular displacement of the flexible links has dy-

namics given by:

$$\begin{bmatrix} 9+\cos(2\theta_2) & 0 \\ 0 & 2 \end{bmatrix} \begin{bmatrix} \ddot{\theta}_1 \\ \ddot{\theta}_2 \end{bmatrix} + \begin{bmatrix} -2\dot{\theta}_1\dot{\theta}_2\sin(2\theta_2) \\ \dot{\theta}_1^2\sin(2\theta_2) \end{bmatrix} + c \begin{bmatrix} \dot{\theta}_1 - \dot{\phi}_1 \\ \dot{\theta}_2 - \dot{\phi}_2 \end{bmatrix} + k \begin{bmatrix} \theta_1 - \phi_1 \\ \theta_2 - \phi_2 \end{bmatrix} = \begin{bmatrix} 0 \\ 0 \end{bmatrix} \tag{4.1}$$

where (θ_1, θ_2) are the flexible joint angles and the dot notation represents the time derivative. Nominally, both parameters are set to be $(c, k) = (1, 1)$. A model for the motion of the rotor with angular displacement (ϕ_1, ϕ_2) is given by

$$\begin{bmatrix} \ddot{\phi}_1 \\ \ddot{\phi}_2 \end{bmatrix} - c \begin{bmatrix} \dot{\theta}_1 - \dot{\phi}_1 \\ \dot{\theta}_2 - \dot{\phi}_2 \end{bmatrix} - k \begin{bmatrix} \theta_1 - \phi_1 \\ \theta_2 - \phi_2 \end{bmatrix} = \begin{bmatrix} \tau_1 \\ \tau_2 \end{bmatrix}. \tag{4.2}$$

The control torques (τ_1, τ_2) are transmitted to the links via the flexible effects. The system of second order ordinary differential equations (ODEs) in Eq. 4.1 and 4.2 can be translated into a system of first order ODEs:

$$\begin{aligned}
\dot{x}_1 &= x_3 \\
\dot{x}_2 &= x_4 \\
\dot{x}_3 &= \tfrac{2x_3x_4\sin(2x_2) - c(x_3 - x_7) - k(x_1 - x_5)}{9 + \cos(2x_2)} \\
\dot{x}_4 &= \tfrac{x_3^2\sin(2x_2) - c(x_4 - x_8) - k(x_2 - x_6)}{2} \\
\dot{x}_5 &= x_7 \\
\dot{x}_6 &= x_8 \\
\dot{x}_7 &= \tau_1 + c(x_3 - x_7) + k(x_1 - x_5) \\
\dot{x}_8 &= \tau_2 + c(x_4 - x_8) + k(x_2 - x_6).
\end{aligned} \tag{4.3}$$

The dynamics, along with nominal values for the model parameters, can be used to formulate deterministic control problems. However, the model parameters, for example (c, k), are generally difficult to measure, or estimate, which introduces

uncertainty into the model and increases the potential for unwanted vibrations and drifting as will become clear in the following section.

4.2 Minimum Effort Nominal Control

Using the DGM model with flexible effects, an optimal control problem for executing a minimum control torque slew can be formulated. Denoting the dynamics given by Eq. (4.3) as

$$\dot{x} = f(x(t;p), p) + hu(t),$$

where the state and control vectors are given by

$$\begin{aligned} x &:= \begin{bmatrix} \theta_1 & \theta_2 & \dot{\theta}_1 & \dot{\theta}_2 & \phi_1 & \phi_2 & \dot{\phi}_1 & \dot{\phi}_2 \end{bmatrix}^T \\ u &:= \begin{bmatrix} \tau_1 & \tau_2 \end{bmatrix}^T, \end{aligned} \tag{4.4}$$

and p is a vector of parameters, in this case the damping and stiffness parameters $p = [c, k]$ and $h = [0\ 0\ 0\ 0\ 0\ 0\ 1\ 1]^T$. The optimal control problem for minimal control effort is given by

$$(FG) \begin{cases} \text{Minimize} & J[x(\cdot), \tau(\cdot)] := \int_{t_0}^{t_f} (\tau_1^2 + \tau_2^2)\, dt \\ \text{Subject to} & \dot{x} = f(x(t;p_0), p_0) + hu(t) \\ & (x(t_0), t_0) = (x_0, t_0) \\ & x(t_f) = x_f \\ & |\tau_{1,2}| \leq 1.5 \\ & t_f = 25, \end{cases}$$

where x_0 is the initial condition of the DGM and x_f is the target endpoint. Simulations in this chapter consider an example slew with initial condition at $x_0 = (10, 20, 0, 0, 10, 20, 0, 0)$ and final condition set to $x_f = (0, 25, 0, 0, 0, 25, 0, 0)$. The optimal control problem (FG) can be solved for the control state pair for given nominal parameter values $p_0 = [1, 1]$.

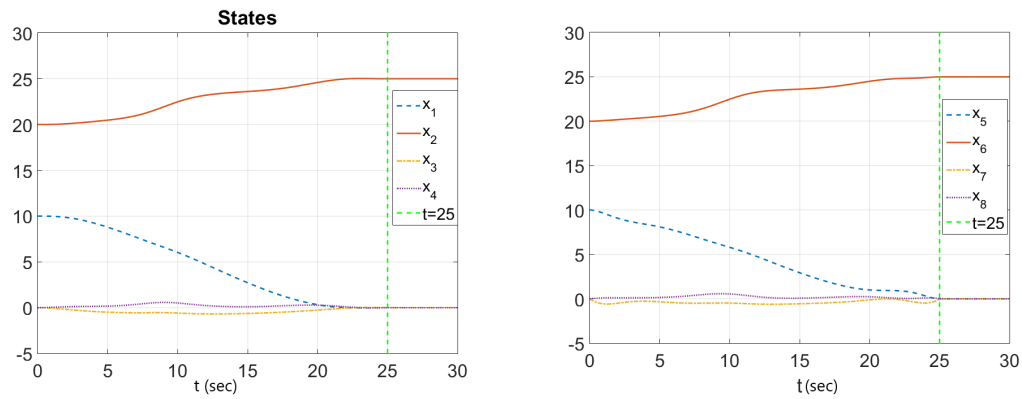

Figure 4.5: Optimal state trajectories generated by propagating controls generated by problem (FG).

Figure 4.5 shows the state trajectories of the nominal optimal control problem (FG) with $(c, k) = (1, 1)$ generated by the controls in Figure 4.6. The system is driven from the initial condition to the desired final condition precisely as seen by the interpolated controls and Runge-Kutta generated trajectories. Indeed, after the control horizon has concluded, the system is in equilibrium and remains stationary as there is no residual energy.

We can verify that the Hamiltonian is constant along these optimal controls. Figure 4.7 shows the constant Hamiltonian along with the KKT multipliers, which for problem (FG) should be zero as the controls never saturate.

The constant Hamiltonian and zero-valued KKT multipliers along with the feasibility of the generated controls help confirm the validity of the solution to problem (FG). This indicates that the solution provided by the computational optimal control algorithm successfully generated an optimal control candidate

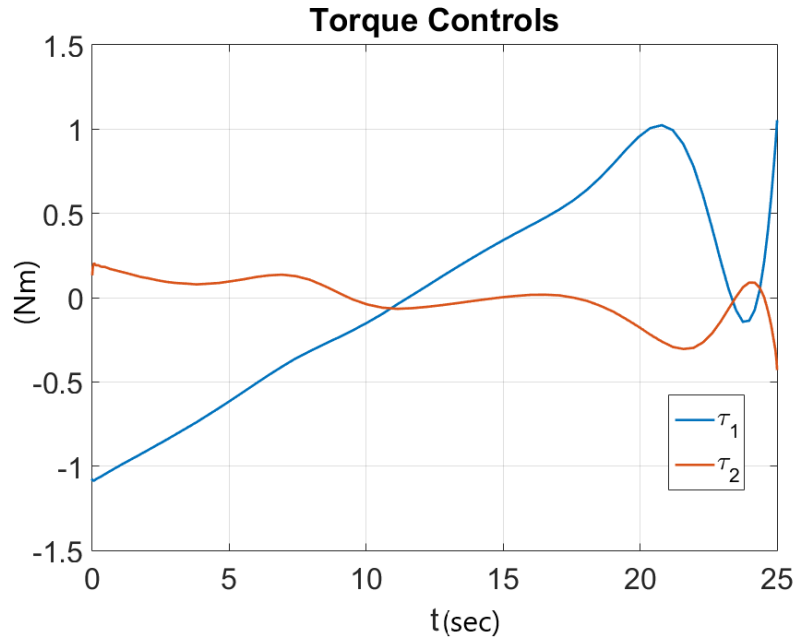

Figure 4.6: Optimal controls generated by problem (FG) interpolated for the desired time range.

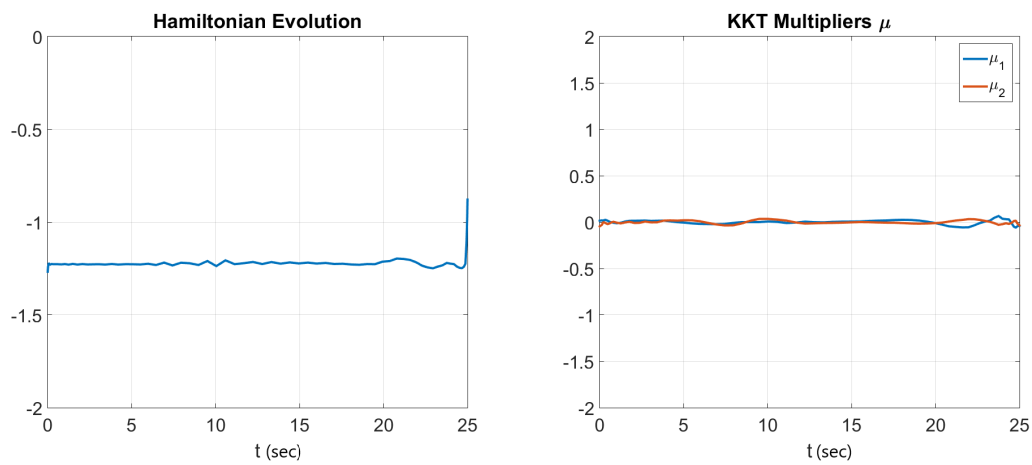

Figure 4.7: Necessary conditions for the minimum effort optimal control generated by problem (FG). Hamiltonian evolution (left) and KKT multipliers (right).

according to the Hamiltonian Minimization Condition.

4.3 Effects of Parameter Uncertainty

Problem (FG) assumes precise knowledge of the parameters which model the flexible effects, however, if uncertainty is introduced, the ability of the computed controls to finish the maneuver without exciting vibrations and/or drift is effected, especially for the long maneuver time slews. The two main parameters which model the flexible connection are stiffness parameter k and damping coefficient c. For this chapter uncertainty in the stiffness parameter will be exclusively considered, however, for a more complete picture of the uncertainty in the model both parameters can be explored.

The stiffness parameter can have a significant effect on unwanted drift once the maneuver has been completed. This can be seen clearly in Figure 4.8 and 4.9 which shows the state trajectories generated by the controls from Figure 4.5 for different $k \in [0.5, 1.5]$ values sampled from an assumed uniform distribution. In Figure 4.8 and 4.9. The trajectories associated with the off nominal parameter values tend to drift from the designated endpoint.

In order to understand the mechanism behind the drift it is important to note that the dynamics given by Eq. (4.2) have an equilibrium at rest when the state positions are aligned. The endpoint conditions from problem (FG) require that this equilibrium is reached, therefore, no additional motion should occur. Any divergence from the desired endpoints have potential for shifting away from the at rest equilibrium which is described by the stiffness parameter. The energy remaining in the system is the driving force behind the divergence from the desired endpoints.

A practical measure, which can be used as a metric describing the residual

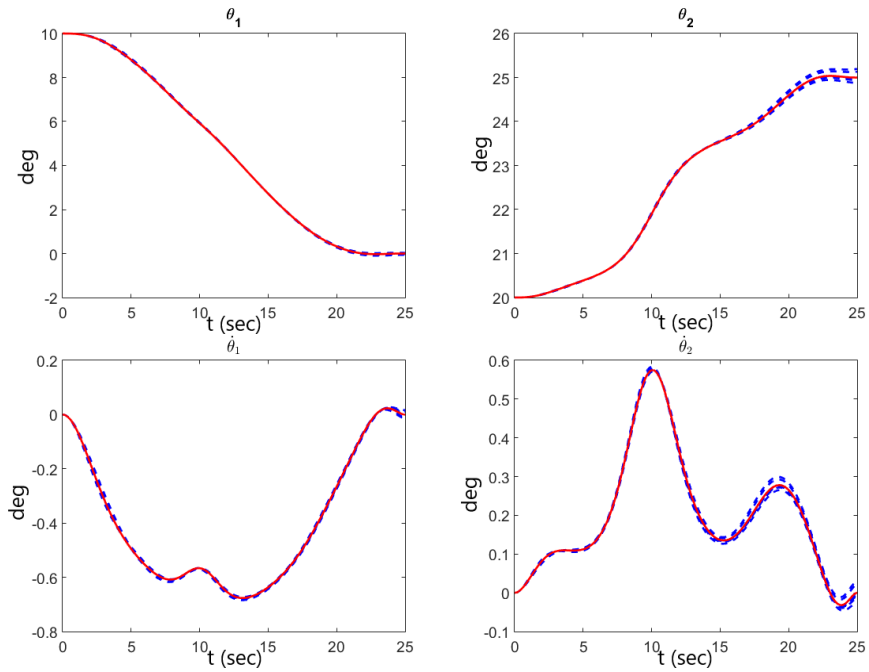

Figure 4.8: Effects of uncertain parameter k on the trajectories of θ and $\dot{\theta}$ for the nominal control signals. Nominal trajectories plotted in solid red.

energy at the final time, can be defined as

$$\begin{aligned} RE &= \frac{1}{2}k\left[(\theta_1(t_f)-\phi_1(t_f))^2+(\theta_2(t_f)-\phi_2(t_f))^2\right] \\ &+ \frac{1}{2}c\left[\dot{\theta}_1^2(t_f)+\dot{\theta}_2^2(t_f)+\dot{\phi}_1^2(t_f)+\dot{\phi}_2^2(t_f)\right], \end{aligned} \tag{4.5}$$

which describes a measure of kinetic summed with the potential energy at the endpoint of the controlled trajectory. We expect to see that, for the nominal case when there is no induced drift, there is no remaining energy in the system. Indeed Figure 4.10 shows that at the nominal stiffness value $k = 1$, there is no residual energy indicating the equilibrium of the system.

In order to quantify the effects of parameter uncertainty seen in Figure 4.8, A Monte Carlo simulation was used to compute the residual energy as a function of the uncertain stiffness parameter, k. The result shown in Figure 4.10 demon-

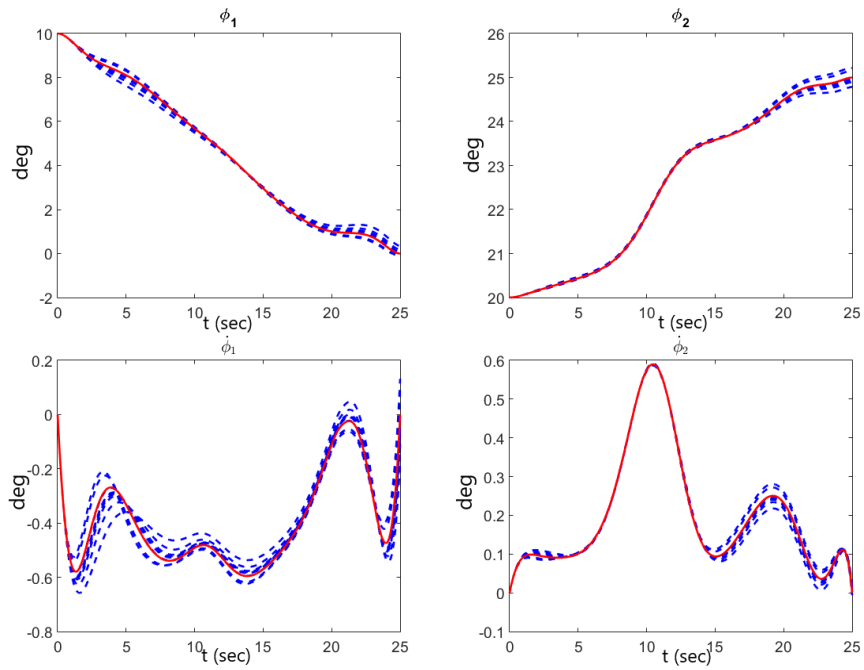

Figure 4.9: Effects of uncertain parameter k on the trajectories of ϕ and $\dot{\phi}$ for the nominal control signals. Nominal trajectories plotted in solid red.

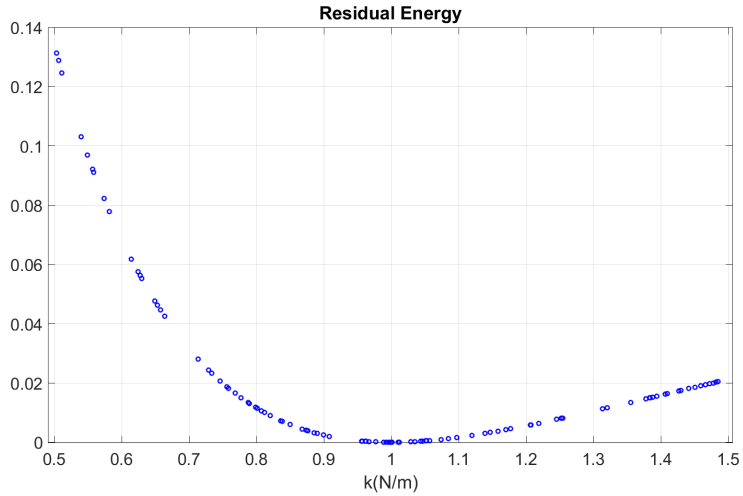

Figure 4.10: Residual energy for a range of uncertain k values for the nominal open loop minimum effort controls generated by problem (FG).

strates a nonlinear relationship between the residual energy and the uncertainty in the spring stiffness $k \in [0.5, 1.5]$. Clearly, except for nominal parameter value, a nonzero residual energy appears. This indicates the need for a mechanism which

manages this residual energy at the endpoints. Explicit consideration of the parameter uncertainty in an optimal control problem can be used to generate both open loop and feedback control signals, however, this generates the need for ways to quantify the effects of the uncertainty.

Figure 4.11 shows the sensitivities for the nominal trajectory generated by problem (FG) with respect to the stiffness parameter, k. The sensitivity functions indicate that the endpoint has non zero sensitivity to uncertainty in the stiffness parameter. This leads to non zero residual energy as in Figure 4.10.

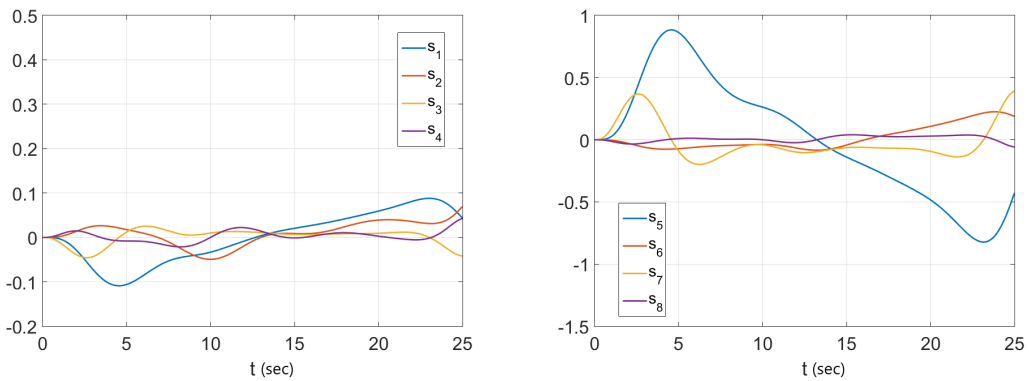

Figure 4.11: Sensitivity states for the first four states (left) and the final four states (right).

By approximating the effects of the parameter uncertainty using the sensitivity functions, we are able to quantify a time dependent expression which can be exploited to improve the robustness to the uncertainty. Higher order sensitivity functions can also be derived to further increase the order of the approximation.

In the following sections it will be demonstrated that these sensitivity functions can be used to formulate an optimal control problem for reducing local parameter effects via the sensitivity neighborhood feedback control outlined in the previous chapter. Additionally, the effectiveness of the unscented neighboring control design will be demonstrated for both the design of the feedback gains and for the design of robust open-loop controls.

4.4 Feedback

When information about the state variables is measurable, it is frequently advantageous to implement a feedback rule for managing the uncertainty in the model parameters. In the following section the feedback gains, which are designed according to the sensitivity neighboring and unscented neighboring problem are generated for the flexible gimbal.

4.4.1 Sensitivity Neighborhood

The flexible gimbal model includes eight states and two control variables which, for the control affine structure of interest, generates sixteen feedback gains. In order to get an idea of the effectiveness of the sensitivity based feedback control, we assume a partial state feedback where the states describing the flexible end are measurable. Conceptually, this could be considered a desirable case for the feedback information as knowing these states implies we are able to directly measure the amount of flex induced in the system.

The flexible gimbal model is of the form

$$\dot{x}(t;p) = f(x,p) + h_1\tau_1(t) + h_2\tau_2(t), \tag{4.6}$$

where $f(x,p)$ is a vector of dynamic functions and h_1, h_2 are constant vectors and the parameter of interest is one dimensional set as the stiffness parameter $p = k$.

Using the controls and states provided by the minimum effort problem (FG), we expand the open loop controls (τ_1, τ_2) in terms of the first four state variables

(x_1, x_2, x_3, x_4)

$$\begin{aligned} \tau_1 &= M_{11}(t)x_1 + M_{12}(t)x_3 + g_1(t) \\ \tau_2 &= M_{21}(t)x_2 + M_{22}(t)x_4 + g_2(t). \end{aligned} \tag{4.7}$$

where the feedback gain vectors are $M_1(t) \in \mathbb{R}^2, M_2(t) \in \mathbb{R}^2$ and $g_1(t), g_2(t)$ are scalar functions of time. With the expanded controls, the sensitivity states $s(t) \in \mathbb{R}^8$ are of the form

$$\dot{s} = \left[\left.\frac{\partial f}{\partial x}\right|_{k_0, x^{\text{Nom}}} + h_1 M_1(t) + h_2 M_2(t) \right] s(t) + \left.\frac{\partial f}{\partial k}\right|_{k_0, x^{\text{Nom}}}, \tag{4.8}$$

which we aim to minimize in order to reduce the effects of the stiffness parameter on the desired trajectory endpoints x_f. Using a cost functional for the endpoint sensitivity subject to the dynamics of the sensitivity states and with the feedback gains as the control variables, an optimal control problem based in the form of problem (FC) can be expressed as

$$(FC) \begin{cases} \text{Min} & J = \alpha ||s(t_f)||^2 + \int_{t_0}^{t_f} \beta \left(||M(t)||^2 + ||s(t)||^2 \right) dt \\ \text{S.t.} & \dot{s} = \left[\left.\frac{\partial f}{\partial x}\right|_{k_0, x^{\text{Nom}}} + h_1 M_1(t) + h_2 M_2(t) \right] s(t) + \left.\frac{\partial f}{\partial k}\right|_{k_0, x^{\text{Nom}}} \\ & s(t_0) = 0 \\ & t_f = 25. \end{cases}$$

The tuning parameters $(\alpha = 1, \beta = 10)$ are chosen to weight more heavily the feedback gains.

Once the feedback gains have been generated the open loop term can be solved for by forcing the controls to satisfy the nominal control along the nominal tra-

jectory

$$g(t) = u^{\text{Nom}} - M(t)x^{\text{Nom}}. \tag{4.9}$$

We now have a two degree of freedom (TDF) control that reduces the sensitivity at the trajectory endpoints, which is optimal for the nominal parameter value, and decreases the potential for endpoint drift.

Solving problem (FC) generates the feedback gains for sensitivity reduction and the open loop terms to satisfy the controls for the nominal model as seen in Figure 4.12. Evaluating the two degree of freedom control along the nominal

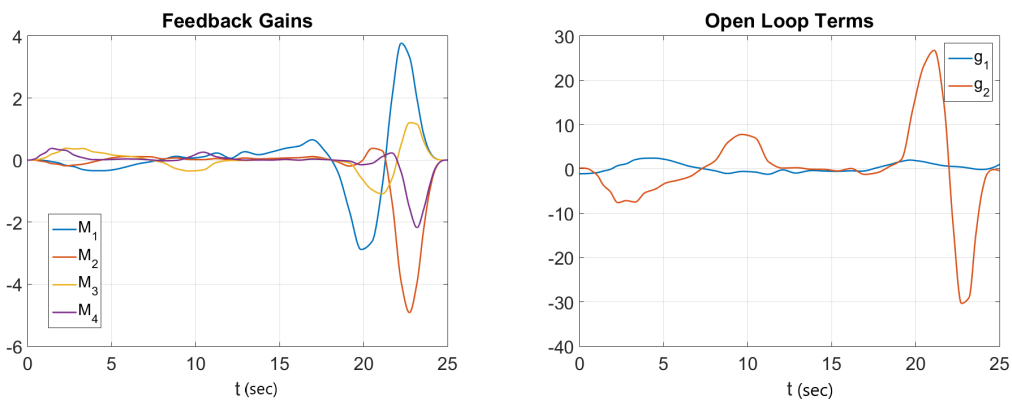

Figure 4.12: Feedback gains from optimal control problem (left) and the open loop controls (right).

trajectory recovers the nominal control shown in Figure 4.13.

The sensitivity functions with respect to parameter k are shown in Figure 4.14. Comparing to the ones shown in Figure 4.11, we clearly see a substantial decrease in the magnitudes of the endpoints of the sensitivity functions as expected.

The implemented TDF control successfully manages the sensitivity functions at the endpoint of the maneuver which should translate to a reduction in residual energy for a range of different stiffness values. Figure 4.15 shows the range of of the residual energies generated by the Monte Carlo simulations, illustrating the

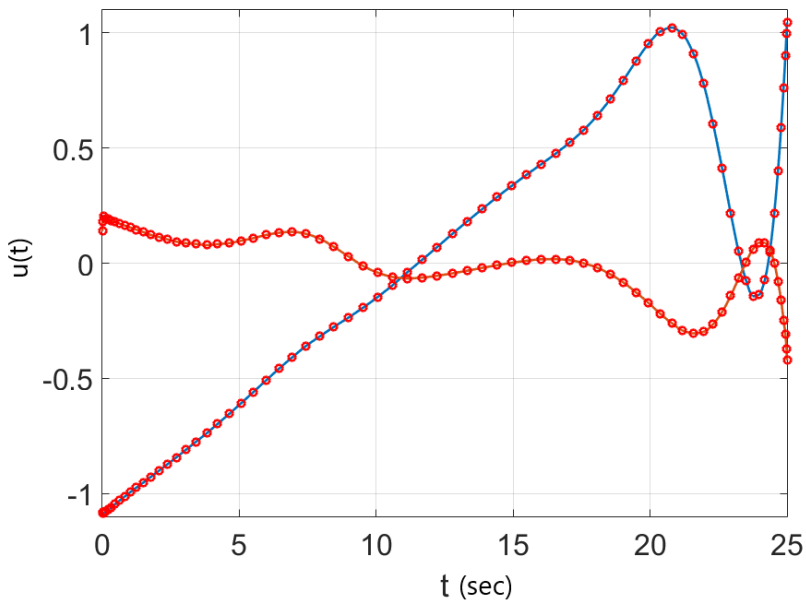

Figure 4.13: Nominal control signals (red dot) and TDF control (blue solid) for nominal state trajectories.

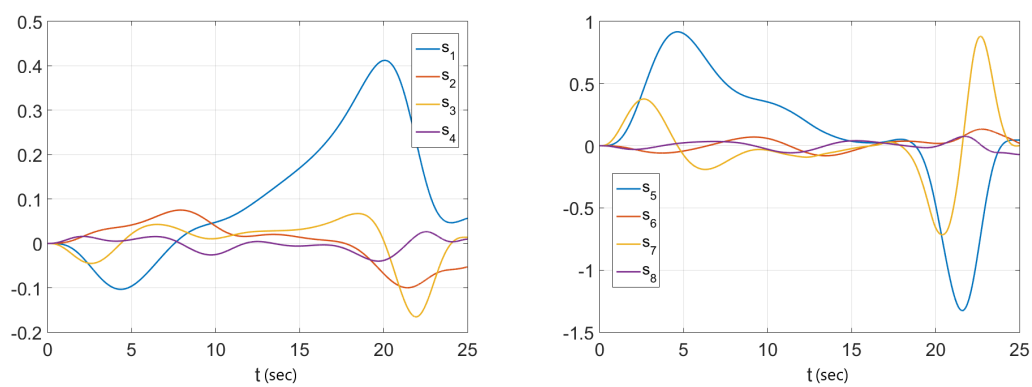

Figure 4.14: Sensitivity functions for sensitivity feedback control trajectory generated by the TDF controls.

effect of the sensitivity reduction on the residual energies compared to the nominal controls.

It is clear that by reducing the endpoint sensitivity the TDF control decreases the residual energy, therefore, reducing the potential for uncontrolled endpoint drift. Table 4.1 shows the statistics of the residual energy for a Monte Carlo

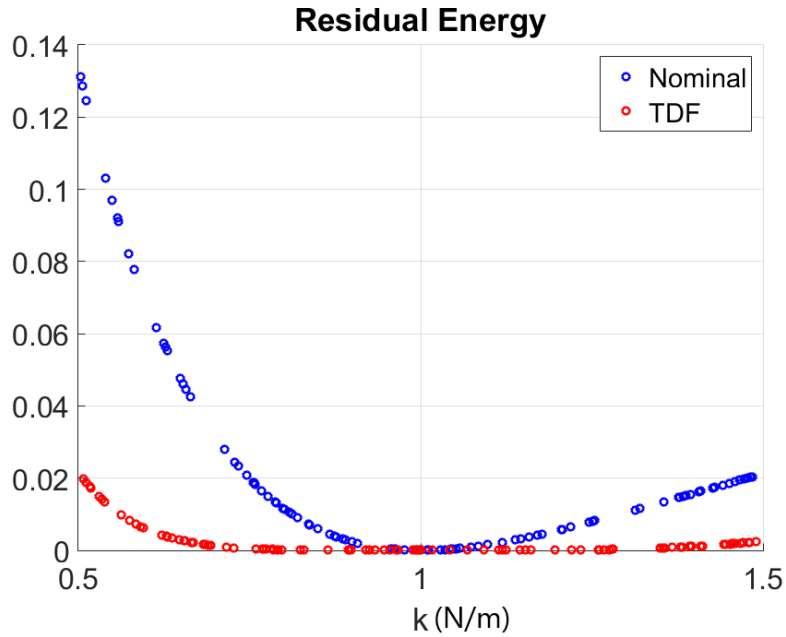

Figure 4.15: Residual energy for a range of uncertain k values for the nominal and TDF sensitivity controls.

simulation of 500 stiffness values sampled from the assumed uniform distribution. There is a -88% change in the mean residual energy and a -99% change in the variance from the nominal control.

4.4.2 Unscented Neighborhood

We now seek to design linear feedback gains according to the unscented neighboring optimal control outlined in the previous section. Discretizing the PDF of the stiffness parameter

$$k \in \mathcal{U}(0.5, 1.5)$$

using the spherical simplex sigma points [29] generates a number of samples needed for the single parameter uncertainty problem, in the case of the uniform distribu-

tion three samples. These parameter samples

$$k_{1,2,3} = (1, 0.8334, 1.1663),$$

and associated weights

$$w_{1,2,3} = (\frac{1}{4}, \frac{3}{8}, \frac{3}{8}),$$

form the state space of the unscented neighborhood

$$\begin{aligned} \delta x_i &= x(t, k_i) - x^{\text{Nom}}(t, k_0), \\ \delta \dot{x}_i &= f(x_i, t, k_i) - f(x^{\text{Nom}}, t, k_0) + h\delta u, \end{aligned}$$

for $i = 1, 2, 3$. The cost function is defined as

$$J_{unsc} = \sum_{i=1}^{3} w_i \|\delta x_i(t_f)\|^2 + \int_{t_0}^{t_f} \|K(t)\|^2 dt,$$

for minimizing the error state at the endpoints while also penalizing the control effort of the feedback gains. Therefore, the unscented neighboring optimal control problem for these feedback gains, which have the same partial feedback structure as in Eq. (4.7),

$$\delta x_i \in \mathbb{R}^{n_x}, \quad K(t) \in \mathbb{R}^{2\times 2}, \quad i = 1, 2, 3$$

$$(UDGM) \begin{cases} \text{Min} & J_{unsc} = \sum\limits_{i=1}^{3} w_i \|\delta x_i(t_f)\|^2 + \int_{t_0}^{t_f} \|K(t)\|^2 dt \\ \text{S.t.} & \delta \dot{x}_1 = f(x_1, t, k_1) - f(x^{\text{Nom}}, t, k_0) + h\delta u \\ & \delta \dot{x}_2 = f(x_2, t, k_2) - f(x^{\text{Nom}}, , t, k_0) + h\delta u \\ & \delta \dot{x}_3 = f(x_3 t, k_3) - f(x^{\text{Nom}}, t, k_0) + h\delta u \\ & \delta \dot{x}_i(t_0) = 0, \ t_f = 25 \end{cases}$$

can be solved computationally. Figure 4.16 shows the discrete controls interpolated over the maneuver time produced by solving problem ($UDGM$).

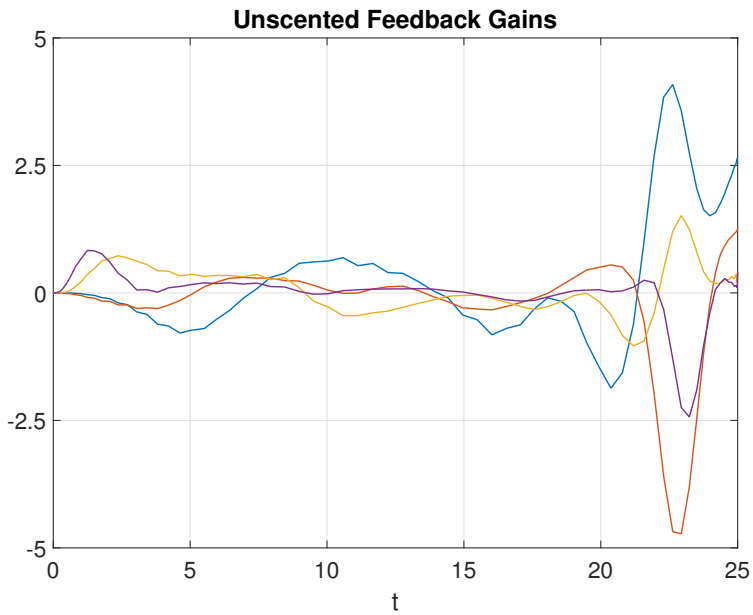

Figure 4.16: Unscented linear feedback gains.

To ensure the solution in Figure 4.16 is truly an optimal candidate, in addition to validating the dynamic constraints and endpoint constraints are met through propagation, verification of the partial derivative of the Hamiltonian is shown in Figure 4.17. Additionally, because the Hamiltonian has no explicit dependence on time the Hamiltonian Evolution Equation dictates that the Hamiltonian should be constant along the optimal trajectory. This also is verified in Figure 4.18.

The effectiveness of these unscented linear feedback gains is clear in Figure 4.19 where the same samples of the parameter as the previous cases is used for the propagation of the interpolated controls. There is a larger deviation along the nominal trajectory for the unscented feedback case compared to the trajectories for the sensitivity feedback gains however, this allows for a noticeably tighter grouping of the trajectory endpoints around the nominal. By not relying on

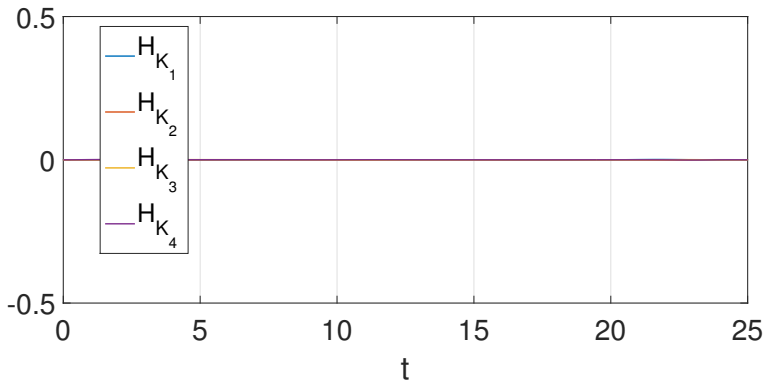

Figure 4.17: Minimized Hamiltonian partial derivatives evaluated along the optimal trajectories generated by the computational solver.

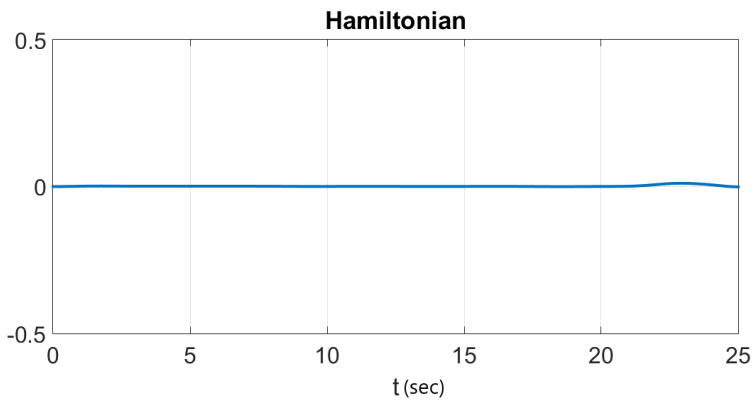

Figure 4.18: Hamiltonian evaluated along the optimal trajectories generated by the computational solver.

purely local measures of the error states like the sensitivity based case, there is conceptually more freedom for the unscented problem to seek a control using information perhaps outside the range of the linear neighborhood.

Figure 4.20 shows the Monte Carlo simulation for samples from the uniform distribution for the nominal open loop control and both the sensitivity and unscented feedback cases. Both feedback cases demonstrate a significant reduction in the residual energy values over the range of stiffness values, as expected. Furthermore, the unscented neighboring gains show an improved reduction across the entire range of parameter values.

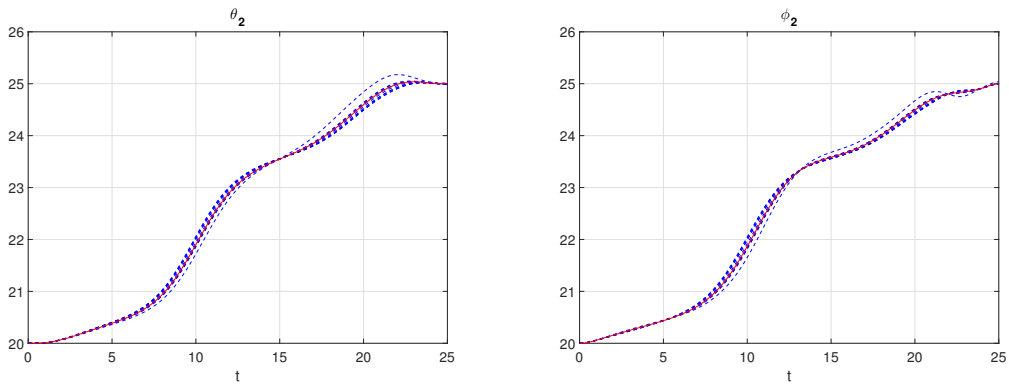

Figure 4.19: Effects of uncertain parameter k on the trajectories of θ_2 and ϕ_2 for the unscented TDF control signals. Nominal trajectories plotted in solid red.

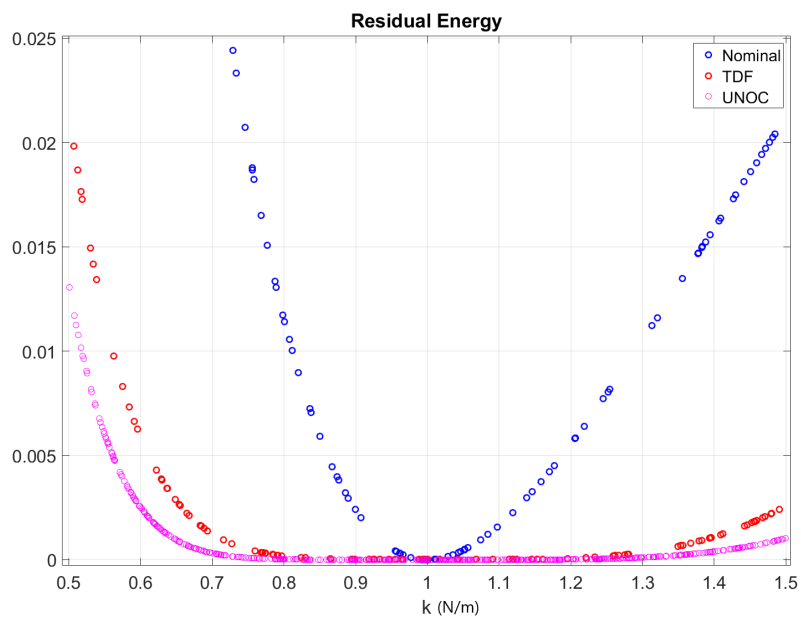

Figure 4.20: Residual energy for a range of uncertain k values.

In order to quantify the effects of the feedback improvements the mean and variance of these residual energies are shown in Table 4.1, which indicates roughly a 90% decrease from the nominal mean residual energy in the case of the linear neighborhood and a 97% decrease relative to nominal in the unscented neighborhood. Similarly, a 98% decrease in the variance relative to the nominal for the

linear and a 100% decrease for the unscented.

	Nominal	**LNOC**	**UNOC**
Mean(RE)	0.0206	0.0025	0.0008
Var(RE)	7.76e-4	1.02e-5	3.65e-6

Table 4.1: Mean and variance of the residual energy for the Monte Carlo simulations for the nominal, unscented and sensitivity TDF controls.

The improvement in robustness through the feedback portion of the TDF control laws adds an additional cost to the nominally designed open-loop controls, which is a well documented aspect of feedback sensitivity reduction. A measure of the extra effort defined as

$$\Delta u := \int_{t_0}^{t_f} |\delta u(t)| dt,$$

which is the integral of the absolute value deviation from the nominal control over the whole maneuver gives a metric to compare control effort relative to the nominal control. Due to the feedback nature of the control deviation, the value of this integral is different depending on the actual value of the stiffness parameter and must be computed for each sampled case of the Monte Carlo simulation. The mean and variance of these control efforts for both the sensitivity and unscented TDF controls are shown in Table 4.2. There is a clear increase in both mean and variance of the additional control efforts in the case of the unscented TDF which results in the improved performance seen in Table 4.2.

	LNOC	**UNOC**
Mean(Δu)	1.548	1.899
Var(Δu)	0.964	2.014

Table 4.2: Mean and variance of the deviation from the nominal control effort for the Monte Carlo simulations of the TDF unscented and sensitivity controls.

The unscented gains invoke a 23% increase in mean control effort over the range of parameter values relative to the sensitivity based gains and a 108% increase in the variance. In a small neighborhood around the nominal parameter value the control efforts of the two types of feedback are closely matched, however the benefit of the unscented gains seen in Figure 4.20 for larger parameter deviation account for much of the increase in the variance of the control effort over the sensitivity gains.

The unscented neighborhood feedback control demonstrates a significant improvement in robustness to the uncertainty in the spring constant compared with the nominal controls and sensitivity neighborhood controls. This is a novel approach to time-varying feedback gain design using the unscented framework. The efficacy of such optimal gains is clearly illustrated in this nonlinear example and proves to be a very promising tool for feedback gains design, however, the unscented neighborhood problem is not limited to purely feedback design. Using the same problem formulation it is possible to design open-loop controls which are inherently more robust to the uncertainty without the need for state information.

4.5 Open Loop

In the case where the information about the states is unavailable or difficult to measure, the unscented neighboring optimal control can be used to generate a new set of controls and trajectories which can reduce the risk of inducing unwanted vibrations and drift without the need for feedback.

A useful cost functional, which is based on the vector norm of the error states at the final time, can be formulated as

$$J = \int_{supp(k)} ||\delta x(t_f, k)||^2 g(k) dk. \tag{4.10}$$

which describes the endpoint spread from the nominal trajectory over the distribution of k. For the stiffness parameter $k \sim \mathcal{U}(0.5, 1.5)$, a discretization with three sigma points based on the spherical simplex points [29] can be generated the same as the samples used for feedback,

$$k_{1,2,3} = (0.8334, 1.1663, 1.0)$$

with weights

$$w_{1,2,3} = (\frac{3}{8}, \frac{3}{8}, \frac{1}{4}).$$

Using these sigma points and weights, the cost functional in Eq. 4.10 can be discretized as

$$J \approx \sum_{i=1}^{3} w_i ||\delta x_i(t_f, k_i)||^2.$$

The soft constraint on the feedback gains from the previous section is no longer strictly necessary. In the case of purely open-loop controls the control constraint can be formally applied as

$$u^L - u^{\text{Nom}} \leq \delta u \leq u^U - u^{\text{Nom}}$$

because the control effort will remain the same regardless of the deviations in the states.

The resulting open-loop neighboring unscented optimal control problem is

given by

$$\delta x_i \in \mathbb{R}^{n_x}, \quad \delta u(t) \in \mathbb{R}^2, \quad i = 1, 2, 3$$

$$(UDG) \begin{cases} \text{Min} & J_{unsc} = \sum_{i=1}^{3} w_i \|\delta x_i(t_f)\|^2 \\ \text{S.t.} & \delta \dot{x}_1 = f(x_1, t, k_1) - f(x^{\text{Nom}}, t, k_0) + h\delta u \\ & \delta \dot{x}_2 = f(x_2, t, k_2) - f(x^{\text{Nom}}, t, k_0) + h\delta u \\ & \delta \dot{x}_3 = f(x_3, t, k_3) - f(x^{\text{Nom}}, t, k_0) + h\delta u \\ & \delta \dot{x}_i(t_0) = 0, \ t_f = 25, \\ & u^L - u^{\text{Nom}} \leq \delta u \leq u^U - u^{\text{Nom}}. \end{cases}$$

Problem (UDG) is a fully deterministic optimal control problem and can be solved using the same computational method as problem (FG). The solution of problem (UDG) is the control perturbation shown in Figure 4.21. When combined with the nominal control designed for the minimum effort control, the resulting time-varying control signal is nicely behaved.

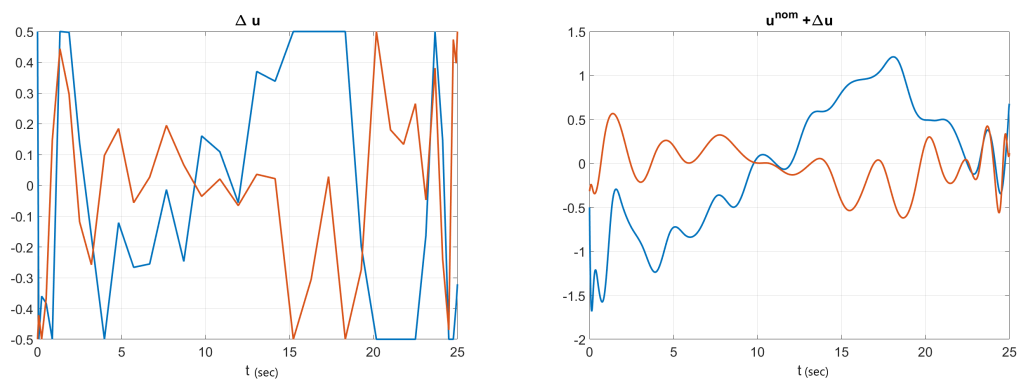

Figure 4.21: Control perturbation and total control resulting from the open-loop unscented neighborhood problem

Figures 4.22 and 4.23 show the trajectories for different parameter values using the unscented optimal control. Compared to Figure 4.8 and 4.9, the unscented optimal control significantly reduces endpoint drift in the open loop. Addition-

ally, the nominal trajectories generated by the unscented controls are noticeably different from the nominal trajectories used in the feedback case. This variation demonstrates that it is possible to design trajectories which are inherently more robust using the neighboring unscented framework.

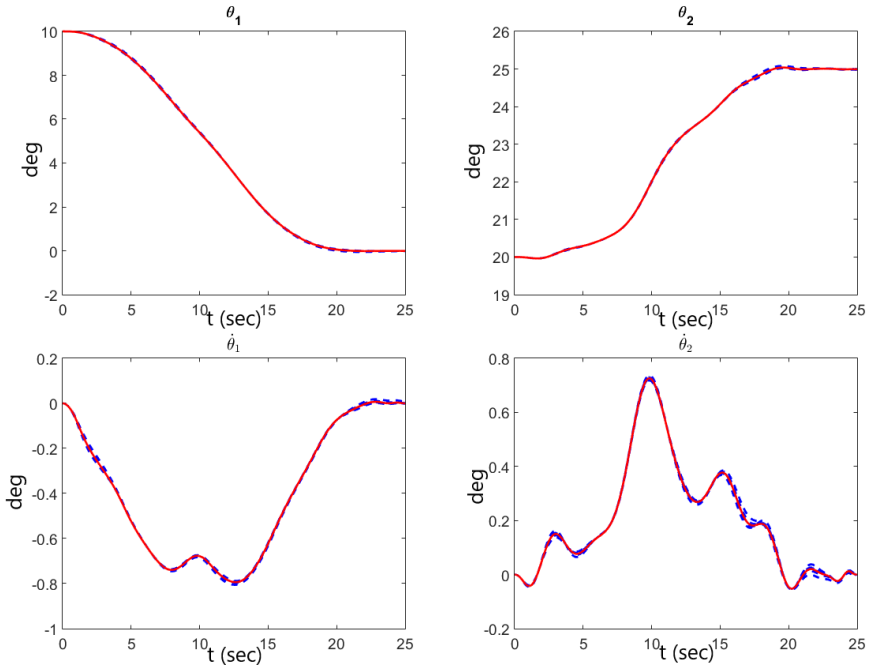

Figure 4.22: Effects of uncertain parameter on the unscented trajectories

We can compare the performance to the nominal and unscented feedback control by sampling the same uniform distribution of possible stiffness parameter values via the Monte Carlo simulation. Figure 4.24 demonstrates the effectiveness of the open loop controls generated by the unscented problem formulation. This open loop performance has been achieved with only three samples of the uncertainty distribution. There is a clear reduction in the residual energies compared to the nominal case for a large span of the uncertainty. In fact, the open-loop unscented controls achieve much of the performance of the sensitivity neighborhood feedback controls without relying on state measurement.

Table 4.3 shows there is a -67% change in the mean residual energy and a

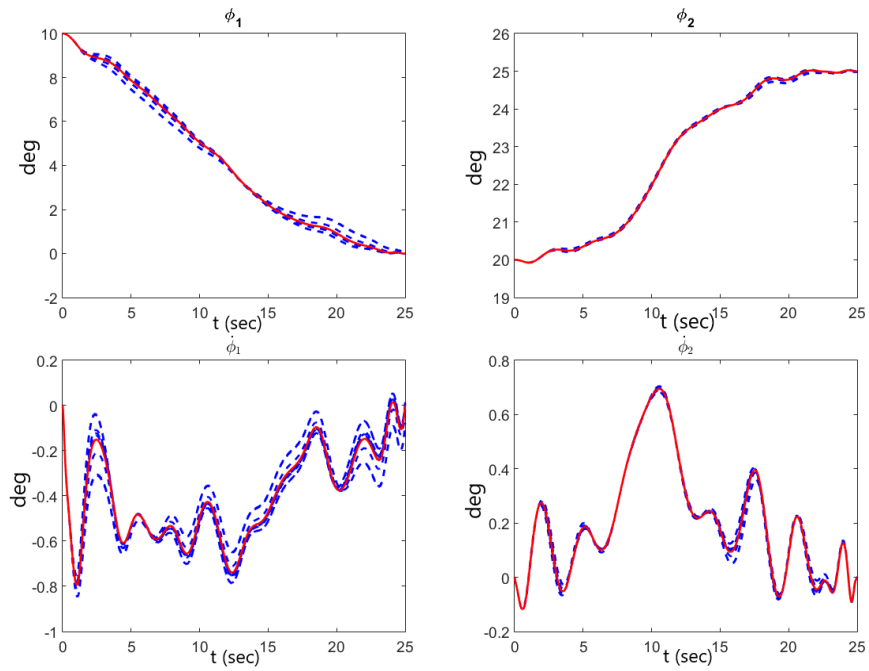

Figure 4.23: Effects of uncertain parameter on the unscented trajectories

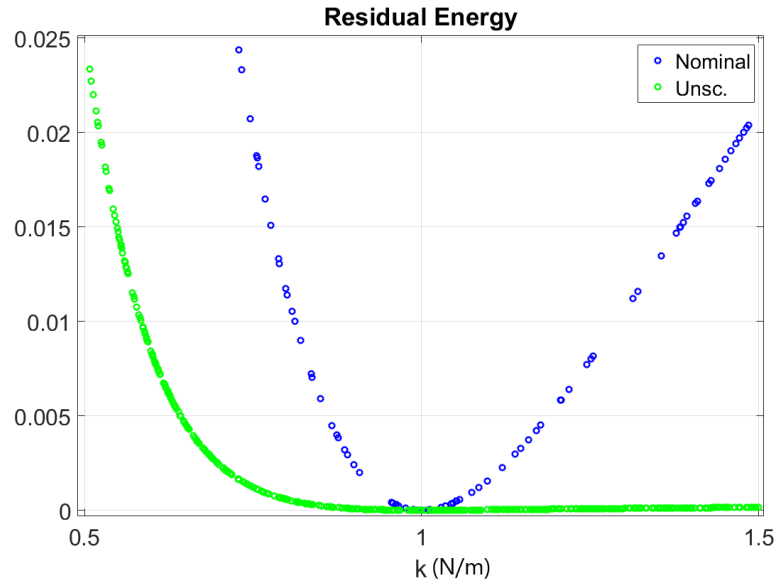

Figure 4.24: Residual Energy of the nominal and unscented optimal controls for the uncertain k.

-82% change in the variance indicating that a large improvement over the nominal open-loop control can be obtained without resorting to feedback. The unscented

	Nominal	Unscented	UNOC
Mean(RE)	0.0206	0.0023	0.0008
Var(RE)	7.76e-4	2.06e-5	3.65e-6

Table 4.3: Mean and variance of the residual energy for the Monte Carlo simulations for the nominal, open-loop unscented and unscented neighboring controls.

feedback controls still achieve a greater reduction in the mean and variance of the residual energy, however, the performance of the open-loop method is still significant. As demonstrated in the case of the linear spring system in previous chapters, one advantage of designing the robust open-loop maneuver is that it has the potential to rely less on a feedback controller.

4.6 Conclusion

The flexible gimbal model explored numerically in this chapter provides a clear demonstration of the usefulness of the neighboring sensitivity and unscented optimal control that was developed earlier in this dissertation. In both the feedback and open-loop case, there was significant improvement in the robustness of the nonlinear system to the uncertainty in the spring constant term. While open-loop unscented controls have been computed for other applications, not specifically the double gimbal, the framework by which the control problem was formulated in this case is novel. Additionally, this chapter presents the first example of an unscented neighboring feedback control problem for nonlinear, or linear, plants.

Chapter 5

Two Link Flexible Robot Arm Experiment

In this chapter, the efficacy of the unscented optimal controls for managing uncertainty in model parameters is demonstrated on a laboratory robotic arm with flexible effects. The robotic arm is a flexible two-link robotic arm (FTLRA) from Quanser shown in Figure 5.1.

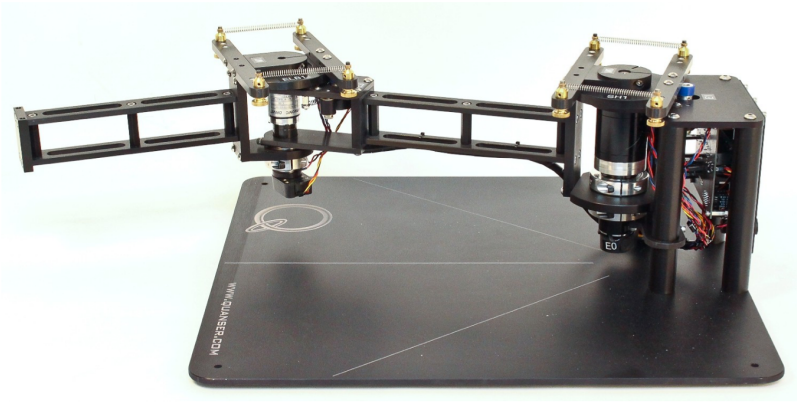

Figure 5.1: Two flexible link robotic arm from Quanser.

The mathematical model for the FTLRA shares the structure of the double

gimbal with flexible effects explored in the previous chapter, however, the model for the Quanser arm is more complex and contains twenty model parameters which have either been measured in lab or provided by Quanser.

In this chapter the open loop controls for the Quanser arm, without consideration of uncertainty, are shown to be ineffective for a minimum effort maneuver. Considering the difference between the computational model and the actual FTLRA is due to inaccuracy in the measurement of the model parameters, specifically in the spring constant of the first link, the two degree of freedom unscented neighboring control is used to design both open-loop and feedback controls for closing the gap between the simulation and actual responses.

5.1 Model of the Flexible Arm

Similar to the double gimbal model introduced in the previous chapter, the dynamics of the two-link flexible arm can be written in the form

$$M(q)\ddot{q} + C(q,\dot{q})\dot{q} + Kq = F(u) \tag{5.1}$$

for $M, C, K \in \mathbb{R}^{4\times 4}$, $F \in \mathbb{R}^{4\times 1}$, and the state, $q \in \mathbb{R}^{4\times 1}$ and control $u \in \mathbb{R}^{2\times 1}$ vectors are

$$q = \begin{bmatrix} \theta_1 & \theta_2 & \phi_1 & \phi_2 \end{bmatrix}^T, \qquad u = \begin{bmatrix} i_1 & i_2 \end{bmatrix}^T.$$

The coefficient matricies are state dependent resulting in a nonlinear model with twenty model parameters give by

$$M = \begin{bmatrix} m_{1,1} & m_{1,2} & 0 & 0 \\ m_{2,1} & m_{2,2} & 0 & 0 \\ 0 & 0 & I_{r,1} & 0 \\ 0 & 0 & 0 & I_{r,2} \end{bmatrix},$$

where the upper left submatrix is given by

$$\begin{aligned} m_{1,1} &= I_1 + I_2 + m_1 d_1^2 + m_2(l_1^2 + d_2^2) + 2m_2 l_1 d_2 cos(\theta_2) \\ m_{1,2} &= I_2 + m_2 d_2^2 + m_2 l_1 d_2 cos(\theta_2) \\ m_{2,1} &= I_2 + m_2 d_2^2 + m_2 l_1 d_2 cos(\theta_2) \\ m_{2,2} &= I_2 + m_2 d_2^2. \end{aligned}$$

The damping matrix is given by

$$C = \begin{bmatrix} -m_2 l_1 d_2 sin(\theta_2)\dot{\theta}_2 + c_1 & -m_2 l_1 d_2 sin(\theta_2)(\dot{\theta}_1 + \dot{\theta}_2) & -c_1 & 0 \\ m_2 l_1 d_2 sin(\theta_2)\dot{\theta}_1 & c_2 & 0 & -c_2 \\ -c_1 & 0 & c_1 + \Delta c_1 & 0 \\ 0 & -c_2 & 0 & c_2 + \Delta c_2 \end{bmatrix},$$

and the spring matrix and forcing vector are

$$K = \begin{bmatrix} k_1 & 0 & -k_1 & 0 \\ 0 & k_2 & 0 & -k_2 \\ -k_1 & 0 & k_1 & 0 \\ 0 & -k_2 & 0 & k_2 \end{bmatrix}, \qquad F = \begin{bmatrix} 0 \\ 0 \\ \eta K_{T,1} K_{g,1} i_1 \\ \eta K_{T,2} K_{g,2} i_2 \end{bmatrix}.$$

Symbol	Value	Symbol	Value
m_1	$2.64kg$	m_2	$0.873kg$
d_1	$0.159m$	d_2	$0.055m$
I_1	$0.0392kgm^2$	I_2	$0.00808kgm^2$
l_1	$0.343m$	η	0.75
c_1	$0.0176Nms/rad$	c_2	$0.0282Nms/rad$
k_1	$9.9Nm/rad$	k_2	$4.2Nm/rad$
$I_{r,1}$	$0.0637kgm^2$	$I_{r,2}$	$0.00351Kgm^2$
Δc_1	$4.05Nms/rad$	Δc_2	$0.125Nms/rad$
$K_{T,1}$	$0.119Nm/A$	$K_{T,2}$	$0.0232Nm/A$
$K_{g,1}$	$100:1$	$K_{g,2}$	$50:1$

Table 5.1: Model parameter values for the two link flexible Quanser robotic arm.

The input controls are the currents provided to the motors attached to both shafts of the arm. A nominal set of model parameters is determined via a combination of previously performed experimentation and documentation of the robotic arm provided by Quanser. These parameter values are shown in Table 5.1.

A Simulink model for applying controls is provided by Quanser. The Simulink model is versatile in how it lets the user apply various controls and reference state trajectories. Additionally, the software provides pre-computed LQR constant feedback gains specifically designed for a linearized version of the FTLRA model. These gains can accommodate both full and partial state feedback as desired by the user.

The feedback gains designed for the flexible arm are

$$K_{LQR1} = [15.2974, -1.1552, 0.70934, 1.7291]$$

$$K_{LQR2} = [9.3175, -2.9929, 0.20336, 0.24391],$$

which are used to generate the feedback current contribution by multiplying the difference between the designed reference states and the measured states of the arm as

$$K_{LQR1}\begin{bmatrix}(\phi_1^{meas}-\phi_1^{nom})\\(\theta_1^{meas}-\theta_1^{nom})\\(\dot{\phi}_1^{meas}-\dot{\phi}_1^{nom})\\(\dot{\theta}_1^{meas}-\dot{\theta}_1^{nom})\end{bmatrix}$$

$$K_{LQR2}\begin{bmatrix}(\phi_2^{meas}-\phi_2^{nom})\\(\theta_2^{meas}-\theta_2^{nom})\\(\dot{\phi}_2^{meas}-\dot{\phi}_2^{nom})\\(\dot{\theta}_2^{meas}-\dot{\theta}_2^{nom})\end{bmatrix}. \tag{5.2}$$

Figure 5.2 shows the control diagram used by the Quanser robotic arm. The LQR gains provided by the Quanser group can be modified to allow for fully open-loop, partial feedback and full feedback by setting specific gains to zero.

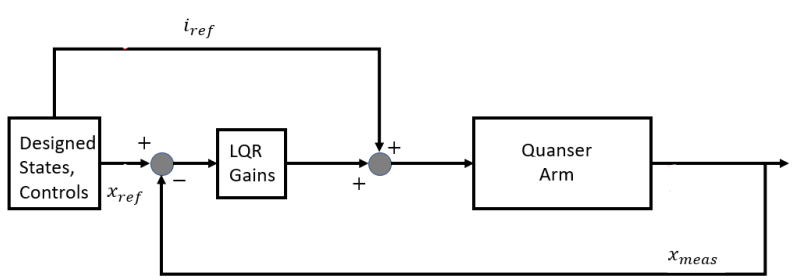

Figure 5.2: Control diagram of the Quanser robotic arm.

Using this model and control structure a nominal reference maneuver can be designed and implemented on the Quanser arm.

5.2 A Nominal Minimum Current Maneuver

Previous work done on this Quanser flexible arm indicated that, in the purely open-loop, there exists some error between the model of the arm and the actual device. This was determined to be likely due to inaccuracies in the model parameters measured for the model shown in the previous section. This discrepancy can be shown using a minimum current nominal maneuver designed using the mathematical model in Eq. (5.1).

A sample maneuver which drives the system from

$$q(0) = [0^\circ, 0^\circ, 0^\circ, 0^\circ]^T, \quad \dot{q}(0) = [0, 0, 0, 0]^T$$

to

$$q(t_f) = [-30^\circ, 30^\circ, -30^\circ, 30^\circ]^T, \quad \dot{q}(t_f) = [0, 0, 0, 0]^T$$

is used for final time $t_f = 1$. This choice of final time is related to the minimum time maneuver for this model, which terminates $0.71s$, with additional time included to allow for a minimum effort control. The maneuver of interest is depicted in the diagram shown in Figure 5.3.

Figure 5.3: Test maneuver for the Quanser robot arm for a -30 degree movement in the shoulder joint and a +30 degree movement of the elbow joint.

An optimal control problem for the motor currents can be formulated as

$$x = [q, \dot{q}]^T \in \mathbb{R}^8, \quad u = [i_1, i_2]^T \in \mathbb{R}^2$$

$$(FRA) \begin{cases} \text{Minimize} & J[x(\cdot), u(\cdot)] := \int_{t_0}^{t_f} (i_1^2 + i_2^2)\, dt \\ \text{Subject to} & \dot{x} = \begin{bmatrix} \dot{q} \\ M^{-1}[-C\dot{q} - Kq + F(u)] \end{bmatrix} \\ & (x(t_0), t_0) = (x_0, 0) \\ & (x(t_f), t_f) = (x_f, 1) \\ & |i_{1,2}| \leq [0.47, 0.60]^T. \end{cases}$$

The control constraints on i_1, i_2, are chosen such that there is sufficient control effort remaining for the addition of feedback. Solving problem (FRA) generates the input currents for the designated maneuver shown in Figure 5.4.

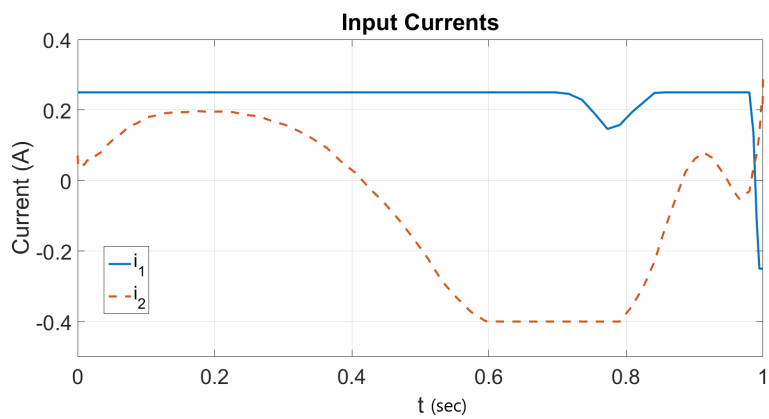

Figure 5.4: Minimum current controls for Quanser robotic arm.

Ideally, when feeding the input currents from Figure 5.4 to the Quanser arm the expected maneuver will be executed. This assumes that the model is accurate with precise model parameters. Passing these designed input currents to the Quanser arm, the desired input currents and the actual measured input currents can be compared. Figure 5.5 shows these designed and measured currents. The

controller has built in friction compensation which accounts for the fairly constant deviation from the desired.

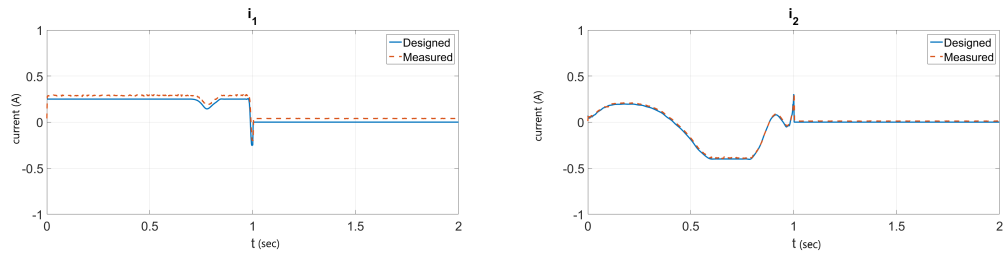

Figure 5.5: Implemented nominally designed currents.

These currents, which match very closely with the desired, generate measured states which have a large error at the endpoints. Figure 5.6 shows the designed and measured angle states of both the shoulder and elbow shaft and link angles. The applied current ends at the one second march at which time the system is allowed to settle to the steady state. It is clear in Figure 5.6 that the steady state reached is significantly different from the desired final angles.

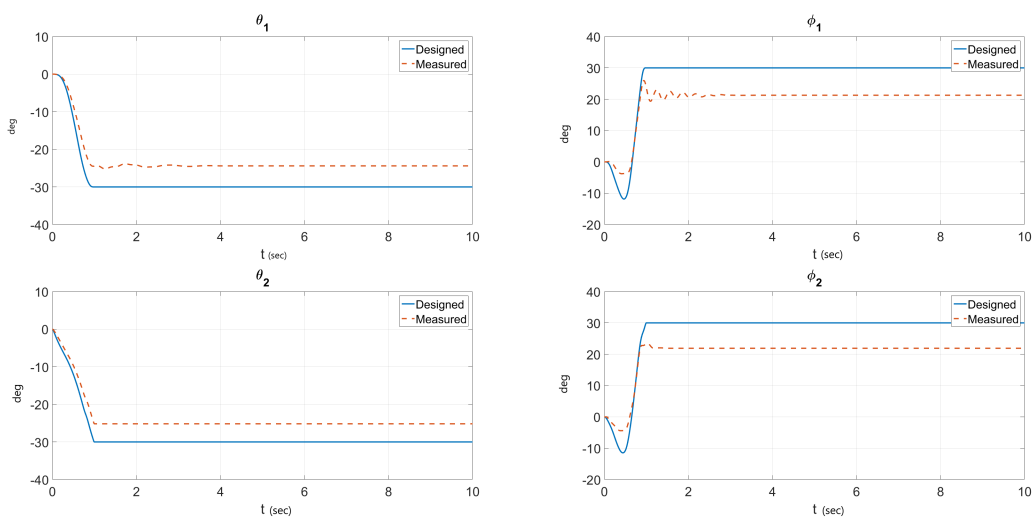

Figure 5.6: open-loop state trajectories generated by the nominally designed current signals.

The error seen in Figure 5.6 is likely due to measurement or approximation error in the model parameters. Without dedicating the time to investigate each

parameter individually, an intuition of model uncertainty in the system can be gained via the sensitivity functions. The sensitivity of the maneuver to uncertainty in the various model parameters is shown in Table 5.2. The table shows the endpoint sensitivity function values for the relative sensitivity functions, the sensitivity functions scaled by the nominal parameter value. For the values which have a larger value, any uncertainty in the measurement of the associated model parameter has more of an effect on the ability of the input currents to achieve the desired endpoint condition. In which case, the spring constant of the shoulder joint k_1, appears to be fairly large, as well as the damping coefficients $\Delta c_{1,2}$.

$\mathbf{c_1}$	$\mathbf{k_1}$	$\mathbf{c_2}$	$\mathbf{k_2}$	$\mathbf{\Delta c_1}$
1.62e-4	1.231	0.0047	0.4959	1.1361
$\mathbf{\Delta c_2}$	$\mathbf{I_1}$	$\mathbf{I_2}$	$\mathbf{m_1}$	$\mathbf{m_2}$
1.8371	0.016	0.3717	0.0463	0.4088
$\mathbf{d_1}$	$\mathbf{d_2}$	$\mathbf{l_1}$	$\mathbf{K_{T,1}}$	$\mathbf{K_{T,2}}$
0.1851	0.0659	1.1573	0.6990	0.6094
$\mathbf{K_{g,1}}$	$\mathbf{K_{g,2}}$	$\mathbf{I_{r,1}}$	$\mathbf{I_{r,2}}$	$\boldsymbol{\eta}$
0.6991	0.6101	0.1521	0.4875	1.1480

Table 5.2: Norm of the scaled endpoint sensitivity functions, $\|s(t_f)\|^2$, of the nominal maneuver

The error from the nominal maneuver can be managed using the feedback gains designed for the Quanser arm according to Eq. (5.2) and Figure 5.2. Figure 5.7 shows that the constant gains can be used to close the gap between the open-loop states and the desired states for partial feedback on the shaft angles and angular velocity of the shoulder and elbow.

In the case of the double gimbal, the unscented open-loop and feedback control perturbations δu demonstrated marked improvement in simulations to uncertainty in the spring parameter. For the Quanser arm, potential measurement error in the shoulder spring constant may have a relatively large effect on the endpoints.

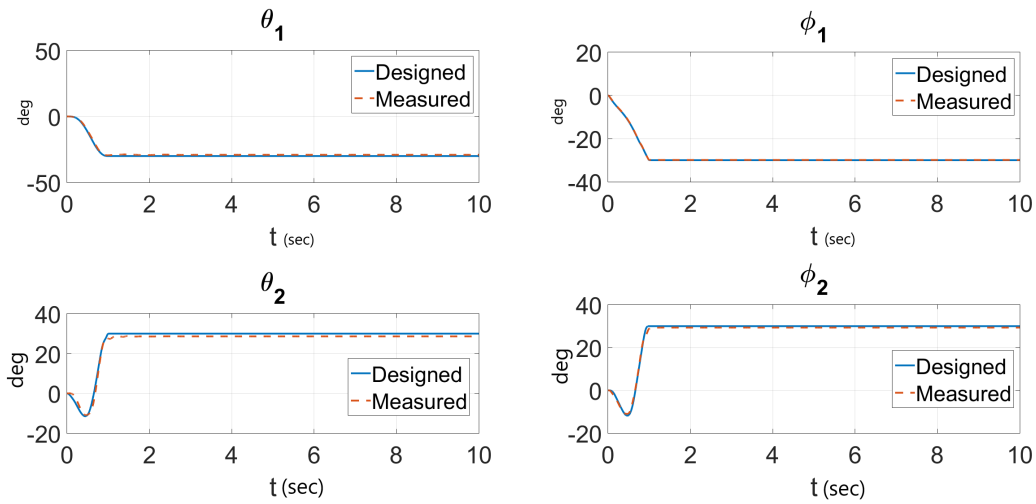

Figure 5.7: Implemented nominal maneuver using the constant partial feedback gains provided by the Quanser software.

This observation is further supported via inspection of the Quanser arm. Figure 5.8 shows the spring apparatus for the shoulder joint where there is a noticeable difference in the two springs which make up the flexibility of the shoulder. The

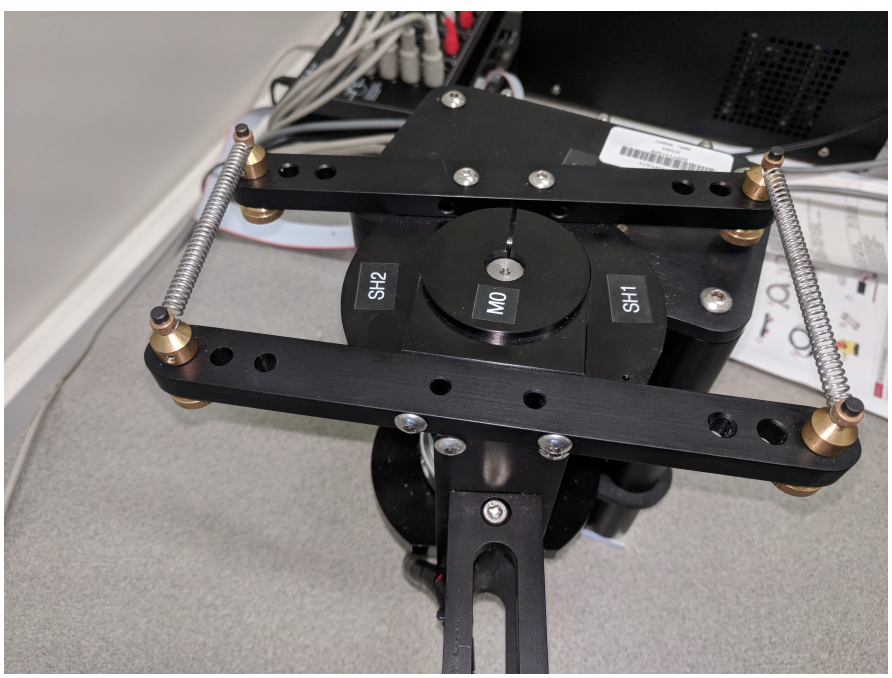

Figure 5.8: Observed inequality in spring action for shoulder joint of the Quanser arm.

model used for designing the nominal maneuver assumes symmetric spring values which is clearly not the case. A new model can be derived which does not used this assumption, or, the spring constant of the shoulder can be assumed to be uncertain and the neighboring unscented optimal control problem can be used to generate both open-loop and feedback controls to try and obtain more desirable results.

5.3 Unscented Neighboring Control for Spring Constant

A clear improvement in robustness was demonstrated via simulation of the double gimbal, which motivates the application of neighboring unscented control to the Quanser arm. The spring constant of the shoulder joint, which is likely incorrect and also has a large endpoint sensitivity value, is a strong candidate for the unscented controls. Assuming the uncertainty in k_1 is subject to a Gaussian distribution with a 15% standard deviation

$$k_1 \in \mathcal{N}(9.9, 1.41^2),$$

the samples and weights can be generated according to the simplex sigma points of the Gaussian, which in one dimension, are the Hermite-Gauss quadrature points. These samples and weights are

$$k = [9.9, 8.49, 11.31] \qquad w = [1.18, 0.2954, 0.2954].$$

The cost function for minimum endpoint error spread using these weighted sigma points becomes

$$J_{unsc} = \sum_{i=1}^{3} w_i \|\delta x_i(t_f)\|^2.$$

The neighboring unscented control problem for the open-loop control perturbations can be formulated as

$$\delta x_i \in \mathbb{R}^8, \quad \delta u(t) \in \mathbb{R}^2, \quad i = 1, 2, 3$$

$$(UFA) \begin{cases} \text{Min} & J_{unsc} = \sum_{i=1}^{3} w_i \|\delta x_i(t_f)\|^2 \\ \text{S.t.} & \delta \dot{x}_1 = f(x_1, t, k_1) - f(x^{\text{Nom}}, t, k_0) + h\delta u(t) \\ & \delta \dot{x}_2 = f(x_2, t, k_2) - f(x^{\text{Nom}}, t, k_0) + h\delta u(t) \\ & \delta \dot{x}_3 = f(x_3, t, k_3) - f(x^{\text{Nom}}, t, k_0) + h\delta u(t) \\ & (\delta x(t_0), t_0) = (0, 0) \\ & t_f = 1. \end{cases}$$

Solving problem (UFA) generates the control perturbations shown in Figure 5.9. The figure shows that more effort is used in modifying the currents applied to the shoulder motor than is applied to the elbow motor. The overconstrained controls in the nominal system allow for a reasonable amount of control effort to be used to improve the robustness.

When these control perturbations are combined with the nominal control currents and implemented via the Quanser software the resulting applied currents are shown in Figure 5.10. The shaft and link angle states generated from these input controls are shown in Figure 5.11.

There is a significant improvement in the steady state errors for the open-

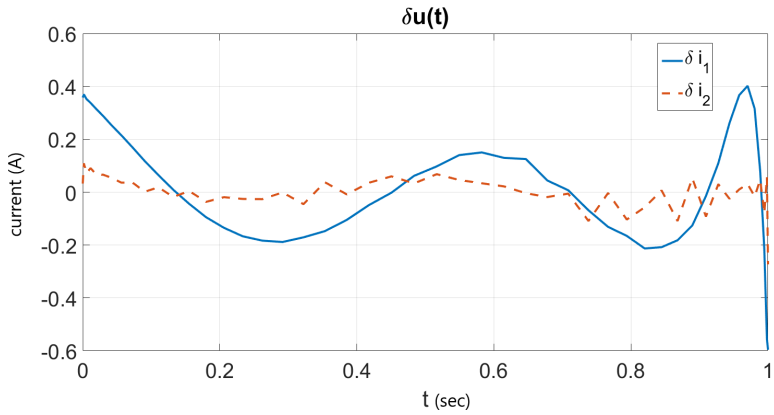

Figure 5.9: Unscented control contributions generated by the neighboring unscented problem for open-loop control.

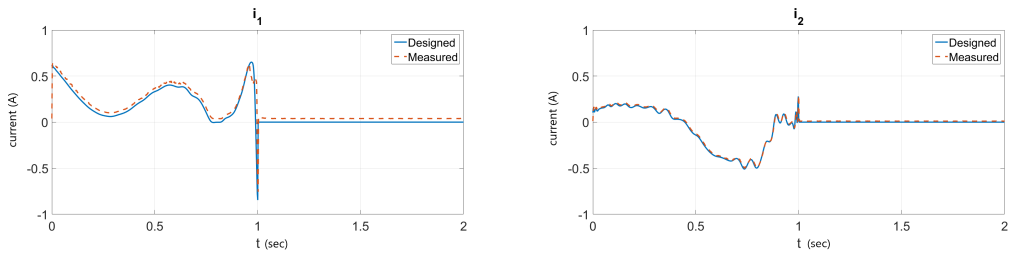

Figure 5.10: Implemented unscented designed currents.

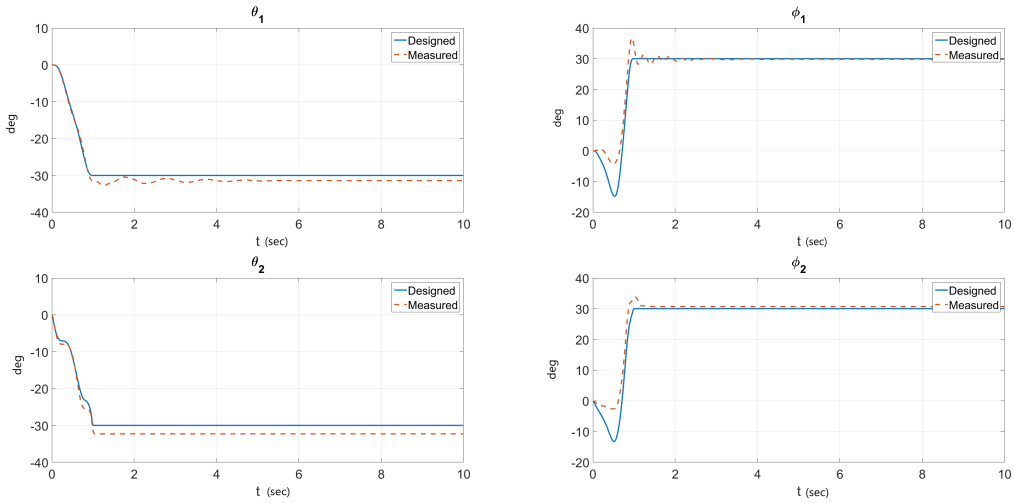

Figure 5.11: States generated by the including the unscented open-loop contributions.

loop unscented controls. The elbow joint has virtually no error in the steady state position of either the shaft or links, roughly 0.5°, while a small error in the shoulder shaft and link, roughly 1.5°, remains. The performance of these open-loop controls, which use no information about the measured states, are comparable with the full state feedback implemented on the nominally designed maneuver.

The endpoint sensitivity norms for the unscented open-loop controls clearly illustrates the improvement to sensitivity of the shoulder spring constant when compared with the values in Table 5.2. These values are shown in Table 5.3. There is an improvement of roughly an order of magnitude in the sensitivity of the endpoint to the spring constant k_1 indicating that deviations in the spring constant have less of an effect on achieving the desired endpoints. Additionally, there are noticeable changes in the endpoint sensitivities for other parameters, some are increased and some are decreased. One potential problem to be carefully considered is whether the unscented controls designed negatively impact the sensitivity to other potentially uncertain model parameters. In this case, the parameters whose sensitivity was increased are likely accurately measured which allows for the sensitivity to increase without negatively impacting the experiment.

$\mathbf{c_1}$	$\mathbf{k_1}$	$\mathbf{c_2}$	$\mathbf{k_2}$	$\mathbf{\Delta c_1}$
2.45e-4	0.1436	0.0037	0.4550	1.7856
$\mathbf{\Delta c_2}$	$\mathbf{I_1}$	$\mathbf{I_2}$	$\mathbf{m_1}$	$\mathbf{m_2}$
2.4857	0.0156	0.4844	0.0452	0.2026
$\mathbf{d_1}$	$\mathbf{d_2}$	$\mathbf{l_1}$	$\mathbf{K_{T,1}}$	$\mathbf{K_{T,2}}$
0.1808	0.1650	0.3876	0.7612	0.7301
$\mathbf{K_{g,1}}$	$\mathbf{K_{g,2}}$	$\mathbf{I_{r,1}}$	$\mathbf{I_{r,2}}$	$\boldsymbol{\eta}$
0.7611	0.7300	0.8987	0.4872	1.1632

Table 5.3: Norm of the scaled endpoint sensitivity functions, $\|s(t_f)\|^2$, of the unscented open-loop maneuver

Table 5.4 shows the endpoint error norm squared of the steady state error for

	NOL	NPD	UOL	UPD
$\|\mathbf{SSE}\|^2$	196.43	3.71	7.789	3.68

Table 5.4: Steady state error of the nominal open-loop (NOL), nominal PD partial feedback (NPD), unscented open-loop (UOL), unscented PD partial feedback (UPD), and unscented with partial UNOC gains (UUFB).

the nominal open-loop, both with and without partial LQR feedback gains, and the unscented open-loop, also with and without partial LQR feedback.

It is clear from the table that the included feedback gains do a good job of eliminating the error from the desired orientation for both the nominal and unscented maneuvers. It is also worth while to note that much of the improvement provided by state feedback can be achieved purely in the open-loop with the unscented controls.

In the next section the unscented neighboring problem will be used to generate feedback gains in an effort to further manage the uncertainty in the spring constant.

5.3.1 Partial Feedback Unscented

In this section, partial state feedback, feedback when the only measured quantities are the shaft angle and velocity of the shoulder and elbow joint, is designed to manage the uncertainty in the spring constant of the shoulder joint. This feedback structure represents the most likely sensor information available for many devices.

Assuming the full control with feedback structured as

$$i_1 = i_1^{nom} + K_1(t)(\phi_1^{meas} - \phi_1^{nom}) + K_2(t)(\dot{\phi}_1^{meas} - \dot{\phi}_1^{nom})$$
$$i_2 = i_2^{nom} + K_3(t)(\phi_2^{meas} - \phi_2^{nom}) + K_4(t)(\dot{\phi}_2^{meas} - \dot{\phi}_2^{nom}),$$

which is partial feedback scaled by the error of the shaft angle and velocity of both the shoulder and the elbow joints, the feedback gains $K(t)$ can be designed via the neighboring unscented control problem. This problem can be formulated as

$$\delta x_i \in \mathbb{R}^8, \quad \delta u = K(t) \in \mathbb{R}^4, \quad i = 1, 2, 3$$

$$(UFB) \begin{cases} \text{Min} & J_{unsc} = \sum_{i=1}^{3} w_i \|\delta x_i(t_f)\|^2 + \int_{t_0}^{t_f} \|K(t)\|^2 dt \\ \text{S.t.} & \delta \dot{x}_1 = f(x_1, t, k_1) - f(x^{\text{Nom}}, t, k_0) + h\delta u(t) \\ & \delta \dot{x}_2 = f(x_2, t, k_2) - f(x^{\text{Nom}}, t, k_0) + h\delta u(t) \\ & \delta \dot{x}_3 = f(x_3, t, k_3) - f(x^{\text{Nom}}, t, k_0) + h\delta u(t) \\ & (\delta x(t_0), t_0) = (0, 0) \\ & t_f = 1. \end{cases}$$

Solving problem (UFB) generates the time-varying feedback gains seen in Figure 5.12. These gains aim to take any measured deviation from the desired nominal maneuver due purely to uncertainty in the nominal spring value k_1, and correct them. These gains vary significantly from the LQR gains designed for the arm. This is likely due to the fact that the unscented gains only aim to reduce the effects of the one spring constant while the LQR gains are designed for general disturbances of the trajectories.

Implementing the feedback gains in Figure 5.12 generates the states in Figure 5.13. There is a clear reduction in the error in the shoulder joint angles from the nominally designed open-loop measured states. Additionally, there is a significant reduction in the endpoint error of the elbow joint as well, which is not specifically addressed by these feedback gains.

The feedback gains have a steady state endpoint error norm squared of 76.13

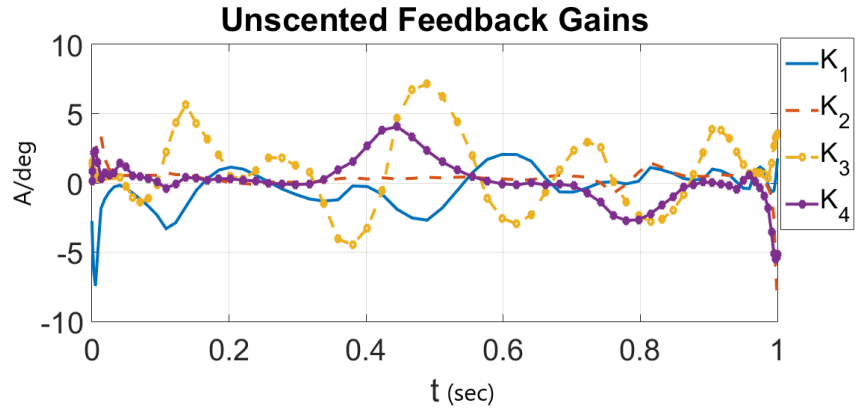

Figure 5.12: Feedback gains generated by the neighboring unscented problem for partial state feedback on the shaft angles of both the shoulder and elbow joints.

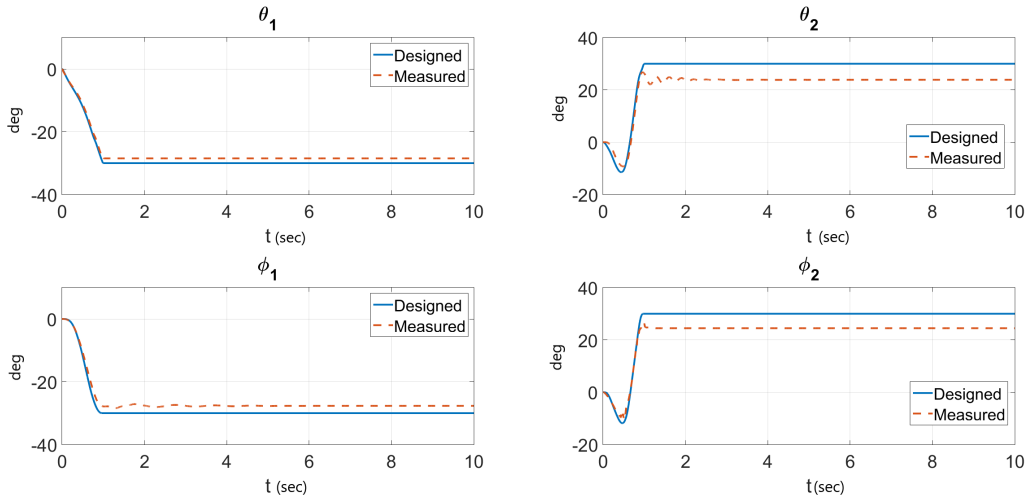

Figure 5.13: Nominal maneuver with unscented partial state feedback for the uncertain spring constant.

which is nearly all due to the error in the elbow joint. The endpoint error norm squared contribution of the shoulder joint is just about 7 while the other 70 is the elbow. The nominal open loop maneuver had endpoint error norm squared for the shoulder joint of roughly 55 which is nearly 8 times larger than the unscented feedback case. The partial state feedback gains for the spring constant greatly reduce the steady state error of the shoulder.

These feedback gains only use information about the deviations due to error in

the spring constant of the shoulder joint k_1 and therefore are unlikely to manage all error in the nominal model. In order to further improve the performance of the feedback solution, a multi-parameter unscented problem could be designed to address much of the remaining error in the elbow joint.

The difference between using the unscented feedback gains for uncertainty in the spring constant and using the LQR constant gains is shown in Figure 5.14 for the shoulder shaft and link angles.

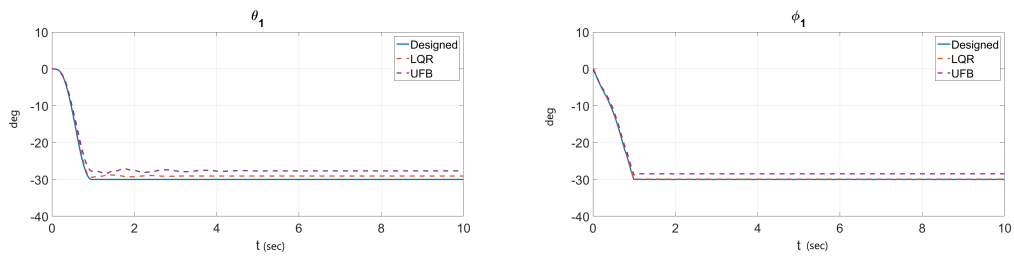

Figure 5.14: Shoulder link and shaft angle comparisons for the nominal maneuver with both LQR and unscented feedback.

The response to both these feedback gains is very close, though, the LQR, for the same partial feedback, gains show a slight improvement over the unscented gains. As mentioned, it is likely due to the unscented gains purely aiming to minimize uncertainty in the spring constant, while the LQR gains aim to remove all disturbances. The difference in the effort that each feedback is applying is another important comparison between the two methods. Figure 5.15 shows the absolute value of the feedback gains for both cases.

The figure clearly illustrates the difference between the time-varying and constant feedback gains. The LQR gains on the shoulder shaft angle ϕ_1 and velocity $\dot{\phi}_1$ are mainly larger in amplitude to the gains designed via the unscented problem. Computing the difference between the nominally demanded current and the

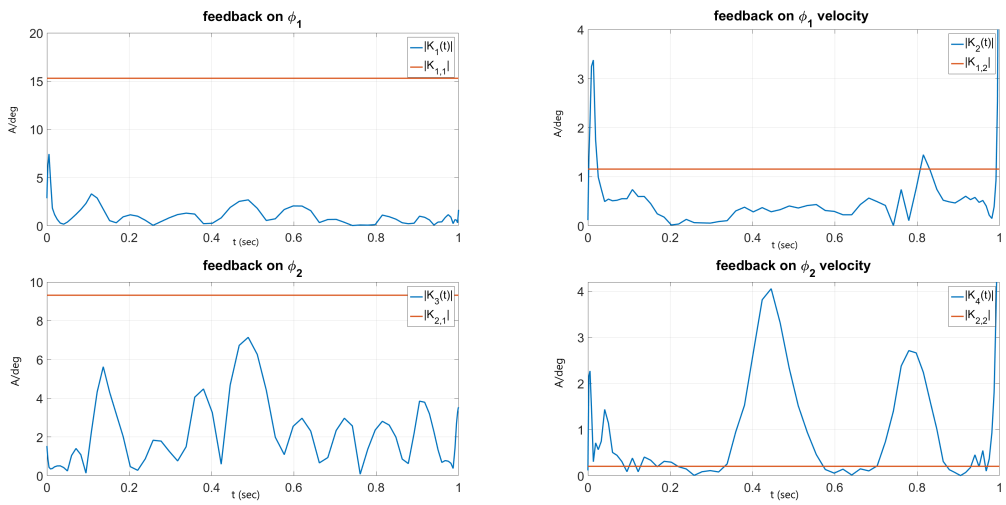

Figure 5.15: Partial state feedback gains for the unscented neighboring control and LQR control.

applied current to each of the motors,

$$\Delta i = |i_{measured} - i_{nom}|,$$

a measure of the control effort commanded by the feedback portion can be quantified as

$$\int \Delta i(t) dt.$$

The LQR gains extend beyond the 1 second maneuver time to decrease error, however, from the figure it appears to finish moving by three seconds. Therefore, a control effort from one to three seconds is computed. The feedback control efforts for the shoulder joint are shown in Table 5.5

	LQR	**Unsc**
Δi_1	0.0829	0.0372
Δi_2	0.2989	0.2890

Table 5.5: Control effort comparison for the first three seconds of the partial feedback gains for the LQR and unscented cases.

The unscented gains show a significant reduction in feedback effort in the feedback gains for the shoulder joint, roughly 55%, while maintaining much of the performance of the LQR gains. This is one of the potential advantages of using full nonlinear error dynamics and represents a promising avenue for designing time-varying feedback gains for these types of mechanical structures.

5.4 Conclusion

In this chapter a laboratory experiment on a two-link flexible arm manufactured by Quanser was performed. A minimum current maneuver was designed for the nominal set of model parameters of the robotic arm which failed to achieve the desired endpoint angles. By generating a set of purely open-loop control contributions for the nominal controls via the neighboring unscented control problem for uncertainty in the spring constant k_1, the error between the desired and measured states was achieved. Using the same framework of the neighboring unscented problem but for feedback gains, a large improvement in the shoulder joint was accomplished while a significant improvement in the elbow joint, though less than the shoulder, was observed. A neighboring unscented problem which considers more than just the single parameter uncertainty could likely be used to further improve the performance of the feedback case.

Chapter 6

Conclusions

Error in the dynamic model used to design input controls for a desired state maneuver can have large effects on the ability to achieve the endpoint conditions of interest. Historically, the deviations from a nominally defined model are managed using information provided by sensors, which can be used to correct many potential trajectory perturbations. In the case of no sensor feedback, it has been demonstrated recently that there are methods by which the maneuver itself can be designed to be more robust, such as unscented optimal control.

Using a classical tool of sensitivity functions (both a first order local measure and higher order terms), to quantify deviations due to parameter uncertainty, a new lens for studying the machinations of the unscented optimal control was outlined. This insight provides an avenue for those familiar with sensitivity analysis to understand unscented optimal control and use the intuitive information provided by the sensitivity functions to gain insight and intuition about how to design the optimal control problem.

The sensitivity functions also provide a means by which a neighboring optimal control type problem can be designed for generating a set of feedback gains for managing parameter deviations in the nominal model. Extending the concept

of the neighboring control for perturbation dynamics that avoid linearization of the error, a new unscented neighboring optimal control problem is defined. This unscented problem can be used to generate both open-loop and feedback controls for managing parameter uncertainty.

The results in this dissertation provide systematical tools to analysis and design optimal control that are inherently robust to parameter uncertainties. These tools are first tested on a simple mass-spring system, and then applied to a more challenging flexible double gimbal nonlinear model with uncertainty in the spring constant. In both cases, a large improvement in robustness to the uncertainty was achieved via feedback and purely open-loop controls. An experimental demonstration of the neighboring unscented controls, both open-loop and feedback, was conducted on a two-link robotic arm with flexible effects. The improvement gained from the open-loop consideration of a single uncertain parameter was significant over the nominally designed minimum current maneuver. The partial state feedback gains designed showed a marked improvement in the shoulder joint for which the uncertainty was relevant.

As an important future research direction, the scalability of the proposed methods with respect to the dimension of uncertainty deserves further study. Applications of current approaches to high dimensional cases entail more computationally efficient algorithms due to fast increase in the dimension of the resulting optimal control problems. This is true for both open-loop and feedback cases. Improvement along this direction will significantly expand application areas and further improve the performance of the robustness.

Bibliography

[1] I. M. Ross, R. J. Proulx, and M. Karpenko. Unscented optimal control for orbital and proximity operations in an uncertain environment: A new Zermelo problem. In *Proceedings of AIAA Space and Astronautics Forum and Exposition: AIAA/AAS Astrodynamics Specialist Conference*, San Diego, CA., August, 2014.

[2] S. Wojdakowski. Rapid slewing of flexible space structures. Master's thesis, Naval Postgraduate School, 2015.

[3] I. M. Ross. *A Primer on Pontryagin's Principle in Optimal Control, second edition*. Collegiate Publishers, San Francisco, CA, 2015.

[4] M. K. Savage. Design and hardware-in-the-loop implementation of optimal canonical maneuvers for an autonomous planetary aerial vehicle. Master's thesis, Naval Postgraduate School, 2012.

[5] I. M. Ross and M. Karpenko. A review of pseudospectral optimal control: from theory to flight. *Annual Reviews in Control*, 36(2):182–197, 2012.

[6] F. Fahroo and I. M. Ross. Enhancing the practical agility of uavs via pseudospectral optimal control. In *Recent Advances in Research on Unmanned Aerial Vehicles*, pages 1–30. Springer, 2013.

[7] Q. Gong, W. Kang, and I. M. Ross. A pseudospectral method for the optimal control of constrained feedback linearizable systems. *IEEE Transactions on Automatic Control*, 51(7):1115–1129, 2006.

[8] W. Kang, Q. Gong, and I. M. Ross. Convergence of pseudospectral methods for a class of discontinuous optimal control. In *44th IEEE Conference on Decision and Control and European Control Conference*, pages 2799–2804, 2005.

[9] C. Phelps, J. O. Royset, and Q. Gong. Optimal control of uncertain systems using sample average approximations. *SIAM Journal on Control and Optimization*, 54(1):1–29, 2016.

[10] C. Phelps, Q. Gong, J. O. Royset, C. Walton, and I. Kaminer. Consistent approximation of a nonlinear optimal control problem with uncertain parameters. *Automatica*, 50(12):2987–2997, 2014.

[11] I. M. Ross, R. J. Proulx, M. Karpenko, and Q. Gong. Riemann-Stieltjes optimal control problems for uncertain dynamical systems. *AIAA Journal of Guidance, Control, and Dynamics*, 38(7):1251–1263, July 2015.

[12] C. Phelps. *Computational optimal control of nonlinear systems with parameter uncertainty*. PhD thesis, UC Santa Cruz, 2014.

[13] C. L. Walton. *The design and implementation of motion planning problems given parameter uncertainty*. PhD thesis, UC Santa Cruz, 2015.

[14] I. M. Ross, R. J. Proulx, and M. Karpenko. Unscented guidance. In *Proceedings of the American Control Conference*, Chicago, IL, July 1-3, 2015.

[15] I. M. Ross, R. J. Proulx, and M. Karpenko. Unscented optimal control for space flight. In *Proceedings of the 24th International Symposium on Space Flight Dynamics*, Laurel, MD., May, 2014.

[16] I. M. Ross, M. Karpenko, and R. J. Proulx. Path constraints in tychastic and unscented optimal control: Theory, application and experimental results. In *2016 American Control Conference (ACC)*, pages 2918–2923, July 2016.

[17] R. Shaffer, M. Karpenko, and Q. Gong. Unscented guidance for waypoint navigation of a fixed-wing uav. In *Proceedings of the American Control Conference*, Boston, MA, July 6-8, 2016.

[18] R. Shaffer, M. Karpenko, and Q. Gong. Robust control of a flexible double gimbal mechanism. In *American Control Conference*, 2018.

[19] S. J. Julier, J. K. Uhlmann, and H. F. Durrant-Whyte. A new approach for filtering nonlinear systems. In *Proceedings of the American Control Conference*, Seattle, Washington, June, 1995.

[20] S. J. Julier. The spherical simplex unscented transformation. In *Proceedings of the 2003 American Control Conference, 2003.*, volume 3, pages 2430–2434 vol.3, June 2003.

[21] C. Phelps, J. O. Royset, and Q. Gong. Sample average approximations in optimal control of uncertain systems. In *52nd IEEE Conference on Decision and Control*, pages 1958–1965, Seattle, Washington, 2013.

[22] I. M. Ross, M. Karpenko, and R. J. Proulx. A lebesgue-stieltjes framework for optimal control and allocation. In *Proceedings of the American Control Conference*, Chicago, IL, July 2015.

[23] I. M. Ross and F. Fahroo. Pseudospectral knotting methods for solving nonsmooth optimal control problems. *Journal of Guidance, Control, and Dynamics*, 27(3):397–405, 2004.

[24] Q. Gong, F. Fahroo, and I. M. Ross. A spectral algorithm for pseudospectral methods in optimal control. *Journal of Guidance, Control and Dynamics*, 31(3):460–471, 2008.

[25] H. K. Khalil. *Nonlinear Systems*. Pearson Education. Prentice Hall, 2002.

[26] A. Ansari and T. Murphey. Minimal parameteric sensitivity trajectories for nonlinear systems. In *Proceedings of the American Control Conference*, Washington, DC, June 17-19, 2013.

[27] A. Ansari and T. Murphey. Minimum sensitivity control for planning with parameteric and hybrid uncertainty. *The International Journal of Robotics Research*, October 2015.

[28] Q. Liu and B. Wie. Robust time-optimal control of uncertain flexible spacecraft. *AIAA Journal of guidance, control, and dynamics*, 15(3):597–604, 1992.

[29] S. J. Julier. The spherical simplex unscented transformation. In *Proceedings of the American Control Conference*, pages 2430–2434, 2003.

[30] A. E. Bryson. *Applied Optimal Control*. Hemishpere New York, 1975.

[31] J. Breakwell, J. Speyer, and A. Bryson. Optimization and control of nonlinear systems using the second variation. *SIAM Journal on Control*, 1:193–223, 1963.

[32] M. Hassan and M. Singh. The optimization of non-linear systems using a new two level method. *Automatica*, 12:359–363, 1976.

[33] H. Yan, F. Fahroo, and I. M. Ross. Real-time computation of neighboring optimal control laws. In *AIAA Guidance, Navigation, and Control Conference and Exhibit*, page 4657, 2002.

[34] A. E. Bryson and J. L. Speyer. A neighboring optimum feedback control scheme based on estimated time-to-go with application to re-entry flight paths. *AIAA Journal*, 6(5):769–776, 1968.

[35] M. Spong. Modeling and control of elastic joint robots. *Journal of dynamic systems, measurement, and control*, 109(4):310–318, 1987.

[36] A. Sears, R. Gargano, and M. Karpenko. Rapid maneuvering of multi-body dynamic systems with motion compensation. In *AIAA/AAS Astrodynamics Specialist Conference*, page 4297, 2014.